IMPACT OF CONNECTING DIFFERENT TYPES OF ENERGY SIMULATION MODELS FOR DATA CENTER COOLING AND WASTE HEAT RE-UTILIZATION

A Thesis
Presented to
The Academic Faculty

By

Seungho Mok

In Partial Fulfillment
Of the Requirements for the Degree
Master of Science in the
School of Mechanical Engineering

Georgia Institute of Technology

August, 2016

IMPACT OF CONNECTING DIFFERENT TYPES OF ENERGY SIMULATION MODELS FOR DATA CENTER COOLING AND WASTE HEAT RE-UTILIZATION

Approved by:

Dr. Yogendra K. Joshi, Co-advisor
School of Mechanical Engineering
Georgia Institute of Technology

Dr. Satish Kumar, Co-advisor
School of Mechanical Engineering
Georgia Institute of Technology

Dr. Ronald R. Hutchins
Information Technology
University of Virginia

Date Approved: July 25, 2016

ACKNOWLEDGMENTS

TABLE OF CONTENTS

LIST OF TABLES

LIST OF FIGURES

NOMENCLATURE

Symbols

A	area, m^2
a	side length of channel, m
C	fluid heat capacity, W/°C
C_r	heat capacity-rate for solid matrix
c_p	specific heat, J/kg·K
D	diameter, m
E	power consumption, W
F	cross-sectional area of channel, m^2
f	Darcy friction coefficient
h	convection heat transfer coefficient, W/m^2·K
i	numbering for wheel designs
k	thermal conductivity of fluid, W/m·K
L	length, m
$\dot{m}$	mass flow rate of fluid, kg/s
m_s	mass of wheel, kg
N	rotational speed of wheel, rev/s
n	number of objects described in subscript
Nu	Nusselt number
NTU	number of transfer units
P	pressure, Pa

pe	periphery of channel, m
Pr	Prandtl number
Q	rate of heat transfer, W
r	ratio of area (gap) to area (circle)
Re	Reynolds number
T	Temperature, °C
U	overall heat transfer coefficient, W/m^2·K
$\bar{u}$	mean velocity of fluid in channel, m/s
V	volume, m^3
$\dot{V}$	volumetric flow rate, m^3/s
v	fluid velocity, m/s
WP	power consumption of the wheel, W
y	loss coefficient
Z	dimensionless coordinate

Greek symbols

α	absolute roughness, mm
ε	overall effectiveness of heat exchanger
ε_0	effectiveness of counter-flow heat exchanger
Θ	heat transfer factor
θ	thermal resistance, °C/W
η	efficiency
ν	kinematic viscosity of fluid, m^2/s

ρ	density of fluid, kg/m^3
Φ	heat transfer factor
φ_r	correction factor for rotational speed
ψ	shape factor

Subscripts

a	air
add	additional
atl	air-to-liquid heat exchanger
C	cold
c	cold side
co	coil
cp	cold plate
cpu	central processing unit
dimm	dual in-line memory module
dc	data center side
eq	equivalent
f	fan
fi	filter
gw	groundwater side
H	hot
h	hot side
I	in Imperial unit

i	inlet
ltl	liquid-to-liquid heat exchanger
m	miscellaneous
max	maximum
min	minimum
o	outlet
open	open for air flow
pf	pipe fittings
pi	pipe
pu	pump
s	server
side	side of triangle
TE	thermoelectric element
TEG	thermoelectric generator
total	total
tri	triangle
w	water
wh	wheel

Superscripts

*	dimensionless

Abbreviations

CRAC   computer room air conditioning

CRAH   computer room air handler

DX   direct expansion

EIR   Energy Input Ratio

HVAC   heating, ventilation, and air conditioning

IT   information technology

ITD   initial temperature difference

PUE   power usage effectiveness

TEG   thermoelectric generator

TIM   thermal interface material

SUMMARY

Data centers are the facilities that house information technology (IT) equipment used for our daily digital activities. They are considered as one of the largest energy consumers and also the fastest growing industries in the world. Since data centers consume a significantly large amount of electricity, which results in a large amount of heat that must be dealt with, "data center cooling" has been a very important topic. Due to the expense a large-scale system, such as a data center may require, it is critical to start with meticulously investigating cooling strategies for the data center before construction. The main purpose of this study is to develop energy simulation models that can be used to estimate overall data center efficiency for various equipment options for the location of interest. This large-scale modeling can be accomplished by developing several component-level models, which may be built in different modeling tools and interact with each other.

This study considers four cooling scenarios for a 400 kW notional data center: (a) an air cooled data center with a rotary regenerative heat exchanger and DX cooling system, (b) a hybrid cooled data center with an air cooled chiller and DX cooling system, (c) a hybrid cooled data center utilizing warm water through a liquid-to-liquid heat exchanger and DX cooling system, (d) a hybrid cooled data center that uses rear door heat exchangers and a water cooled chiller. This study also considers currently available or developmental low-grade waste heat re-use techniques including domestic heating, water pre-heating, and direct power generation from thermoelectric generators.

This thesis is presented in four chapters. In the first chapter, the four cooling scenarios, which have been chosen based on the past, current, and future trends of data center industry, are explained. This chapter also introduces a building energy simulation tool, EnergyPlus used as a core simulation tool. The second chapter discusses the modeling of each cooling and waste heat re-utilizing component. The component-level models are developed in different modeling tools including EnergyPlus, COMSOL, and MATLAB and are linked to run annual energy simulation for selected climates. In the third chapter, the annual simulation results which are calculated from scenario-level models are presented with deep and adequate discussions. In the final chapter, the suitability and detailed comparison of each cooling scenario are discussed.

CHAPTER 1

INTRODUCTION

1.1 Review of Common Cooling Techniques in Data Center

For the past decades, the increasing demand for data processing, data storage, and IT equipment have resulted in a rapid growth rate in the data center industry. The total electricity consumed by data centers worldwide doubled from 2000 to 2005 and increased by 58 % from 2005 to 2010 [1, 2]. In 2013, it was estimated that U.S. data centers consumed 91 billion kilowatt-hours of electricity, which was enough to power all the households in New York City two times [3]. By 2020, it is expected that data center energy consumption will reach about 140 billion kWh [3]. Along with the increasing energy consumption, the server manufacturers have been trying to increase the power density in order to meet the data demand, as well as the space constraints. Rack heat loads have been growing at a compounded annual growth rate of between 16.5 and 30.6% prior to 2005, and between 3.8 and 4.6% thereafter [4]. Driven by rising power densities and heat dissipation levels in data centers, the cooling systems consume significant of energy within data centers. In addition to energy efficient cooling strategies, waste heat utilization can also result in possible energy savings.

For many years, most of data centers have been air-cooled, using conventional raised floor systems equipped with computer room air conditioning (CRAC) units. A schematic of a traditional air-cooled data center with a raised floor system is shown in Figure 1.1. A typical CRAC unit consists of fans for air movement and cooling coils that chills the air through a direct expansion (DX) refrigeration cycle. Cold air from CRAC unit is supplied to the cold aisles and enters the server racks, cooling the heat produced from IT equipment. Then, the heated air comes out of the other side of rack, where hot aisles present, and is drawn back to the CRAC unit to be cooled. This conventional system has relatively poor efficiency because powering a refrigeration cycle is not energy efficient. Also, the system may create hot spots due to uneven cooling. Despite its disadvantages, low heat densities enables the system to meet the cooling objective that ensures the server components are maintained within their operational requirements.
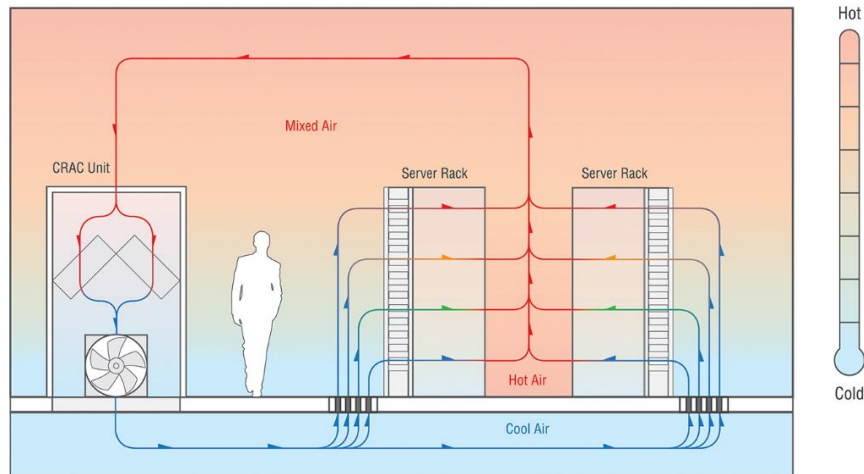
Figure 1.1 Traditional Raised Floor Cooling in Air-cooled Data Centers [5]

The conventional cooling with CRAC had been improved by implementing an air-side economizer, which enables the cooling system to utilize the cold ambient air. When the ambient temperature is below a certain temperature, the data centers can achieve a refrigeration-free cooling, which only requires fans to be powered. An air-side economizer regulates the use of outside air with regard to the temperature and humidity, and cooling with air-side economizer is often referred as free air cooling. Figure 1.2 shows a typical air-side economizer and CRAC unit used in air-cooled data centers.
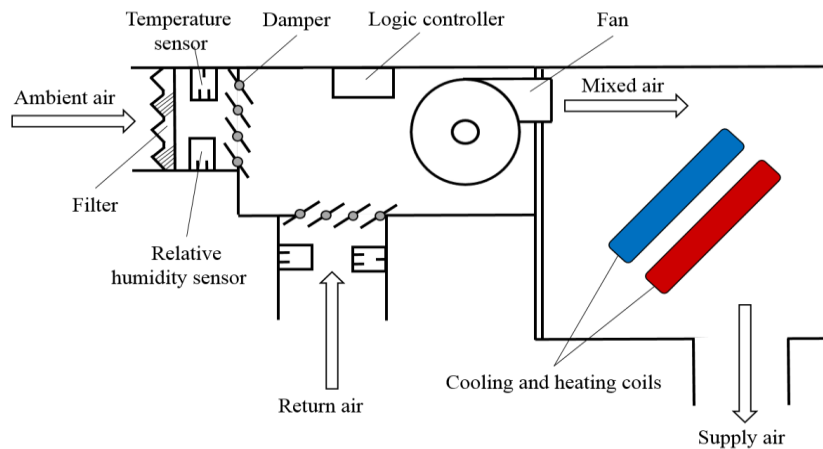
Figure 1.2 Diagram of a typical air-side economizer and CRAC unit

2

An air-side economizer typically consists of temperature sensors, humidity sensors, ducts, dampers, and a filter. As shown in Figure 1.2, the air-side economizer is located next to CRAC unit with ducting both ambient air and return air. This air-side economizer only works when the system can take advantages of brining the outside air into data center. Depending on the condition of the ambient and return air, the return air can be mixed with the ambient air or rejected to the ambient.

Since the power density of data center has continuously increased over time, which makes the traditional air cooling face its practical limit, liquid cooling has started to take people's attentions and been explored to keep up with the increase in server performance. The term "liquid cooling" means that the liquid is directly used to remove the heat generated from server components. There are two main approaches that directly utilize liquid for data center cooling and are as follows: hybrid (liquid/air) cooling and liquid immersion cooling. Hybrid cooling system uses both liquid and air to directly cool the server components. Liquid cooling at the server level is used for the high power components, such as central processing units (CPU) and dual in-line memory modules (DIMM). The remaining components are cooled by air, similar to conventional air-cooled data centers. Hybrid system not only allows the data center to be compatible with legacy IT equipment that should be cooled by air but also offers the majority of the benefits of liquid cooling [6]. Liquid immersion cooling is another method that uses liquid as coolant. It considers a server as one big heat sink. Servers are submerged in non-conductive liquid such as mineral oil or other engineered fluid, and the liquid is maintained below a certain temperature by being circulated using an ordinary chiller, heat exchanger, or two-phase cooling system. In 2013, 3M and Allied Control introduced liquid immersion cooling using Novec Engineered Fluid for its excellent dielectric heat transfer performance with exceptional environmental properties [7]. Their results show that the liquid immersion cooling can reduce the energy used to cool IT equipment by up to 97 percent when compared to conventional data air-cooled data centers [7].

1.2 Review of Modeling Data Centers

As modeling of data center requires not only individual component modeling but also considerations of other factors that affect data center efficiency, there were various modeling efforts for a specific stage in data center. In the early 2000's, Kang et al. [8] first modeled a data center with raised floor plenum by using CFD and fluid network modeling [9]. Patel et al. [10]

have developed a CFD model for a data center using an overhead supply and return air distribution system. Shrivastava et al. [11] have presented experimental-numerical comparison for a high density data center using CFD software. More recently, numerous studies have conducted thermal-fluids analyses of steady-state data centers [12-14] and a data center with transient boundary conditions [15].

In 2011, Demetriou et al. [16] stated that there was no current method for performing coupled simulations of the data center utilizing several cooling components. Then, they presented how two different kinds of simulation software, which were thermodynamic model of the cooling equipment and a hydraulic pipe network for hydraulic characterization, were coupled to evaluate the energy impact of various data center loop configuration and operating conditions [16]. Their study used various methods, including correlation for motor driven chiller, effectiveness-NTU method for cooling tower and CRAH, and hydraulic pipe network, in order to estimate the overall power consumption by their existing data center. The simulation results were fairly accurate when comparing with the actual data. The main difference between the work performed by Demetriou et al. [16] and our study is that we used EnergyPlus as core simulation tool, rather than having to use a number of different kinds of methods for modeling components. Yet, we did not investigate on automating the process of connecting EnergyPlus models to other models developed in MALAB, MLE+, an open source MATLAB/Simulink toolbox for co-simulation with EnergyPlus, can be used for easier communication between the two programs.

1.2 Summary of Cooling Scenarios Considered in This Study

This study presents four different cooling scenarios to be modeled and the modeling procedures of each of the cooling components used in the scenarios. Waste heat reutilization is also investigated when available. The cooling scenarios include one scenario of air-cooled data center with rotary regenerative heat exchanger and three scenarios of hybrid cooled data center. Table 1.1 summarizes the cooling scenarios presented.

Table 1.1 Summary of Cooling Scenarios

Scenario		Cooling Approach		Waste heat Re-use
		Air	Water	
A	Air Cooled	Rotary Regenerative Heat Exchanger and DX Cooling	N/A	Domestic Heating
B	Hybrid Cooled	DX Cooling with Air-side Economizer	Cooling with Air-Cooled Chiller	Thermoelectric Generators
C	Hybrid Cooled	DX Cooing with Air-side Economizer	Warm Water Cooling by Groundwater and Dry Cooler	Pre-heating Water
D	Hybrid Cooled	Air-to-Liquid Heat Exchanger (Rear Door Heat Exchanger)	Cooling with Water-Cooled Chiller	N/A

The first scenario describes an air cooled data center using a rotary regenerative heat exchanger and DX cooling system. Figure 1.3 shows a diagram of heat and air flow for Scenario A.
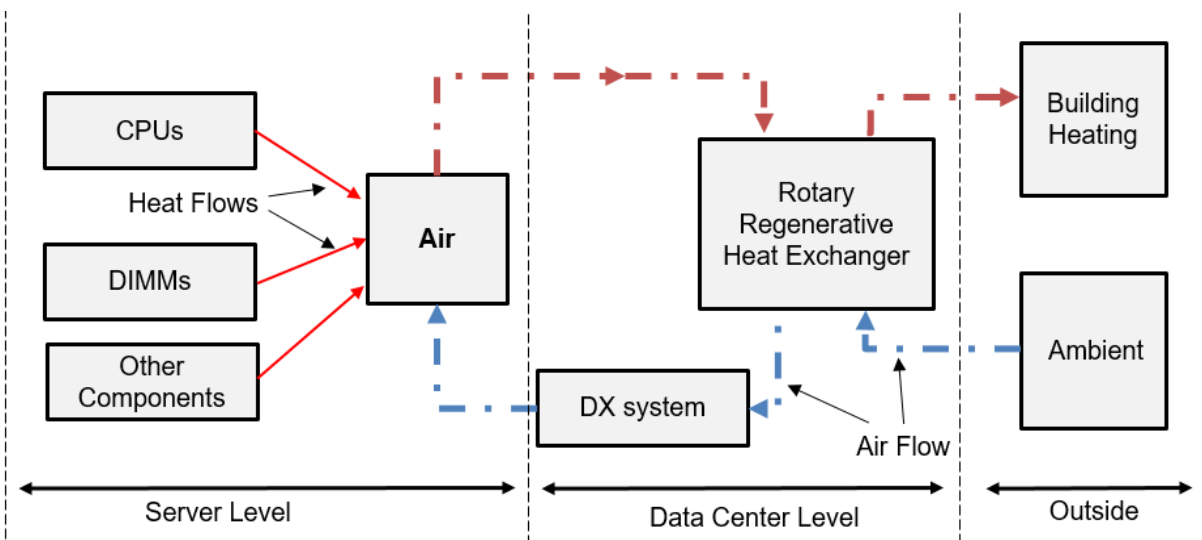
Figure 1.3 Diagram of Heat and Air Flows for Scenario A

All server components are cooled by air using rotary regenerative heat exchanger as main cooling component. When the ambient temperature is too high, DX cooling must be used as a secondary approach. The DX system has been modeled in EnergyPlus, an energy simulation tool. More detailed information regarding EnergyPlus will be presented in Section 1.5. This cooling approach discharges exhaust air to the ambient, which can be reused to heat up neighboring buildings and homes during winter.

Next three scenarios deal with hybrid cooled data centers using different cooling methods. Figure 1.4 shows a diagram of heat, air, and water flows for the first hybrid cooled case, which is Scenario B.
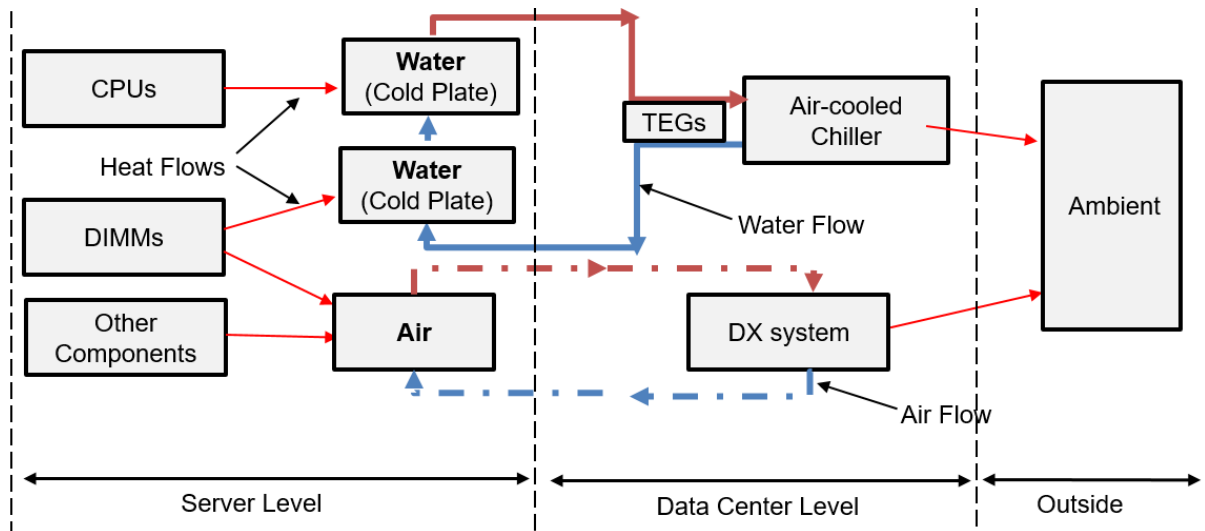
Figure 1.4 Diagram of Heat, Air, and Water Flows for Scenario B

As shown above, DIMMs are cooled by both water and air. The amount of heat transfer rate for each fluid has been determined and discussed later in the paper. The air that cools DIMMs and other server components is cooled by a DX system with an air-side economizer enabled for free air cooling. Water that is used to cool CPU through cold plate is chilled by an air-cooled chiller. By minimizing the water flow rate while making sure the server components are maintained within operating conditions, the water temperature rise can be as high as 40 °C. With this temperature difference, a thermoelectric generator is used for direct power generation as the waste heat re-

6

utilization method. The performance of the air-cooled chiller is determined by EnergyPlus simulations.

The third scenario is another example of a hybrid cooled data center. The main difference between Scenario B and C is that the temperature of the water that goes into the cold plates is as warm as 35 ℃ in Scenario C. Due to the fact that water inlet temperature is usually higher than ambient temperature and ground water temperature, it is possible to achieve a chiller-less system for cooling water. Figure 1.5 displays two diagrams of heat, air, and water flows for Scenario C.
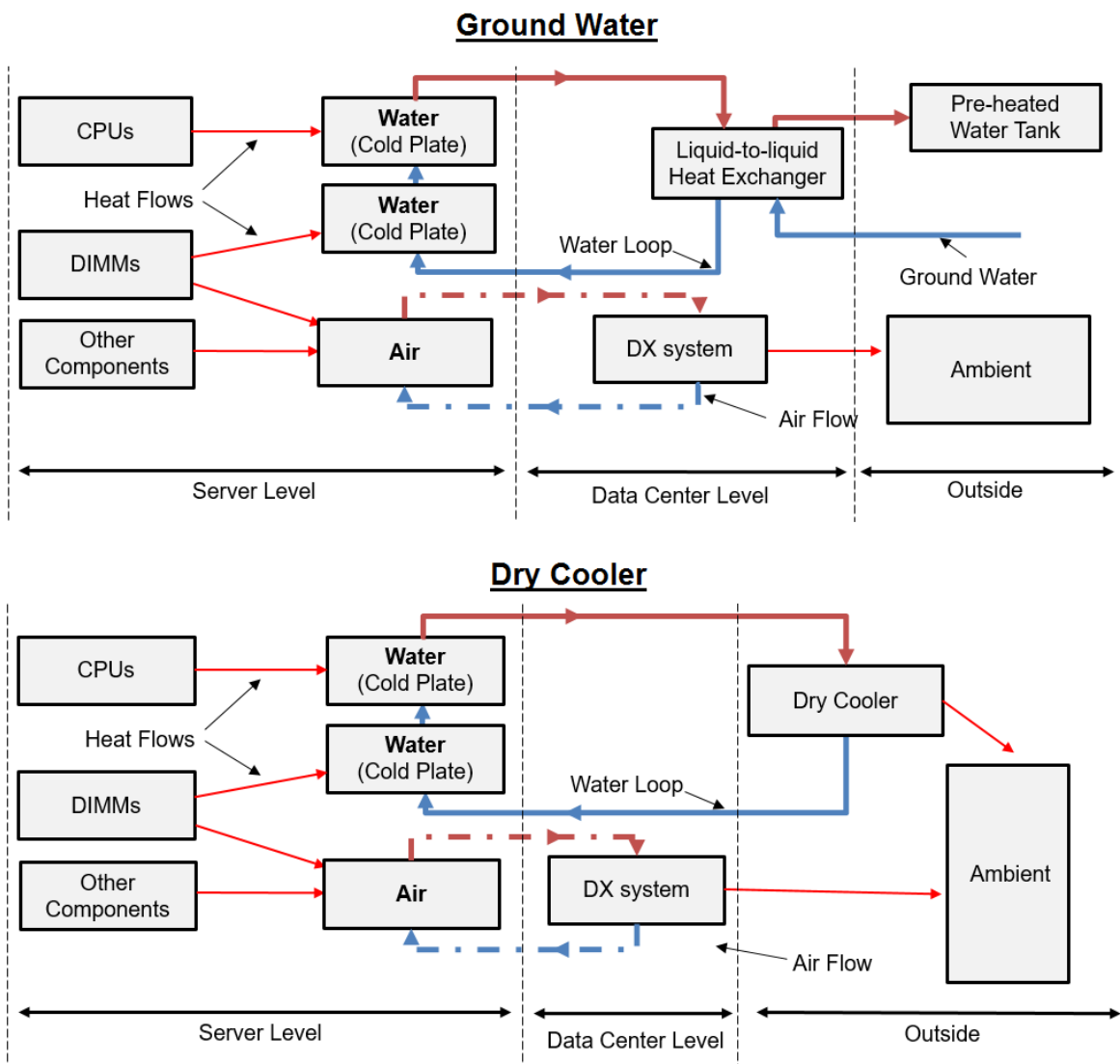
Figure 1.5 Diagram of Heat, Air, and Water Flows for Scenario C

Air is cooled by DX system, as same as scenario B. Water is cooled through a commercial liquid-to-liquid heat exchanger using ground water as coolant at temperatures as high as 25 °C for warmer climates. The ground water captures the heat from servers within liquid-to-liquid heat exchangers, and the heated water is delivered to hot water storage or reservoir containing pre-heated water. The heated water can be distributed to neighboring houses, office buildings, hospitals, and hotels. Since the hot water consumption is not consistent, a secondary system must be used when the data center is not able to manage the groundwater usage. Instead of liquid-to-liquid heat exchanger, dry cooler units located outside of the facility are used to cool the water. Dry cooler units consist of fans, air-to-liquid heat exchanger, and pump.

The last scenario uses air-to-liquid heat exchangers placed on the back of racks to cool down air, instead of DX cooling system. These air-to-liquid heat exchangers are often referred as rear door heat exchangers. The following figure shows a diagram of heat, air, and water flows for Scenario D.
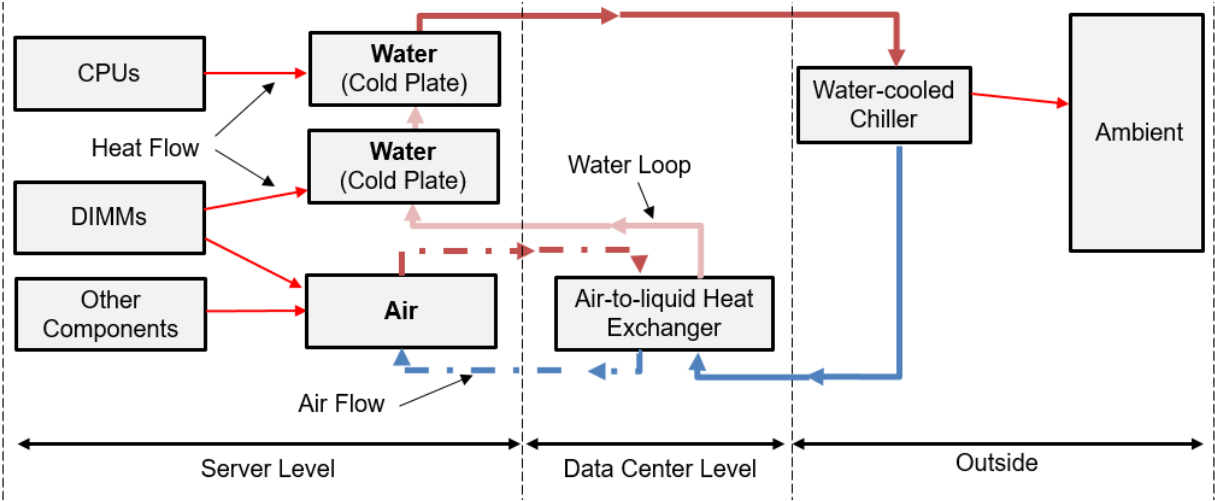
Figure 1.6 Diagram of Heat, Air, and Water Flows for Scenario D

The heat from DIMMs and other server components is transferred to air and then transferred to water through the heat exchanger. After the water leaves the heat exchanger, the water is distributed to the cold plates in servers, cooling DIMMs and CPUs. The water is then chilled by a

water-cooled chiller, which is modeled in EnergyPlus. No waste heat re-utilization is investigated for this case.

IBM LS20 blade server is used as an illustrative example, and power consumptions by the server components have been assumed, based on the server specification. In a single 42-U (1U = 44.45 mm) tall rack, 84 servers of this type can be fit and can consume up to 24 kW of power [17]. The data center considered in this study is 465 m^2 (5000 ft^2) and equipped with 17 racks which consumes about 408 kW at the maximum load. In all scenarios, each blade server has two AMD Opteron 875 CPUs and four typical 4GB-PC3200 DIMMs.

1.3 Air-Cooled Data Center with Rotary Regenerative Heat Exchanger

This section is to provide an introduction and background to Scenario A. Rotary regenerators that use a thermal wheel, also often referred as a heat wheel, have been widely used in gas turbine engines for heat recovery and as air preheaters in steam power plants for many decades [18]. Also, they have been used as an energy recovery component in air conditioning and heating applications [19]. Two distinct advantages of rotary regenerative heat exchangers are as follows: fairly compact design can be achieved with relatively inexpensive heat transfer per unit volume, and the amount of heat transfer can be readily controlled by varying the wheel speed [20]. In the context of data centers, this technology has been examined by and commercially available at KyotoCooling since 2006 [21]. There is an exploratory case study performed by Uptime Institute, regarding regenerative heat exchangers in data centers, however, the white paper does not get into the details of the performance analysis. The objective of developing a computational model for this cooling approach is to provide quantitative assessments of the performance of rotary regenerative heat exchangers in air-cooled data centers.

A regenerative system within a data center can achieve refrigeration-free cooling when the ambient temperature is below a certain maximum. It uses a thermal wheel, which is shown in Figure 1.7, to move the heat generated by the IT hardware to the environment. The thermal wheel consists of a number of equilateral triangle flow channels and is made of aluminum honeycomb material [22].
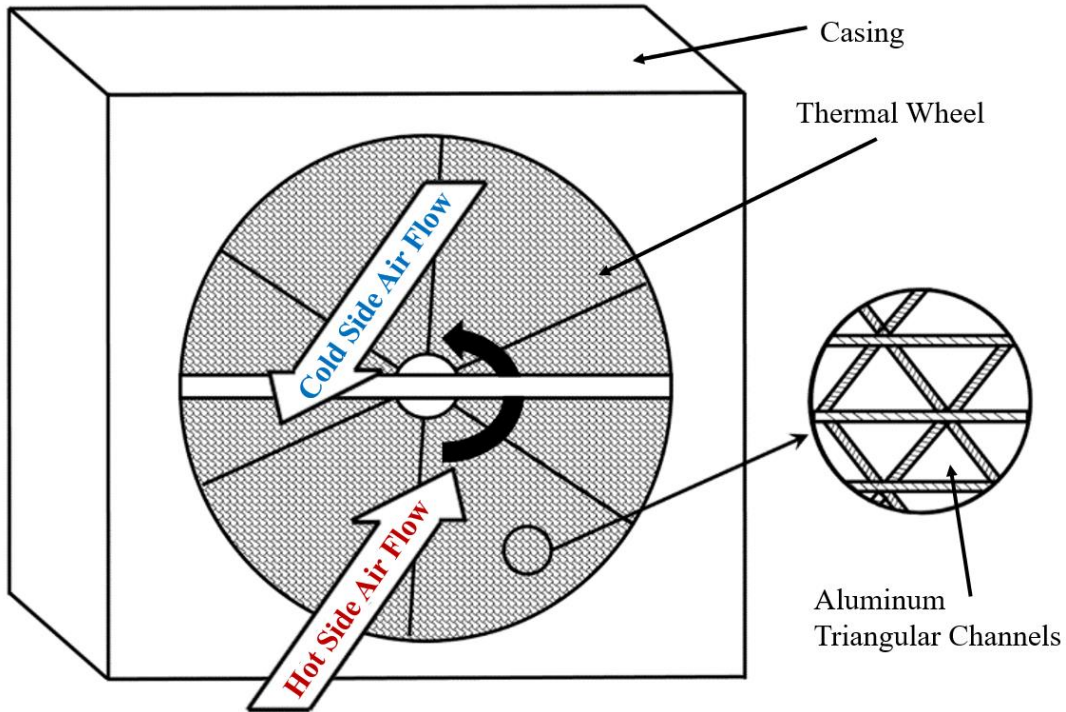
Figure 1.7 Schematic of a Typical Rotary Regenerative Heat Exchanger.

The solid arrow denotes that the thermal wheel is rotating counter-clockwise, and the hollow arrows indicate the directions of the air flow in hot and cold side. The thermal wheel is divided into two sections: the hot side and cold side. To minimize air mixing between the two sides, the rotating speed of the wheel is maintained low. An overview of the regenerative system with air flow patterns is shown in Figure 1.8. The region enclosed by the dashed line occupying the right side of the wheel is the cold side. The ambient air is drawn into the lower chamber by a set of fans. This air cools the wheel, and the discharge air is exhausted back to the ambient. The heated internal air from the data center hot aisles is drawn into the higher chamber by another set of fans. The air passes through the wheel, transferring heat to the external air. The cooled air is then recirculated into the data center. Due to such a small exchange of air between the data center and the ambient, the system is relatively insensitive to the quality of the ambient air, which broadens its applicability. When the ambient temperature is cold enough, cooling can be completely achieved through using only the fans and the motor of the wheel. The system also requires less humidity control, which is a large power saving factor. A cooling load of 400 kW is used as the maximum

load per unit. A cooling unit consists of 8 fans in the cold side, 8 fans in the hot side, and a thermal wheel between the two sides. Other data center parameters are summarized in Table 1.2.
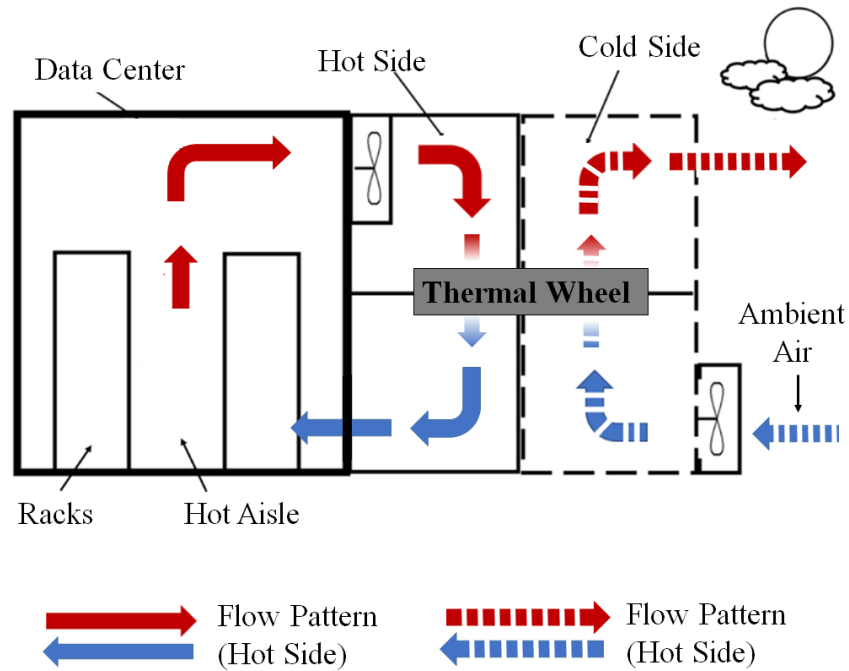
Figure 1.8 An Overview of a Rotary Regenerative Heat Exchanger Installed in Data Center and Overall Air Flow Patterns.

Table 1.2 Data Center Parameters, Descriptions, and Values.

Parameter [unit]	Description	Value
$T_{c,i}$ [°C]	Ambient Air Temperature	Model Input
$T_{c,o}$ [°C]	Discharge Air Temperature	Calculated
$T_{h,i}$ [°C]	Supply Air Temperature	26.7
$T_{h,o}$ [°C]	Return Air Temperature	38.9
Q [kW]	IT Load	400
N [RPM]	Rotating Speed of Wheel	0 to 6 RPM
$\dot{m}_h$ [kg/s]	Mass Flow Rate (hot side)	32.7
$\dot{m}_c$ [kg/s]	Mass Flow Rate (cold side)	Calculated

The ambient temperature is from weather data files for selected locations and contains hourly dry-bulb temperature for one year period. Also, $\dot{m}_h$ is the maximum mass flow rate that can be delivered by the set of fans, as discussed in the next chapter, and $T_{h,o}$ is the return air temperature which ensures that IT equipment is maintained within the operating condition. With fixed values of $T_{h,o}$, Q, and $\dot{m}_h$, $T_{h,i}$ can be calculated by energy balance:

$$Q = c_{p,air}\dot{m}_h(T_{h,i} - T_{h,o}) \tag{1}$$

where $c_{p,air}$ is the specific heat of air evaluated at the average value of supply and return air temperature. In Equation (1), $\dot{m}_h$ is a function of the cooling load, while $\dot{m}_c$ depends on the ambient temperature and the performance of the heat exchanger. Since $\dot{m}_c$ varies over time, a year-long simulation is performed in order to determine the annual energy usage by the fans.

A supplemental system must be used when the ambient temperature is too high for the system to efficiently dissipate the heat. The temperature point where the switch needs to occur depends on the performance of the regenerative system, which is determined later in this paper. In this study, refrigeration-based DX cooling is used as the secondary approach. In this study, the rotary regenerative system and the DX cooling system have been modeled separately. The regenerative heat exchanger is modeled in MATLAB, based on the effectiveness-NTU method and other heat transfer correlations. The DX system is modeled in EnergyPlus. The two separate models are coded in MATLAB to be able to take a weather data file for a particular location as input and to calculate annual power usage effectiveness (PUE) at the location. The details of modeling procedures are presented in the next chapter.

1.4 Hybrid (Liquid/Air) Cooled Data Center

This section is to provide background and more explanations regarding hybrid cooling scenarios considered in this study. Hybrid cooling system uses liquid as coolant to directly reject the heat generated from the high power components in servers, while the remaining low power components are cooled by air. Figure 1.9 shows a schematic view of a hybrid cooled server.
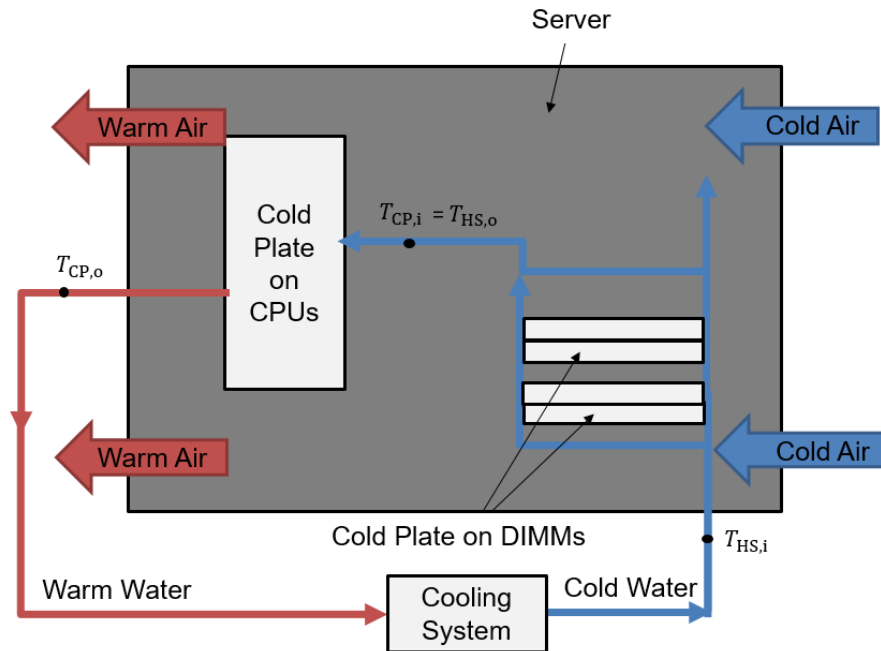
Figure 1.9 A Top View of a Typical Hybrid Cooled Server with 4 DIMMs and 2 CPUs.

As shown in Figure 1.9, cold water is drawn into the server and passes through the cold plates enclosing DIMMs. Heat produced by DIMM is partially transferred to the water, which then enters the cold plate for CPUs that replaces the traditional air cooled heatsink. The water delivered to the CPU cold plate heats up as the CPUs are cooled. Other components in the servers are cooled by air. This concept design described in Figure 1.9 has been studied by Iyengar at el [23]. According to the specifications of IBM LS20 blade server, which has been used for the illustrative case study in this hybrid cooling part, power consumption by CPUs and DIMMs operating at the maximum load can be nearly 50% of the total consumption. By cooling these high power components directly by liquid, a considerable reduction in the energy usage for cooling is expected.

1.5 Energy Simulation Tool: DesignBuilder & EnergyPlus

1.5.1 Introduction

DesignBuilder provides advanced modelling tools in an easy-to-use interface. This enables users to develop comfortable and energy-efficient building designs from concept through to completion [14]. Modelling work that involves EnergyPlus simulations starts with creating

geometries and setting up a number of input parameters in DesignBuilder. Then it takes those inputs to run energy simulations using its core simulation tool, EnergyPlus. EnergyPlus is a whole building energy simulation software developed by the U.S. Department of Energy Building Technologies Office. EnergyPlus can take a number of input parameters, such as weather conditions, building geometry, heating/cooling loads, heating, ventilation, and air conditioning (HVAC) system, temperature set points, volumetric flow rate, schedule, and more. Using these inputs, the software can estimate power usage by each cooling and heating component for a selected period and climate. EnergyPlus also allows users to customize a HVAC system for user-created building geometry and all other inputs. For example, an EnergyPlus model whose HVAC system utilizes a Direct Expansion (DX) coil as the main cooling component can be used to estimate energy consumption of the DX system. The performance of the cooling or heating components at part-load conditions is determined by incorporating performance information at rated conditions, along with curve fits for variations in total capacity, energy input ratio and part-load fraction [25, 26]. The DX cooling coil requires 5 curves as follows: (1) Total cooling capacity as function of temperature, (2) Total cooling capacity as function of flow fraction, (3) Energy input ratio as function of temperature, (4) Energy input ratio as function of flow fraction, (5) Part load fraction correlation. The performance curves are obtained from EnergyPlus database and attached in Appendix A. [27]. The rated conditions are the following: air entering the DX coil at 26.7°C dry-bulb/19.4°C wet-bulb, and air entering the condenser coil at 35°C dry-bulb/23.9°C wet-bulb. Other than the DX cooling system, an air-cooled chiller and water-cooled chiller can also be modeled in the same way as for DX system. EnergyPlus simulations for the chillers use performance curves given by the software and also presented in Appendix A.

1.5.2 Software Validation

EnergyPlus enables users to perform energy simulations even if there is unobtainable input data by autosizing. In the case where "autosize" is entered for an input parameter, EnergyPlus will calculate an appropriate value before simulation, based on other data provided. To validate our simulation results calculated using autosized data as well as the given performance curves for cooling components, experimentally measured power consumption of an existing data center and chiller plant located in Poughkeepsie, NY were used [16]. We modeled a data center with all available information from the data center in Poughkeepsie. The goal of this modeling was to compare the measured power consumption by water-cooled chiller with the one calculated by

EnergyPlus. Two different chillers from the EnergyPlus database were selected, based on the known properties of the chiller used in the existing data center. Table 1.3 and 1.4 summarize the chiller and cooling tower properties for the data center and the EnergyPlus models.

Table 1.3 Comparison of the Chiller Properties

	Existing Data Center [16]		EnergyPlus Model	
	Chiller		Chiller 1	Chiller 2
Reference Cooling Capacity [kW]	4220		4667	4396
Reference COP	6.25		6.16	6.63
Reference chiller water flow rate [m^3/s]	0.1767		0.1956	0.1956

Table 1.4 Comparison of the Cooling Tower Properties

	Existing Data Center [16]		EnergyPlus Model	
	Cooling Tower		Cooling Tower 1	Cooling Tower 2
Design Air Flow Rate [m^3/s]	128.5		Autosize	Autosize
Fan Power at Design Air Flow Rate [kW]	44.7		Autosize	Autosize
Reference Condenser Water Flow Rate [m^3/s]	0.189		0.24605	0.24605

According to the 10 measurements from [16], the total cooling load ranged from 4310 kW to 5380 kW, while chiller power consumption ranged from 470 kW to 660 kW and cooling tower consumption stayed constant at 44.7 kW. With varying the cooling load, EnergyPlus simulations were performed to estimate power consumption by chiller and cooling tower. As the exit cooling tower water temperatures varied from 18 °C to 24 °C [16], the same temperature range was used

in EnergyPlus models. Figure 1.10 shows the percent difference between the measured power consumption and the EnergyPlus results for two chillers.
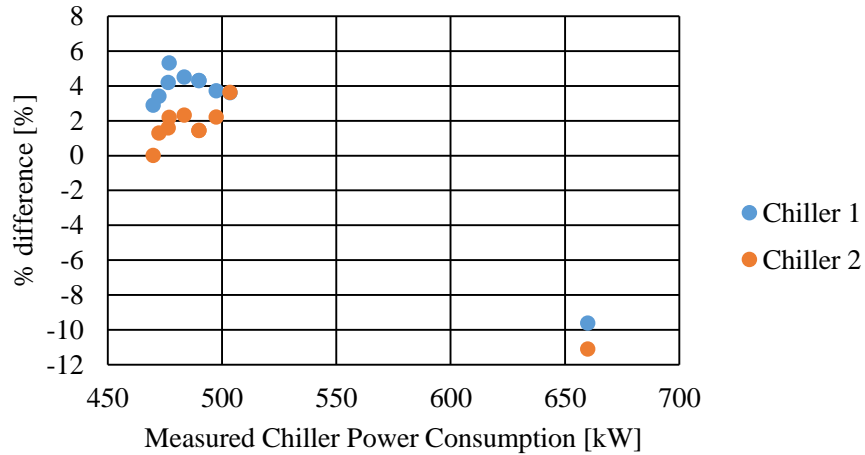
Figure 1.10 Percent Difference between Measured Data and Simulation Model

All the measurement data, EnergyPlus results, error calculations in Figure 1.10 can be seen in Appendix B. Agreements within 6 % was observed in all measurements except the one measured when an exceptionally higher cooling load was assigned. These outliers may be due to the fact that the assigned cooling load was much greater than rated cooling capacity. For cooling tower consumption, EnergyPlus shows that the power consumption by the cooling tower is constant at 44.31 kW, which had a difference of 0.9 % when comparing with the measured power consumption. These results conclude that EnergyPlus models developed for data center-level analysis are useable and fairly accurate even with autosized input data and performance data given by EnergyPlus.

CHAPTER 2

MODELING PROCEDURES

Energy modeling of a data center can be accomplished by developing separate models for all the cooling and waste heat re-utilizing components used in each scenario. This chapter presents component-level modeling procedures, which takes place before the individual models are combined as scenario-level models. The order of subsections in this chapter does not reflect the order of the cooling scenarios listed previously.

2.1 Rotary Regenerative Heat Exchanger

2.1.1 Thermal wheel design

A design of the heat exchanger, a thermal wheel, must be defined in order to evaluate the heat exchanger performance. The dimensions and mass of the thermal wheel are chosen, based on a commercially available thermal wheel, TF-556 from Thermotech Enterprise. A 1556 kg aluminum wheel with a diameter of 3.8 m and a channel length of 0.33 m is used. A top view of possible designs of the thermal wheel is shown in Figure 2.1.
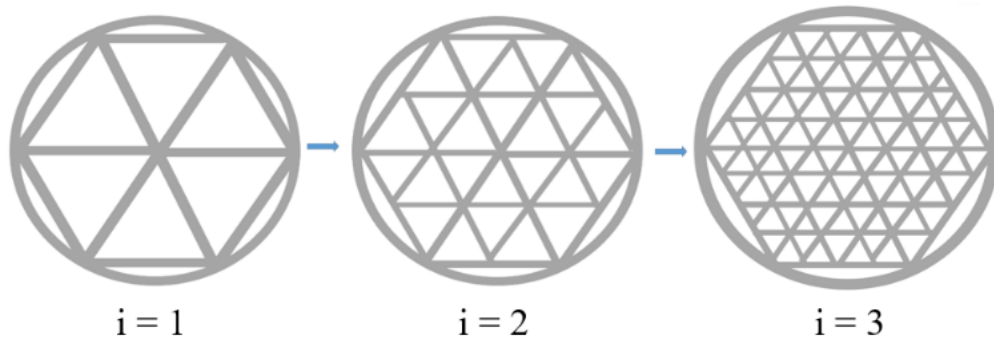
Figure 2.1 Possible Designs of Thermal Wheel.

The thermal wheel design can be as simple as the left design ($i=1$), which contains only 6 equilateral triangle flow channels. The left design will not be efficient enough to be used as a heat exchanger because it has a relatively small heat transfer surface area. From these simple cases ($i = 1, 2,$ and 3) in Figure 2.1, the following equations have been formulated to calculate the number of triangular channels for more complex designs:

$$n_{\text{tri},(i)} = 6\left(4^{i-1}\right) + n_{\text{add},(i)} \tag{2}$$

$$n_{\text{add},(i)} = 6r\left(4^{i-1}\right) \tag{3}$$

$$r = \left(\left(\frac{\pi D^2}{4}\right) - \frac{3\sqrt{3}}{2}\left(\frac{D}{2}\right)^2\right)/\left(\frac{\pi D^2}{4}\right) \tag{4}$$

where n_{tri} is the number of triangular channels and n_{add} is the additional number of the triangles that can fit in the remaining space between the circle and the hexagon. The parameter r is the ratio of the area of the gap to the area of the circle. Equation (3) and (4) should be applied only when i is greater than 4, where triangle channels are small enough to fit in the space. The equations for the number of sides and the total heat transfer area are following:

$$n_{\text{side},(i)} = 2(n_{\text{side},(i-1)} + 1.5\,k_{(i)}) + 3n_{\text{tri},(i-1)} \tag{4}$$

$$A_{(i)} = 2n_{\text{side},(i)}\,a_{(i)}L \tag{5}$$

where n_{side} is the number of sides, and a is the length of the side of the triangle, A is the total heat transfer surface area through the channels, L is the length of the channels. Since it is expected that pressure drop along the channel will increase as the value of i increases, the pressure drop must be considered when selecting the wheel design. Since the flow condition for the hot side is known, it is possible to calculate the average velocity of the fluid. The open area is the area that the air can flow through and can be calculated by the following equation:

$$A_{\text{open}} = \frac{\pi D^2}{4} - \frac{V_w}{L} \tag{6}$$

where V_w is the total volume of the wheel, which can easily be converted from the given mass. The equation for the average fluid velocity of the hot side is given by

$$\overline{u_h} = \left(\frac{\dot{m}_h}{\rho_h}\right)/\left(\frac{A_{\text{open}}}{2}\right) \tag{7}$$

18

The reason for dividing A_{open} by 2 is that the hot side air flows through only the half of the wheel. Again, $\dot{m}_{\text{h}}$ is the mass flow rate required to cool down a cooling load of 400 kW and can be generated when the fans are operating at their maximum. Reynolds number for this flow condition is calculated:

$$Re_{\text{h}} = \frac{\overline{u_{\text{h}}} d_{\text{eq}}}{\nu} \tag{8}$$

where ν is the kinematic viscosity of the fluid and d_{eq} is the equivalent diameter of the flow channel

$$d_{\text{eq}} = \frac{4F}{P} \tag{9}$$

where P is the perimeter of the triangular channel and F is its cross-sectional area. F is defined as

$$F = \frac{\sqrt{3}}{4} a2 \tag{10}$$

Shah and London [28] have presented a useful compendium of laminar flow and heat transfer data for triangular ducts. For an equilateral triangle channel, where the duct apex angle is 60°, the friction factor is calculated by the following equation:

$$f_{\text{h}} = \frac{53.332}{Re_{\text{h}}} \tag{11}$$

The pressure drop across the wheel is given by,

$$\Delta P_{\text{w}} = \frac{f_{\text{h}} \rho_{\text{h}}}{2 D_{\text{eq}}} \overline{U_{\text{h}}}^2 L \tag{12}$$

Table 2.1 summarizes the calculation results that define the thermal wheel design for cases $i = 2$, 3, 9 and 10.

Table 2.1 Parameters of Thermal Wheel Designs

Parameter	$i = 2$	$i = 3$	$i = 9$	$i = 10$
n_{triangle}, [-]	24	96	471858	1887436
n_{side} [-]	42	156	937116	3761668
a [mm]	480	240	3.71	1.86
A [m^2]	20.4	31.7	2302	4613
Re_h, [-]	$9.8{\times}10^4$	$4.9{\times}10^4$	767	388
ΔP [Pa]	-	-	207	828

Based on the flow condition, the pressure drop along the channels, and manufacturability, the result for $i = 9$ has been selected and used in this model.

2.1.2 Overall effectiveness of the heat exchanger

The heat exchanger part is modeled using the effectiveness-NTU method. The overall effectiveness of a rotary regenerative heat exchanger or any other types of heat exchanger is defined as

$$\varepsilon = \frac{Q}{Q_{\text{max}}} \tag{13}$$

where Q_{max} is the maximum possible heat transfer rate:

$$Q_{\text{max}} = C_{\text{min}}(T_{h,i} - T_{c,i}) \tag{14}$$

where C_{min} (C_{max}) is C_h or C_c, whichever is smaller (larger). C_h or C_c are the fluid heat capacity rates of hot side and cold side, respectively. The fluid heat capacity rates are expressed in the following:

$$C_h = \dot{m}_h c_{p,\text{air}} \tag{15}$$

$$C_c = \dot{m}_c c_{p,\text{air}} \tag{16}$$

Since $\dot{m}_h$ is fixed at the maximum volumetric flow rate that the fans can produce, $\dot{m}_c$ is always smaller or equal to $\dot{m}_h$. Thus, it can be seen that C_{min} is C_c and C_{max} is C_h for this condition. The effectiveness of a rotary regenerator can also be expressed in terms of the effectiveness of a stationary counter-flow heat exchanger (ε_0) and the correction factor that takes into account the

influence of rotating wheel (φ_r). The equation for the overall effectiveness of rotary regenerative heat exchanger is expressed as,

$$\varepsilon = \varepsilon_0 \varphi_r \tag{17}$$

As seen in Equation (17), the calculation of the overall effectiveness of the system involves two main steps: calculating the effectiveness of a stationary counter-flow heat exchanger, and the correction factor which comes from the rotational speed of the thermal wheel. It is possible to calculate the overall effectiveness using Equation (13) and the data center parameters defined in Table 1.2. Since the effectiveness values calculated from (13) and Equation (17) should be identical, the unknown parameter, $\dot{m}_c$, presented in the calculation process of ε_0 and φ_r can be found. Therefore, the goal of the presented model is to calculate the cold side mass flow rates of air with different temperature inputs.

2.1.3 Effectiveness of a stationary counter-flow heat exchanger.

The effectiveness of a stationary counter-flow heat exchanger is shown in the following equation:

$$\varepsilon_0 = \frac{1-e^{[-\text{NTU}(1-C^*)]}}{1-C^*e^{[-\text{NTU}(1-C^*)]}} \tag{18}$$

where C^* is the heat capacity ratio, defined as

$$C^* = \frac{C_{\min}}{C_{\max}} \tag{19}$$

NTU in Equation (18) stands for the number of transfer units. It is a dimensionless parameter that is widely used in heat exchanger analysis. NTU is defined as

$$\text{NTU} = \frac{UA}{C_{\min}} \tag{20}$$

where U is the overall heat transfer coefficient of the system and A is the total surface area available for convection heat transfer. Since there are two sides in rotary regenerative heat exchanger, the overall heat transfer coefficient can be expressed as

$$\frac{1}{UA} = \frac{1}{h_h A_h} + \frac{1}{h_c A_c} \tag{21}$$

where h_h and h_c are the convective heat transfer coefficient of hot side and cold side, respectively. The overall heat transfer coefficient is calculated with assuming negligible wall resistance. The

convection heat transfer coefficients are evaluated using the correlation, proposed by Yilmaz and Cihan [29]. This correlation is applicable for laminar flow in the channels of various cross-sections for a constant wall temperature boundary condition:

$$\text{Nu} = \text{Nu}_\infty \left[\frac{1 + 4.212\psi\Phi^3}{ZNu_\infty^3} - 0.8 \left(\frac{\psi\Phi^3}{ZNu_\infty^3} \right)^{\frac{2}{3}} \right]^{1/3} \tag{22}$$

where ψ is the shape factor, Φ is the heat transfer factor, and Z is the dimensionless coordinate. Nu_∞ is the Nusselt number for the limiting case of $Z \rightarrow \infty$:

$$\text{Nu}_\infty = 3.657\Theta \tag{23}$$

where Θ is another heat transfer factor that takes the shape of the cross-section of the flow channel into account for developed velocity and temperature profiles at a constant wall temperature.

$$\Theta = 1 + \frac{\Theta_\infty - 1}{1 + 1/(n-1)} + \Delta\Theta \tag{24}$$

The parameters in Equation (24) are defined by the shape of the flow channel.

$$\Theta_\infty = 0.5155 \frac{D^{*2}}{3 - d^*} \tag{25}$$

$$\Delta\Theta = \Theta_{max} \frac{0.95(n-1)^{0.5}}{1 + 0.038(n-1)^3} \tag{26}$$

where Θ_{max} is defined as

$$\Theta_{max} = \frac{0.007D^{*8}}{\left(1 + 10\, D^{*-28}\right)\left(1 + (6.4 \times 10^{-7})D^{*28}\right)^{0.5}} \tag{27}$$

The parameter d^* and n in Equation (24) through (27) are determined by the shape of the flow channel, described in Figure 2.2.
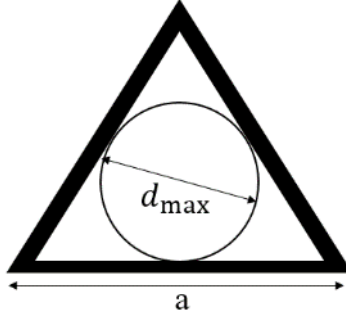
Figure 2.2 Definition of Maximum Diameter in an Equilateral Triangle Flow Channel.

D_{max} is the diameter of the largest circle that can be inscribed in the flow channel, which is, in this case, the same as the equivalent diameter D_{eq}. Now D^* and n can be calculated using the equations below:

$$D^* = \frac{D_{eq}}{D_{max}} \tag{28}$$

$$n = \frac{Pe}{Pe_{eq}} \tag{29}$$

where Pe_{eq} is the periphery of the largest circle in the channel. D^* and n are found to be 1 and 1.653, respectively.

The shape factor in Equation (22) is given by

$$\psi = 1 + \left\{ \frac{\psi_\infty - 1}{[1 + 0.33D^{*2.25}/(n-1)]} \right\} \tag{30}$$

where ψ_∞ is defined as

$$\psi_\infty = \frac{3}{8} D^{*2}(3 - D^*) \tag{31}$$

The heat transfer factor (Φ) and dimensionless parameter (Z) in Equation (22) can be calculated as follows:

$$\Phi = 1 + \frac{[3(D^*/2)^{7/8}/(1+D^*)]-1]}{1 + 0.25/(n-1)} \tag{32}$$

$$Z = \frac{L}{D_{eq} \cdot Re \cdot Pr} \tag{33}$$

23

where Pr is the Prandtl number of the fluid. All necessary parameters for calculating the Nusselt number are described above. Using the definition of Nusselt number,

$$Nu = \frac{hD_{eq}}{k} \qquad (34)$$

ε_0 in Equation (17) can be calculated.

2.1.4 Correction factor for rotational speed.

It is necessary to consider the effect from the rotational speed of the wheel. Worsøe-Schmidt [20]. developed an equation for the correction factor (φ_r), presented in Equation (17) and is given by

$$\varphi_r = 1 - \frac{0.114[1-e^{(-NTU)}]}{C^{*0.44}C_r^{*1.93}} \qquad (35)$$

where C_r^* is the heat capacity ratio of the rotary regenerative heat exchanger. C_r^* is defined as

$$C_r^* = \frac{C_r}{C_{min}} \qquad (36)$$

where C_{min} is the minimum heat capacity rate of the fluid, which has already been defined as C_c. C_r is the heat capacity rate of the solid part of the wheel. The equation for C_r is following:

$$C_r = m_s c_s N \qquad (37)$$

where m_s, c_s, and N are, respectively, the mass, specific heat, and rotational speed of the wheel.

2.1.5 Fan power consumption

Commercially available fans (Type GR56CZID.GL.CR by Ziehl-Abegg) are implemented in this presented model. Fan power is calculated using the following equation:

$$E_{fan} = \frac{\Delta P_{total} \dot{V}}{\eta_f} \qquad (38)$$

where ΔP_{total} is the total pressure drop, $\dot{V}$ is the volumetric flow rate, and η_f is the overall fan efficiency. The volumetric flow rates can be directly converted from the mass flow rates calculated by the heat exchanger analysis. ΔP_{total} can be expressed as

$$\Delta P_{total} = \Delta P_{wh} + \Delta P_{fi} + \Delta P_{co} + \Delta P_m \qquad (39)$$

where ΔP_{wh}, ΔP_{fi}, ΔP_{co}, and ΔP_m are the pressure drop across the wheel, filters, DX cooling/condenser coils, and the miscellaneous pressure drop, respectively. The miscellaneous drop includes external static pressure, discharge loss, and system effect. The total pressure drop is

the pressure that the fans need to overcome to deliver a desired volumetric flow rate. Fan system curves showing the total pressure drop versus volumetric flow rate are obtained from the data sheet by Air Enterprises [30]. Table 2.2 summarizes the pressure drop values of the hot side at the maximum volumetric flow rate per fan, which is 7240 ft^3/min [3.42 m^3/s].

Table 2.2 Pressure Drop Values by Components Evaluated at the Maximum Volumetric Flow Rate of the Hot Side

Location	[Inch-water]	[Pa]
Thermal Wheel	0.61	152
DX Coil	0.53	132
Filters	1.00	248
Miscellaneous	0.6	149

At the maximum volumetric flow rate, the data sheet estimated the pressure drop across the wheel to be 152 Pa, which is about 50 Pa lower than the pressure drop calculated in Equation (12) for the selected wheel design.

Figure 2.3 shows the fan curves and system curves for the presented wheel and commercial wheel in imperial units. It is important to mention that these fan and system curves were evaluated for 8 identical fans in parallel. The performance of multiple fans in parallel increases the volume flowrate by the number of fans [31]. For example, the system would experience around 3 inch of water [746.5 Pa] of pressure drop at about 58000 ft^3/min [27.4 m^3/s], which is 7240 ft^3/min [3.42 m^3/s] times 8 fans. Multiple fans placed in parallel can result in a performance drop in amount of the airflow due to interference effects, if the fans are not identical, the fans are operating at a different speed [32], and the fans are placed too close together [33]. In this model, these effects have been neglected due to the fact that the fans are identical and always operating at the same speed, and the cooling unit is large enough to have fans installed with a distance.
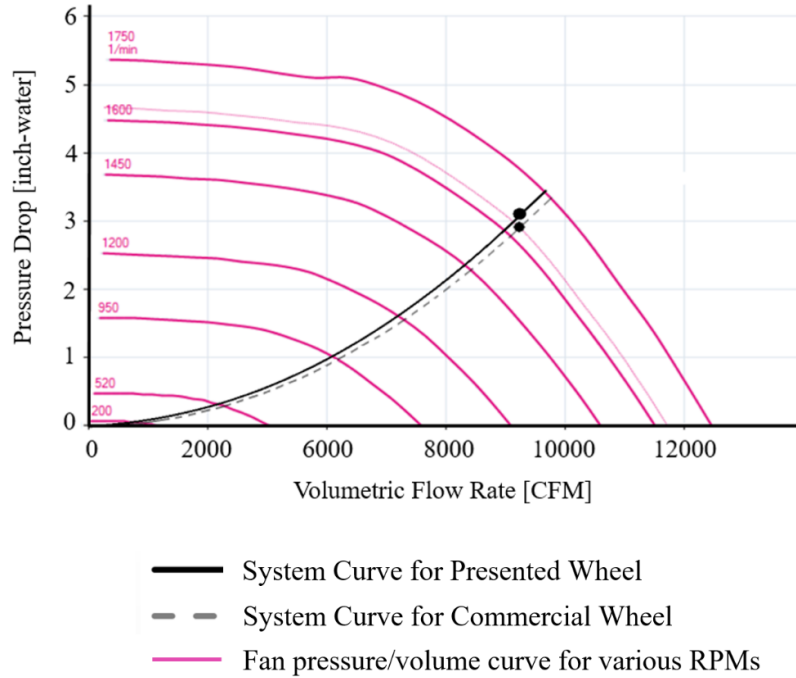
Figure 2.3 Performance/System Curves of the Fans in Hot Side.

As can be seen in Figure 2.3, there are two system curves. The dashed line is the sum of the pressure losses across the commercial wheel and other components, which can be directly obtained from the data sheet. The solid line, for the wheel design selected in this paper, is calculated by the following procedures. The governing equation for pressure loss across any component is defined as [34]

$$\Delta P_I = y \left(\frac{v_I}{1097} \right)^2 \rho_I \tag{40}$$

where ΔP_I is the pressure loss across the component in inch of water, y is the loss coefficient for the component, v_I is the velocity of the fluid in feet per minute, and ρ_I is the density of the fluid in pound per cubic feet. From Equation (40), the pressure loss is a parabolic function of the fluid velocity.

It has been assumed that all the components with pressure drop in the presented model would have the same pressure loss as given from the data sheet, except the pressure loss across the

26

wheel. This is because the design of the wheel used in this paper is different from the commercial wheel. Using Equation (40), it is possible to calculate the loss coefficients for the presented wheel and the commercial wheel at the maximum volumetric flow rate. The difference between the two is used in Equation (40) with different fluid velocities to generate a parabolic curve for the presented wheel.

The overall efficiency of the fan is assumed to be ranging from 0.4 to 0.6. Based on the fan curves and efficiencies, power consumption by the fans can be calculated using Equation (38). The power consumption by the fans placed in the cold side is calculated using the same method presented above.

2.2 Direct Expansion (DX) Cooling System

2.2.1 Background

A DX air conditioning system uses a refrigerant vapor expansion /compression cycle to directly cool the supply air to an occupied space. Warm air is blown over a cooling coil with internal refrigerant flow. For conventional chilled-water systems, the cooled refrigerant first cools the water, which is then used to chill the warm air. A DX cooling system has no middle stage involved for the heat transfer, resulting in a higher cooling efficiency.

2.2.2 DX System without air-side economizer (used in Scenario A)

This cooling component is used in the first scenario where the data center is air cooled. The information regarding this air-cooled data center has previously been introduced in Chapter 1. The reason for not utilizing an air-side economizer is that this system is designed to work with a rotary regenerator, which can be classified as an air-side economizer in a way that they both utilize outside air for cooling. An HVAC system with a single speed DX cooling coil has been modeled in EnergyPlus. The software uses NTU-effectiveness method for simulation of heat exchangers and is used to estimate the power consumption by DX cooling system. Key input parameters used in this model are summarized in Table 2.3

Table 2.3. Input Parameters of DX Coil Used in Scenario A

Rated Cooling Capacity	500 kW
Rated COP	4
Rated Air Flow Rate	32.7 kg/s
Rated Evaporator Fan Power per Volume Flow	1100 W/(m³/s)
Condenser Type	Air-cooled

The rated cooling capacity is the total sensible cooling capacity at the rated condition. The rated COP is the coefficient of performance, cooling power output divided by electrical power input, at the rated conditions. The air flow rate is set to 32.7 kg/s as the air that passes through the wheel is directly blown over the DX coil without any loss. The supply air temperature is fixed at 26.7 °C. This EnergyPlus model takes ambient temperature from weather data and calculates the electrical power usage by the DX system to cool down the air from the ambient temperature to 26.7 °C. A year-long energy simulation produces the relationship between power consumption and ambient temperature.
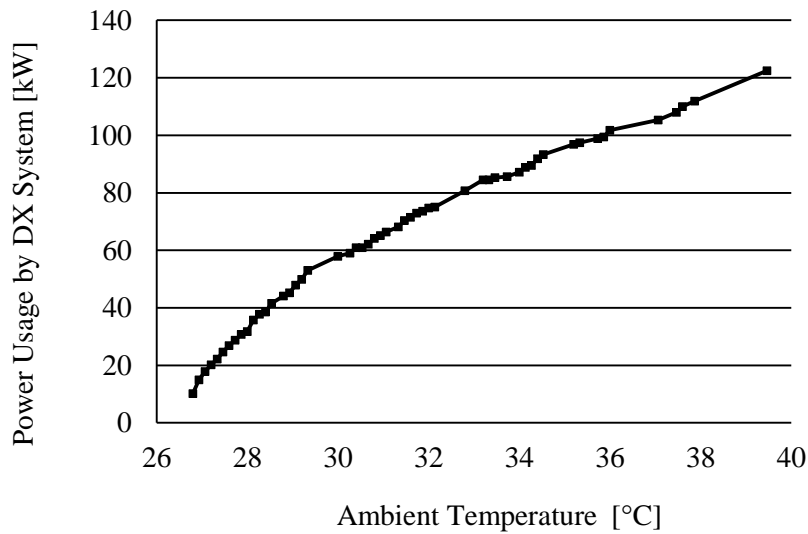
Figure 2.4 Plot showing Ambient Temperature versus Power Usage by DX System.

This figure denotes that the DX system consumes about 30 kW when it takes the ambient air at 28 °C at the mass flow rate defined in Table 1.2 and cools it down to 26.7 °C. The power consumed by the DX system increases as the air temperature increases. This result will be used in Chapter 3 to calculate the overall efficiency of Scenario A.

2.2.3 DX System with air-side economizer (used in Scenario B and C)

This model is similar to the DX model introduced in Section 2.1.3 but has an additional component, air-side economizer. The following figure is a schematic of a DX cooling system with an assisted air-side economizer
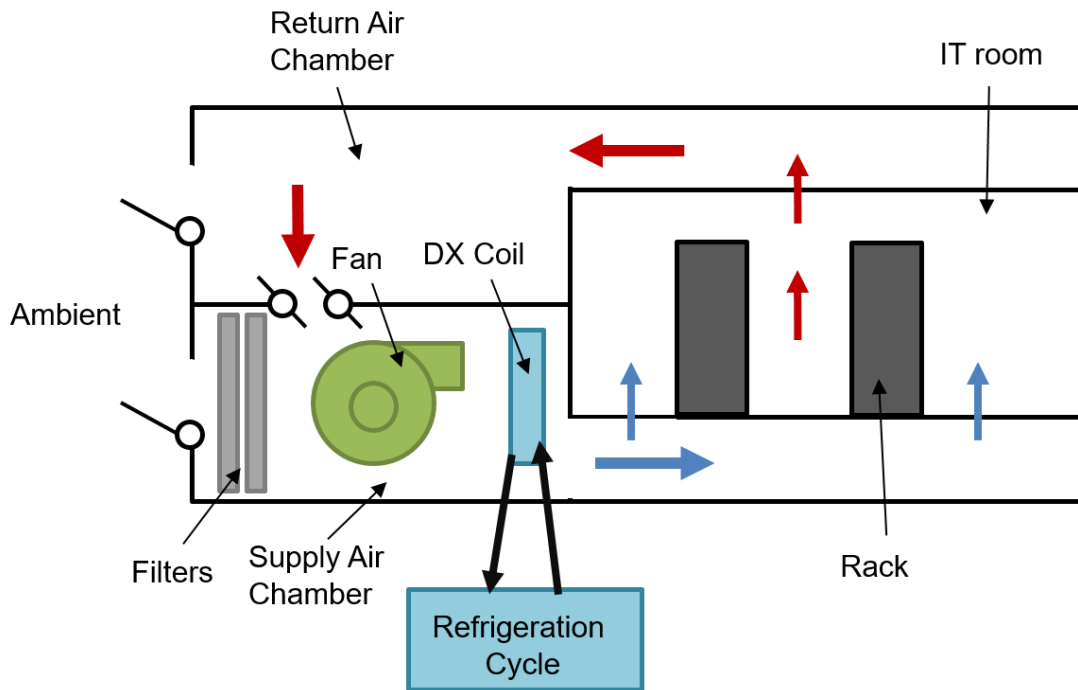
Figure 2.5 Schematic of DX Cooling System with an Assisted Air-side Economizer

When the ambient air is cold enough, the air handler brings it into the supply chamber by a fan. The air is blown over a DX coil and chilled. After cooling the IT equipment, it is returned to the return air chamber and it either re-enters the supply air chamber, or leaves the unit for the ambient. This mechanism depends on the ambient condition. A 465 m^2 (5000 ft^2) heavily insulated data center is simulated in EnergyPlus for a year. Table 2.4, 2.5, and 2.6 list the necessary input parameters. All other input parameters and performance curves used in this EnergyPlus model can be seen in Appendix A.

Table 2.4 Input Parameters of IT Room in Scenario B and C

Cooling Load	191 kW
Set Point Temperature	27 °C, 32 °C, 35°C, or 40 °C
Supply Air Temperature	From 18 °C to 27 °C
Humidity Ratio	Between 0.006 - 0.11

A server consumes about 286 W at the maximum load, while the two CPUs and four DIMMs consume 136 W and 18 W, respectively. From Section 2.3, it is found that 12.5 % of the heat produced by DIMMs is transferred to air, implying that the water cooling load per server is 152 W, and air cooling load per server is 134 W. Therefore, the cooling load for DX system with 17 fully populated racks is 191 kW. Four different set point temperatures have been investigated to determine their effect on the power consumption. The supply air temperatures range from 27°C to 40 °C, which are the recommended and allowable temperature for classes A1 through A4 by 2011 ASHRAE thermal guidelines [35]. Humidity ratio is the ratio between the actual mass of water vapor present in moist air to the mass of the dry air. The range noted in Table 2.4 represents the acceptable humidity ratios for IT equipment [36].

Table 2.5 Input Parameters of Fan

Overall Fan Efficiency	0.4, 0.5, or 0.6
Fan Pressure Rise	750 Pa

The overall fan efficiency is a product of fan efficiency and motor efficiency. It has been assumed that the overall fan efficiency lies between 0.4 and 0.6. Fan pressure rise is the pressure drop that the fan must be able to overcome at the rated volumetric flow rate. We assume a fan pressure rise of 750 Pa as in a similar sized air-cooled data center [30].

Table 2.6 Input Parameters of DX Coil

Rated Cooling Capacity	200 kW
Rated COP	2, 3, or 4
Rated Air Flow Rate	Autosized
Rated Evaporator Fan Power per Volume Flow	1100 W/(m^3/s)
Condenser Type	Air-cooled

A single speed DX coil is used. The rated cooling capacity is the total, full load cooling capacity of the DX coil unit at rated conditions: air entering the cooling coil at 26.7°C dry-bulb/19.4°C wet-bulb, air entering the outdoor condenser coil at 35°C dry-bulb/23.9°C wet-bulb. The rated air flow rate is autosized by EnergyPlus.

2.3 Hybrid Cooled Server

2.3.1 Server Hybrid Cooling - DIMMs

In this study, cold plate liquid cooling for DIMMs in servers is used, enabling DIMMs to reject heat to both liquid and air. Figure 2.6 shows top and side view of the cold plate enclosing 2 DIMMs.
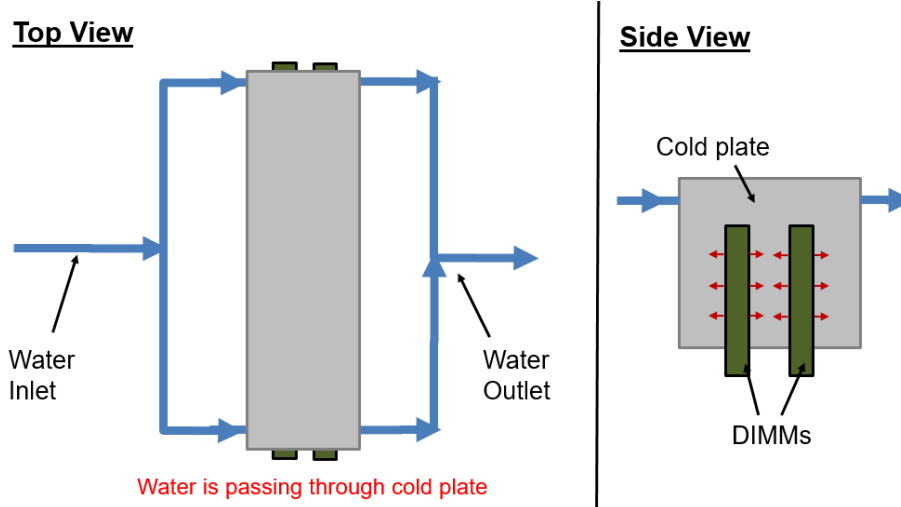
Figure 2.6 Schematics of Cold Plate for DIMMs

As can be seen in Figure 2.6, cold water first enters the server and passes through the DIMM cold plate capturing the heats from DIMMs. Each DIMM is assumed to generate 4.5 W at the maximum load. Since cold air is also blowing over the cold plate, partial heat is transferred to the air. A COMSOL model is used to determine heat removed by the air. In order to calculate the heat transfer coefficient, Reynolds number (Re_L) is needed for the flow over the cold plate:

$$Re_L = \frac{u_a L}{v} \tag{41}$$

where u_a is the average velocity of the cold air, L is the length of the cold plate, v is the kinematic viscosity of air, evaluated at the temperature of the air.

The average convection coefficient for laminar flow is calculated as [37]:

$$\bar{h} = (0.664\, Re_L^{\frac{1}{2}} Pr^{\frac{1}{3}}\, k\,)/\text{L} \tag{42}$$

where $\bar{h}$ is the average convection coefficient, Pr is the Prandtl number, and k is the thermal conductivity of the air. Several different values of convection coefficient are used in the COMSOL model. Figure 2.7 presents the temperature profile of the cold plate when each DIMM produces 4.5 W. The supply air temperature, the inlet water temperature, and the water flow rate are set to 27 °C, 25 °C, and 0.1 L/min, respectively.
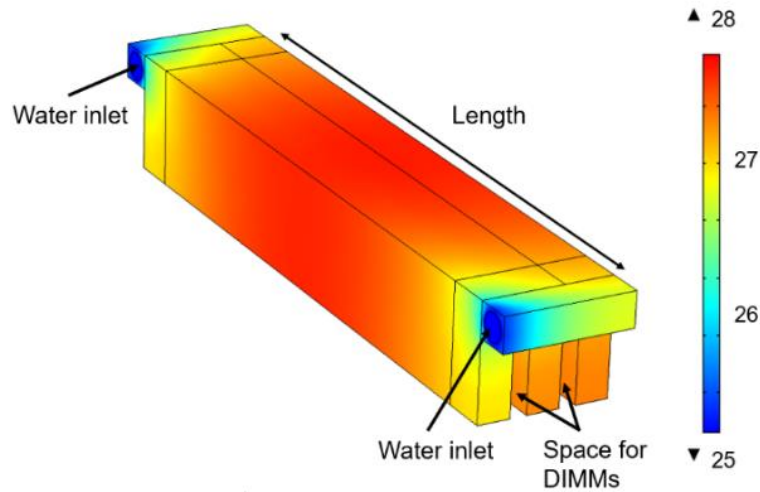
Figure 2.7 Temperature Profile of Cold Plate for 2 DIMMs

According to Figure 2.7, the temperature of the hottest spot is 28 °C, when two DIMMs are operating at the maximum load. This result shows that the difference between the warmest point on DIMMs and the inlet temperature of coolant is lower than 3 °C with 9 W of power. It also ensures that the DIMMs are maintained within their operating temperature. Figure 2.8 presents the rate of heat transferred to water and air with varying air velocity.
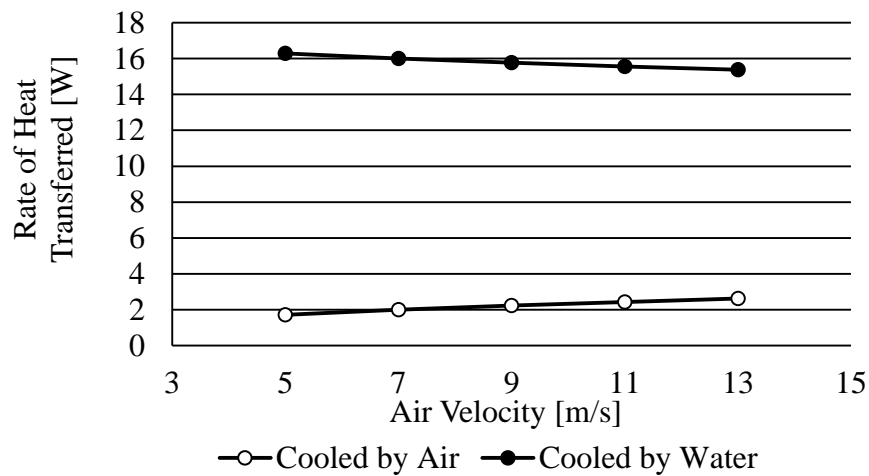
Figure 2.8 Rate of Heat Transferred to Air and Water

Total power consumption by four DIMMs is 18 W. It can be observed that increasing air velocity aids in convection but not significantly. When air velocity is 9 m/s, about 12.5 % of the total heat is transferred to air. This means water can dissipate 87.5 % of the total. We will continue to use 9 m/s as air velocity in the rest of the simulations. The temperature of the water leaving the cold plate can be calculated as follows:

$$T_{hs,o} = \frac{Q_{di}}{C_p \rho \dot{V}_s} + T_{hs,i} \tag{43}$$

where $T_{hs,i}$ is the inlet temperature of the water entering cold plate, $T_{HS,o}$ is the outlet water temperature, C_p is the specific heat of water, ρ is the density of water, and $\dot{V}_s$ is the flow rate of water. Q_{di} is the amount of heat transferred from four DIMMs to water, which can be obtained from Figure 2.8.

2.3.2 Server Hybrid Cooling – CPUs

A commercially available cold plate, CP20G01 with aluminum flat tube from Lytron, is selected to be used for direct CPU cooling. Figure 2.9 shows a side view of the cold plate placed on CPUs with a copper block that connects CPU and cold plate.
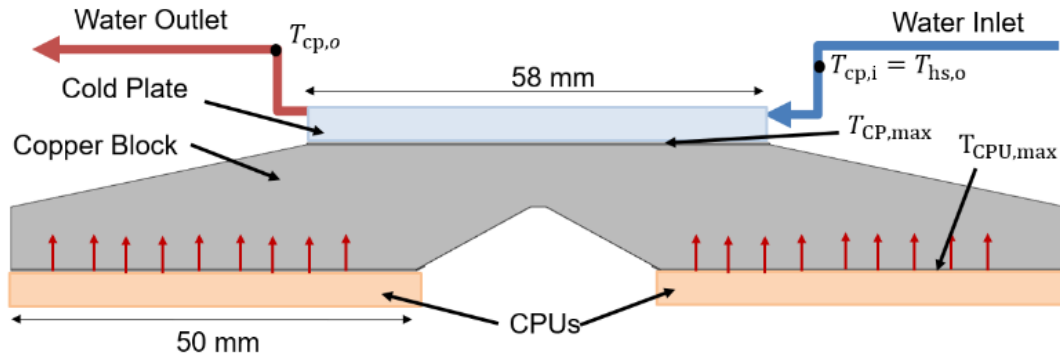
Figure 2.9 Schematic of CPU Cooling With Cold Plate

For the copper block, the exposed surface is thermally insulated. As such, the cold plate captures 100 % of the heat produced by two CPUs. To evaluate the cooling performance, the performance

data showing overall thermal resistance with respect to the liquid flow rate is used for simulations. Figure 2.10 shows the thermal resistance of the cold plate, when water is used as coolant.
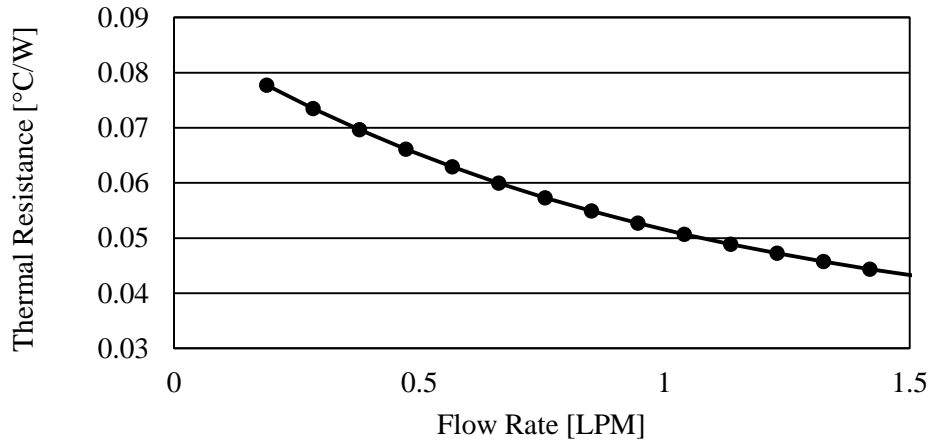
Figure 2.10 Thermal Resistance of the Cold Plate with Varying Water Flow Rate [38]

As shown in Figure 2.10, the thermal resistance increases as the flow rate decreases. The thermal resistance is defined as

$$\theta_{cp} = (T_{cp,max} - T_{cp,o})/Q_{cpu} \tag{44}$$

where θ_{cp} is the thermal resistance of the cold plate, $T_{cp,max}$ is the maximum temperature of the surface of the cold plate, and $T_{cp,o}$ is the outlet temperature of water, and Q_{cpu} is the heat being transferred from CPUs. As the maximum cold plate temperature $T_{cp,max}$ is different from the actual CPU temperature, this cooling block is modeled in COMSOL. With a fixed value for water flow rate, $T_{cp,max}$ can be calculated using Equation (43) and Equation (44). The following figure shows the temperature profiles when $T_{cp,max}$ is 65 °C and each CPU operates at the maximum load consuming 68 W [39].

35
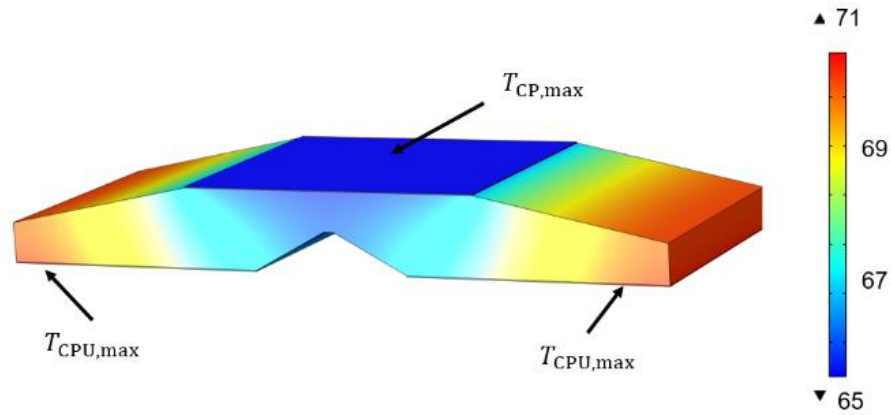
Figure 2.11 Temperature Profile of Cooling Block

In this CFD model, Dow Corning® TC-5022, thermal interface material (TIM), is applied between the copper block and the cold plate, as well as the CPUs. The thermal properties of the TIM have been obtained from the manufacturer [40]. The COMSOL result shows that the maximum CPU temperature is about 6.1 °C higher than $T_{\mathrm{cp,max}}$.

$$T_{\mathrm{cpu}} = T_{\mathrm{cp,max}} + 6.1 \tag{45}$$

where T_{cpu} is the maximum CPU temperature when operating at the maximum power. Using Figure 2.10 and Equation (43) through Equation (45), the relationship between T_{cpu} and the flow rate with different water inlet temperatures is calculated and plotted in Figure 2.12.
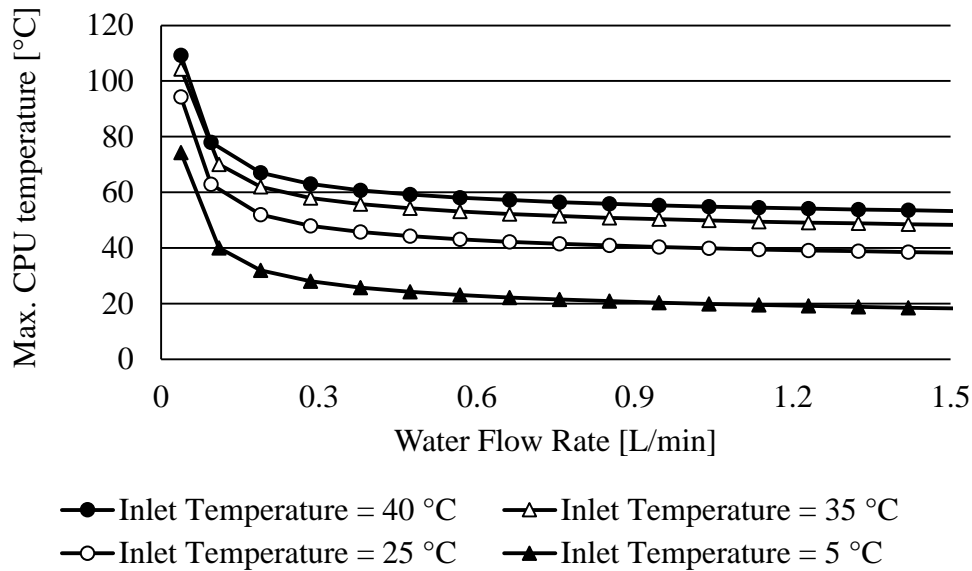
Figure 2.12 Maximum CPU Temperature versus Water Flow Rate with Different Inlet Temperature

As the water flow rate decreases, the temperature of the water leaving the cold plate increases, which results in a higher maximum CPU temperature. According to the specification, AMD Opteron 875 should be maintained at below 71°C, which implies that the system must have a certain minimum flow rate which depends on the inlet temperature of water.

2.4 Rear Door Heat Exchanger (Air-to-liquid Heat Exchanger)

The heat exchangers placed in the back of the racks, also known as rear door heat exchangers have been used in data centers. This air cooling approach is used in Scenario C. Figure 2.13 displays a schematic of rack-level cooling system with air-to-liquid heat exchangers placed.
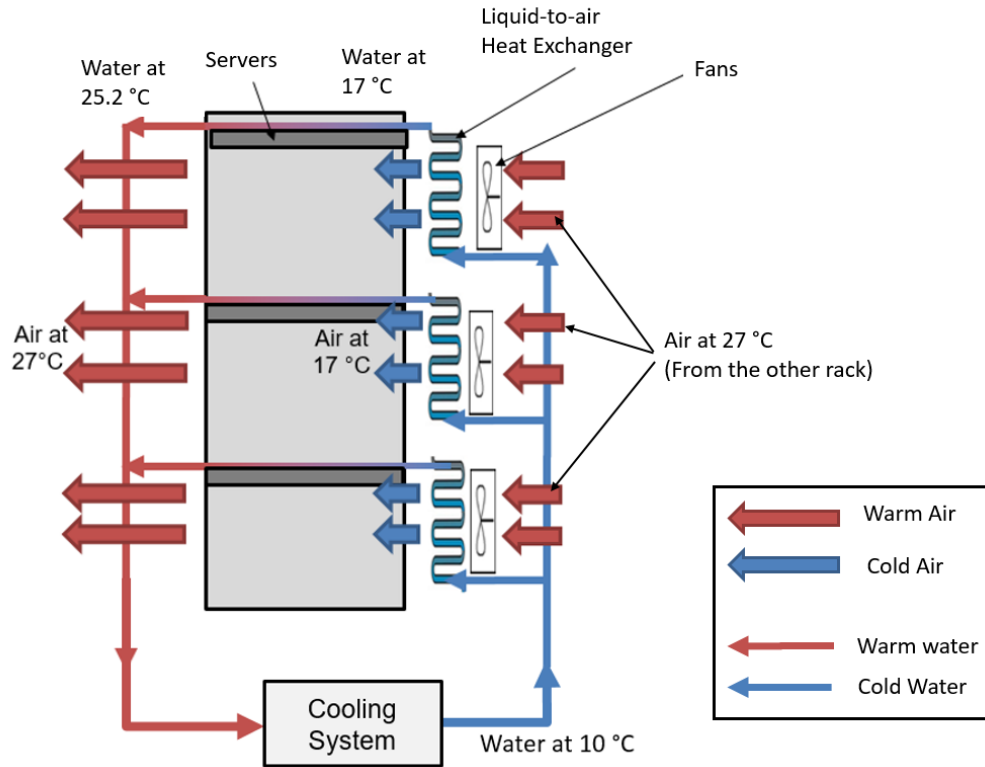
Figure 2.13 Schematic of Cooling with Rear Door Heat Exchanger

The warm air from one rack is drawn to the air-to-liquid heat exchangers by the sets of fans. Chilled air then enters the other rack, cooling low power components. The heat captured from the warm air is transferred to the water through the heat exchanger. A commercial air-to-liquid heat exchanger, M14-240 tube-fin heat exchanger from Lytron, is selected and the performance data is used for simulations. The manufacturer evaluates the heat exchanger performance with the following reference conditions: air flow of 18.4 m³/min, a water flow of 7.5 L/min, and 20 °C of initial temperature difference (ITD). The maximum performance of the heat exchanger is given by 234.9 W/°C [41]. The air-to-liquid heat exchanger performance is defined as

$$\theta_{atl} = \frac{Q}{T_{a,i} - T_{w,i}} \tag{46}$$

where $T_{a,i}$ is the temperature of the air entering the heat exchanger and $T_{w,i}$ is the temperature of the water entering the heat exchanger. Calculated θ_{atl} should be lower than the maximum

performance. At the maximum load, air cooling load per rack is about 11.3 kW. Since there are three heat exchangers per rack, about 3.7 kW is the cooling load for one heat exchanger. Following ASHRAE's recommended temperature limit, $T_{a,i}$ is set to 27 °C. If $T_{w,i}$ is 10 °C, required performance is found to be 223.5 W/°C, which is lower than the maximum heat exchanger performance at the same conditions for air and water. Lower values of $T_{w,i}$ which may be used will decrease the required heat exchanger performance, which increases the feasibility. To create the reference air flow rate, 18.4 m^3/min, two tubeaxial fans from Lytron with a diameter of 254 mm are used. The two fans coupled with one heat exchanger consume 66 W [42] which is used in power consumption calculation.

2.5 Cold Water Cooling with Air/water Cooled Chillers

2.5.1 Air-cooled chiller

The water used in servers can be cooled using an air-cooled chiller. A detailed HVAC system with an air-cooled chiller has been modeled in EnergyPlus. An advantage of modeling a chiller in EnergyPlus is that performance information for more than 160 commercial chillers, including the default DOE-2.1E reciprocating and centrifugal chillers, are provided in the software. Air-cooled chiller is equipped with a condenser cooled by the ambient air. An electric air-cooled chiller from Daikin McQuay (model no. AGZ075D) is selected for simulations. This EneryPlus model takes the weather data for a selected location and calculates the electric power usage by the chiller to cool down an assigned cooling load. The goal is to determine the relationship between the electricity usage by this chiller and the ambient temperature. It is then possible to estimate annual PUE using the relationship and weather data. The calculated energy usage includes the energy consumed by pump, which is determined by pump pressure drop at the reference flow rate. How total pump pressure drop is estimated is explained later in Section 2.9.

2.5.2 Water-cooled chiller

As with the air-cooled chiller, a detailed HVAC system with a water-cooled chiller has been modeled in EnergyPlus. An electric centrifugal water-cooled chiller from Daikin McQuay (model no. PEH 703) is used. The difference between air-cooled chiller and water-cooled chiller is that water-cooled chillers have water-cooled condenser connected to a cooling tower. It is well-known that water-cooled chiller is more energy efficient and environmentally friendly than air-

cooled chiller [43]. However, a water-cooled chiller may not be ideal for a small facility due to a larger space requirement with additional condenser pump installation. Also, it should be considered that cooling towers lose water as it operates. Through this EnergyPlus model, how the ambient temperature influences the overall chiller performance is determined. All other parameters are the same as the air-cooled chiller.

2.6 Warm Water Cooling with Ground Water and Dry Cooler

This water cooling approach utilizes a commercial liquid-to-liquid heat exchanger using groundwater at a fairly constant temperature throughout the year. Kellner and Hubbart have done time-dependent measurements of shallow groundwater temperature in Missouri from 2010 to 2014, and the temperature fluctuated within 4.5 °C [44]. The average temperature of shallow ground water in the U.S. ranges from 2.8 °C to 25 °C [45]. These experimental studies suggests that using ground water as coolant is promising for most of the U.S. cities. Figure 2.14 shows a schematic of warm water cooling by groundwater and dry cooler units, which are used as a supplementary cooling approach.
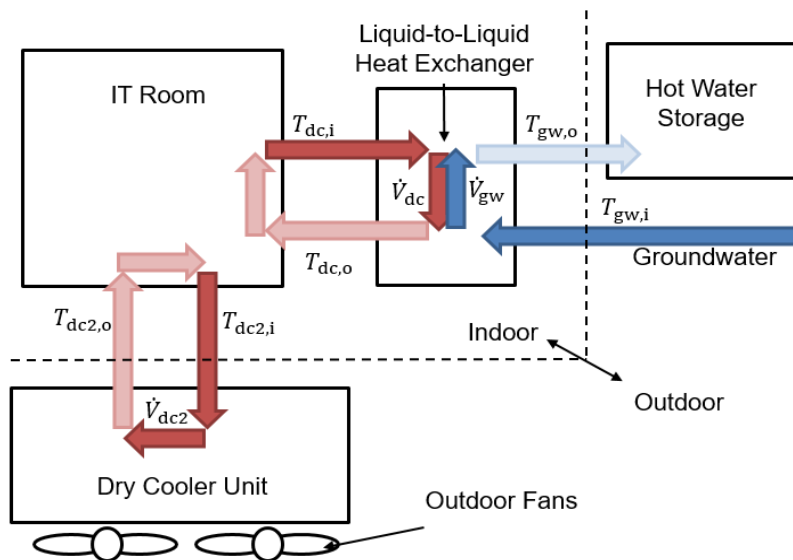
Figure 2.14 Schematic of Warm Water Cooling With Groundwater and Dry Cooler Unit

Detailed explanation can be found in Figure 1.5 on Page 9, where it describes heat, air, and water flows for this cooling approach. A commercial liquid-to-liquid heat exchanger, LCS20 from Lytron, is used in this cooling approach. The performance of the heat exchanger is defined by Q, $T_{dc,i}$, $T_{gw,i}$, $\dot{V}_{dc}$, and $\dot{V}_{gw}$. $T_{dc,o}$ is the temperature of the water leaving the heat exchanger to the data center, and $T_{dc,i}$ is the temperature of the water coming into the heat exchanger. $T_{gw,i}$ is the temperature of groundwater, and $T_{gw,o}$ is the temperature of the heated groundwater. $\dot{V}_{dc}$ is the water flow rate of the data center side, $\dot{V}_{gw}$ is the flow rate of groundwater. The performance of a liquid-to-liquid heat exchanger is defined as

$$\theta_{ltl} = \frac{Q}{T_{dc,i}-T_{gw,i}} \tag{47}$$

where θ_{ltl} is the performance of liquid-to-liquid heat exchanger in terms of thermal resistance. Q can be calculated by the equation below:

$$Q = n_s Q_{s,w} \tag{48}$$

where n_s is the number of server cooled by one heat exchanger and $Q_{s,w}$ is the water cooling load per one server, which is 152 W. The water flow rate of data center side is calculated as follows:

$$\dot{V}_{dc} = n_s \dot{V}_s \tag{49}$$

where $\dot{V}_s$ is the water flow rate for one server. Assuming the data center is located in a warm climate where the average groundwater temperature is around 23 °C, it is necessary to know acceptable range of $T_{dc,o}$ and $\dot{V}_s$ that make sure CPUs are maintained within the operating condition. Figure 2.10 shows that the maximum CPU temperature is 70 °C when $T_{dc,o}$ and $\dot{V}_s$ are 35 °C and 0.11 L/min, respectively. With this flow condition, $T_{dc,i}$ is calculated using the equation below:

$$T_{dc,i} = \frac{Q_{s,w}}{C_p \rho \dot{V}_s} + T_{dc,o} \tag{50}$$

$T_{dc,i}$ is found to be 54.8 °C. It is then possible to calculate required performance using Equation (47), (48), and (49). The following figure presents the given performance of LSC20 and the required performance for data center with varying the water flow rate on the data center side ($\dot{V}_{dc}$)
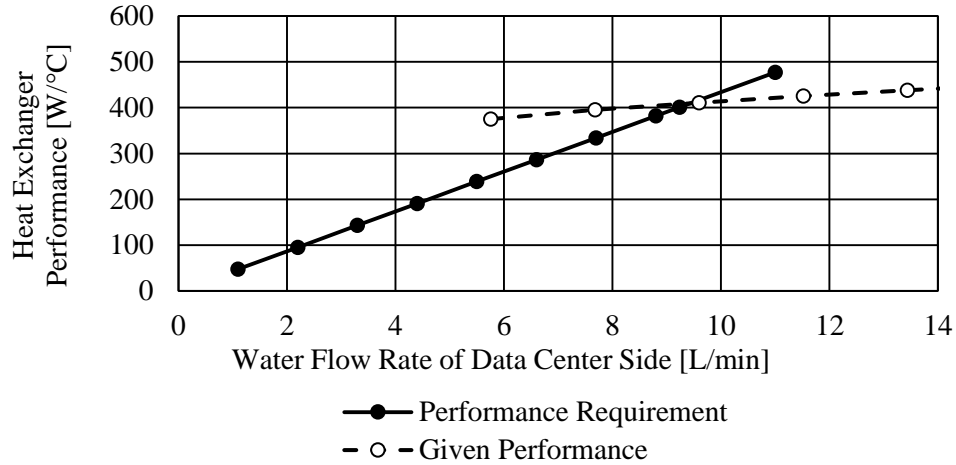
Figure 2.15 Performance of LCS20 [46] and Desired Performance with Varying Water Flow Rate in Data Center Side

These two performance curves are evaluated when $\dot{V}_{gw}$ is 7.7 L/min. The performance requirement linearly increases with $\dot{V}_{dc}$ which is linearly proportional to the number of servers being cooled. As long as the requirement is below the given performance curve at a specific flow rate, the heat exchanger is capable of handling the assigned cooling load. The point where the two curves intersect is the maximum operating point with the flow conditions. From Figure 2.15, it is observed that a LSC 20 can take up to 9.24 L/min, which can be distributed to 84 blade servers, cooling 12.7 kW.

2.7 Domestic Heating (Waste Heat Re-use)

In Scenario A, the exhaust air from the cold side (refer to Figure 1.7), is dumped in the ambient. If the data center is able to deliver the warm exhaust air to neighboring homes during winter, considerable energy can be saved. The computational model for the rotary regenerative heat exchanger, introduced in Section 2.1, calculates the temperature and mass flow rate of exhaust air with regard to ambient temperature. The results are plotted in Figure 2.16.
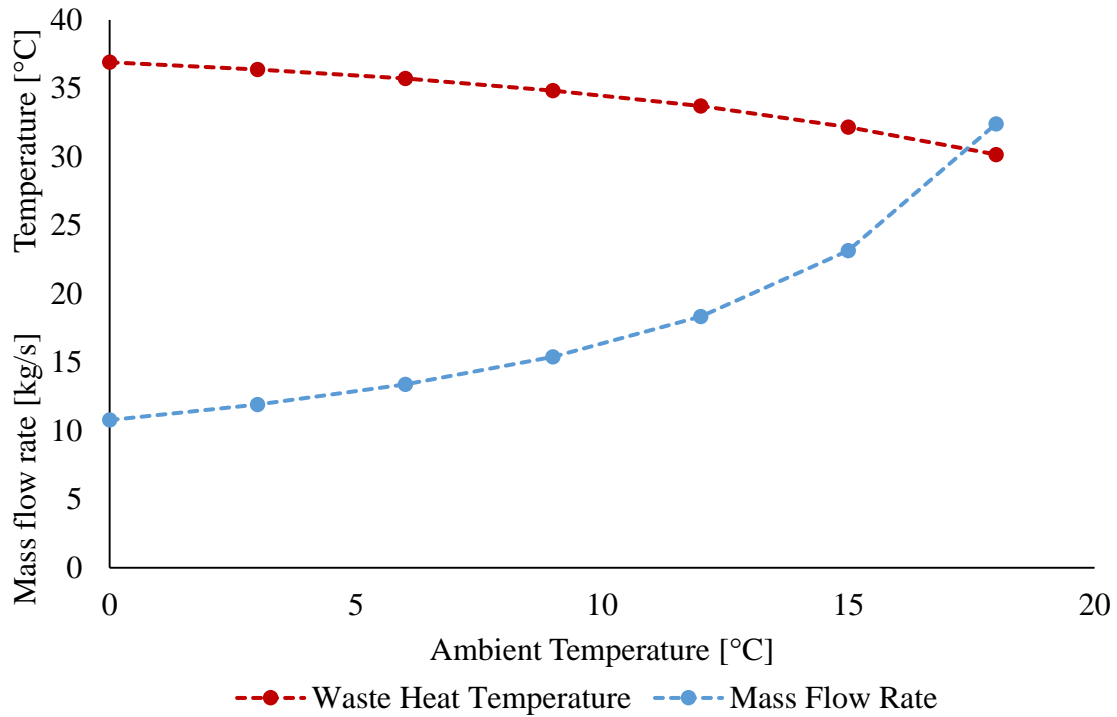
Figure 2.16 Properties of Waste Heat as Air with Respect to Ambient Temperature

It can be observed that when the ambient temperature is 5 °C, air at 35.6 °C will be exhausted from the data center to the ambient at a mass flow rate of 13.39 kg/s. With taking the heat losses that might occur in transit into account, it has been assumed that the temperature of the exhaust air will be as least 32 °C once it reaches the destination. A typical 163 m^2 (1750 ft^2) house with two stories, which can be seen in Figure 2.17, has been modeled in DesignBuilder to calculate how much air at 32 °C must be used for heating up the entire house during the winter period. Table 2.7 summarizes important input parameters used for simulation of this model house.
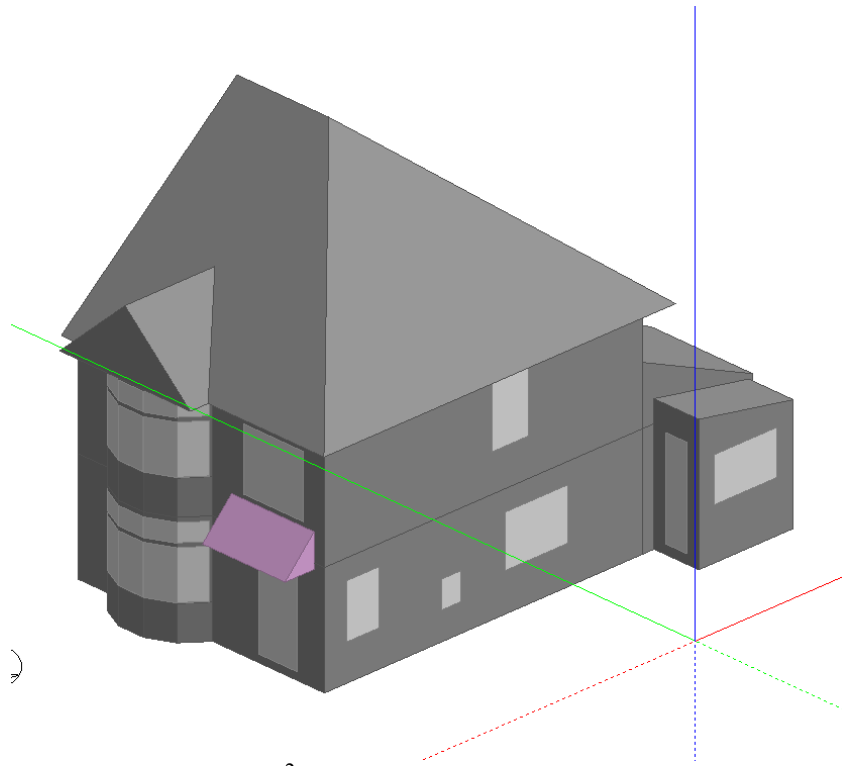
Figure 2.17 A 163 m^2 Typical House Modeled in DesignBuilder

Table 2.7 EnergyPlus Parameters for the House Model

Location	Atlanta, GA
HVAC Type	VAV reheat
Boiler Template	Gas-fired condensing boiler
Nominal Thermal Efficiency	0.89
Nominal Capacity	Auto-sized
Design Water Flow Rate	Auto-sized
Boiler Fluid Type	Water
Heating Supply Air Temperature	32 °C
Heating Setpoint Temperature	20 °C

More input parameters used in this model are listed in Appendix A. The heating supply air temperature is set to 32 °C, and the mass flow rate of supply air is auto-calculated by EnergyPlus. Colder outside temperatures will result in a higher mass flow rate required for heating, as the supply air temperature is fixed. The model is able to estimate how many of these houses can be completely heated by the waste heat.

Next, it is possible to estimate the heating cost for the model house located in Atlanta, GA, using this model. EnergyPlus enables users to review energy usage by components, such as boiler, fan, and pump. Energy consumed by the boiler throughout the winter can be saved by utilizing the waste heat from the data center.

2.8 Thermoelectric Generators (Waste Heat Re-use)

A Thermoelectric generator (TEG) is a solid-state device that transforms thermal energy into electricity using the Seeback effect. TEG has several advantages over conventional electric power generation devices since it is environmentally friendly and has no moving parts, which increases its reliability. TEGs have applications in aerospace and military [47], battery charging [48], and utilizing radioisotopes [49, 50]. More recently, there is a growing interest in using TEG for waste heat recovery from various heat sources, such as combustion in automobiles [51], heat exchangers [52], geothermal energy, and power plants [47]. Since it has been known that TEG efficiency generally increases with higher temperature differences, as well as, higher operating temperatures, there are fewer studies on investigating low-grade waste heat recovery through TEGs. Scenario B will consider implementing TEG modules in between hot and cold water channels connected to air-cooled chiller. Figure 2.18 shows a conceptual design of a TEG integrated in between two water flow channels.
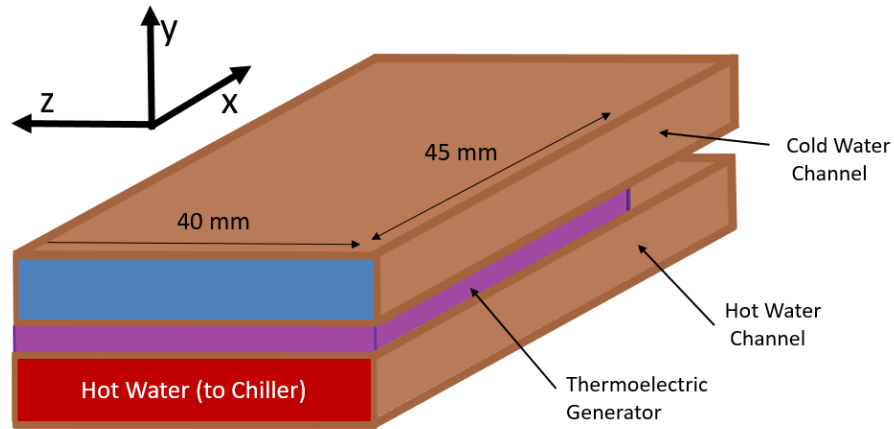
Figure 2.18 Conceptual Design of a TEG placed in between Hot and Cold Water Channel.

The cold water is supplied to servers in data center, and the hot water is returned back to air-cooled chiller. The figures shows one TEG in place, but additional TEGs can be added for more power generation. The following figure shows a 2-Dimensional schematic of the TEG module and directions of water channels.
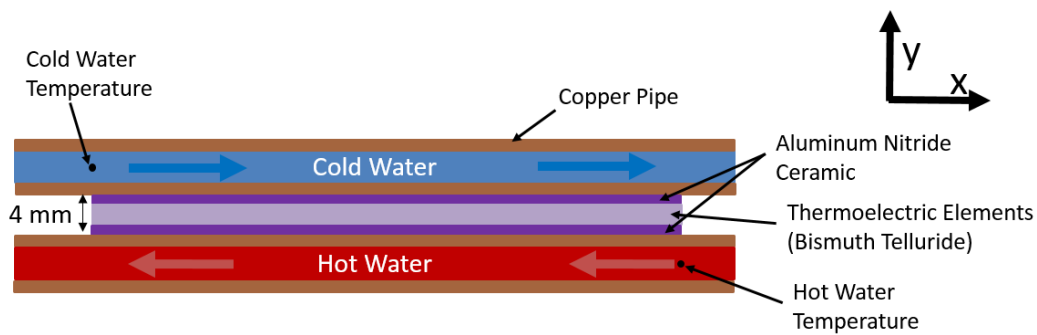
Figure 2.19 Domains of TEG module in 2-D and Water Directions

Based on the dimensions defined previously, a CFD model has been created in COMSOL to produce a temperature profile, which is needed to evaluate TEG performance. The model assumptions are following: (1) the heat transfer along z-axis is negligible, (2) water flow is thermally and hydrodynamically fully developed, and (3) top and bottom of channels are insulated.

There are two domains that are now shown in Figure 2.19 but included in COMSOL simulations as thin thermally resistive layers: copper conductive layer between the ceramic and the thermoelectric element and TIM TC-5022 Dow Corning. The boundary conditions for the model are presented in Table 2.8.

Table 2.8 Boundary Conditions of the TEG model

Mean Velocity [m/s]	Water Flow Rate [kg/s]	Cold Water Inlet Temperature [°C]	Hot Water Inlet Temperature [°C]
0.0583	0.0233	5	50

The mean velocity of water has been chosen by minimizing the mass flow rate of water, while the server components are maintained within their operating conditions, which can be confirmed by using Figure 2.12. This water flow rate is enough for cooling 28 blade servers, which consume about 4256 W. A representative configuration for a TEG and its energy balance are shown in Figure 2.20.
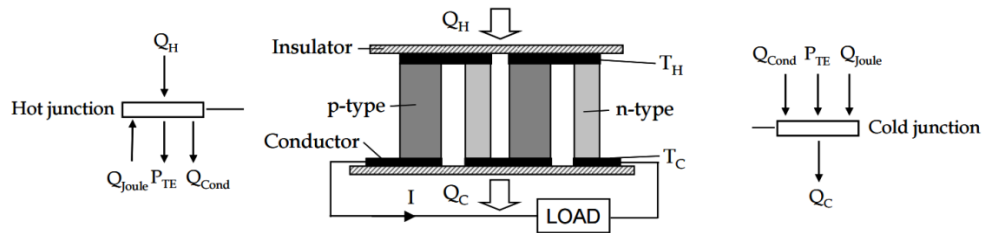
Figure 2.20 Two Series-Connected TEG Unit [53].

The basic energy balance equation is shown in Equation 51:

$$Q_H - Q_C = P_{TEG} \tag{51}$$

where Q_H is the heat input from hot water to TEG, Q_C is the heat transferred to cold water, and P_{TEG} is the electrical power generated by TEG. The power generated by TEG can be expressed as

$$P_{TEG} = V_{TEG}I \tag{52}$$

$$P_{TEG} = [S_{TEG}(\varDelta T_{TEG}) - IR_{TEG}]\,I \tag{53}$$

where S_{TEG} and R_{TEG} are calculated using the material properties of TEG, which in this case, bismuth telluride, and using Equation (54) and (55),

$$S_{TEG} = 2Na_{TEG} \tag{54}$$

$$R_{TEG} = 2N\rho_{TEG}/G \tag{55}$$

where N is the number of N-P couples in the TEG, a_{TEG} is the Seeback Coefficient, ρ_{TEG} is the resistivity of bismuth telluride, and G is the geometry factor, which is area of thermoelectric elements (N-P couples) divided by the length of the elements. A commercially available thermoelectric generator, TG12-6 from Marlow Industries, has been used for this model, and its properties are presented in Table 2.9.

Table 2.9 Properties of Marlow TG12-6 [54]

N	ZT – Figure of Merit at 27.1 °C	Geometry Factor [mm]
128	0.73	1.184

The Seeback coefficient a_{TEG} can be calculated by the equation below:

$$a_{TEG} = \left(\frac{ZT\rho_{TEG}k_{TEG}}{T_{eval}}\right)^{1/2} \tag{56}$$

a_{TEG} for this TEG is found to be 192 uV/K when built-in material properties in COMSOL is used. Using those equations above, it is possible to obtain the optimum power output by performing parametric simulations varying the current. COMSOL simulations generated temperature profiles of the module with the boundary conditions in Table 2.8. The average outlet temperatures of cold and hot water channels are plotted in Figure 2.21.
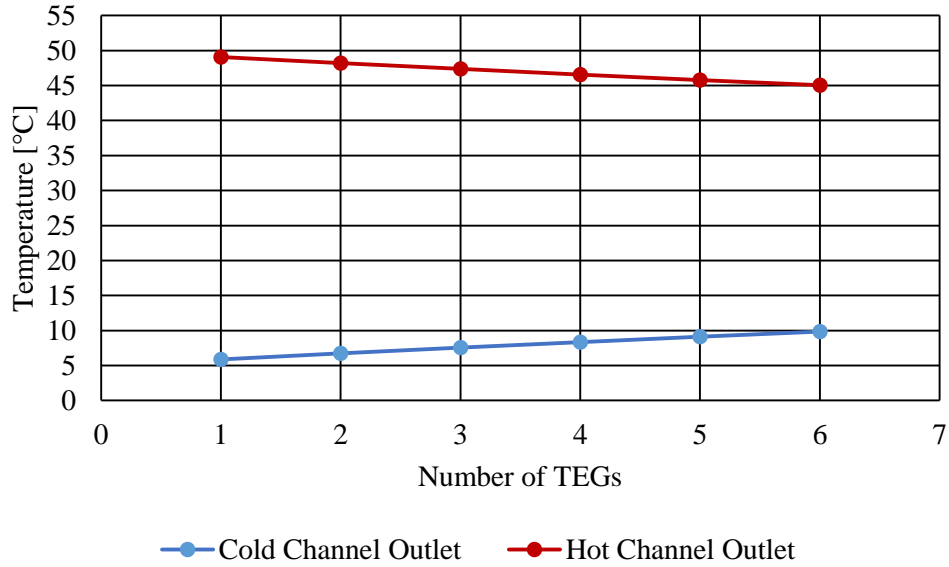
Figure 2.21 Average Outlet Water Temperature of Cold and Hot Channels

Figure 2.21 indicates that when the model has one TEG between hot and cold channels, the water outlet temperature of cold channel is about 5.9 °C. This is a 0.9 °C increase from the inlet temperature, 5.0 °C. As TEGs do conduct heat, more TEGs implemented will increase the water outlet temperature in cold channel and decrease the one in hot channel. This suggests that this technique will become even less efficient as the number of TEGs increases. The power harvested and efficiencies for this TEG model will be discussed in Chapter 3.

2.9 Pump Power Calculations

The pump power consumption can be calculated by the following equation:

$$P_{pu} = \frac{\Delta p_{total} \dot{V}}{\eta_{pu}} \tag{57}$$

where P_{pu} is the power consumed by pump, Δp is the total pressure drop, $\dot{V}$ is the flow rate, η_{pump} is the overall pump efficiency. The overall pump efficiency, combining impeller and motor efficiency, is assumed to be 0.65 as suggested by ASHRAE [55]. The total pressure drop is the sum of the pressure drops across each cooling components and in pipe fittings. In this paper, the pressure drops across the cold plate, liquid-to-liquid heat exchanger, and liquid-to-air heat

exchanger are obtained from the manufacturer's performance information. The pressure drop information for the components is summarized in Table 2.10

Table 2.10 Pressure Drop Information at Maximum and Minimum Flow Rate Used in This Study [38, 41, and 42]

	Cold Plate (CP20)	Air-to-Liquid Heat Exchanger (M14-240)	Liquid-to-Liquid Heat exchanger (LCS20)
Pressure Drop at The Minimum Flow Rate Used	325 Pa at 0.05 L/min	27.5 kPa at 7.5 L/min	6.9 kPa at 9.24 L/min
Pressure Drop at The Maximum Flow Rate Used	1380 Pa at 0.2 L/min		

The pressure drop along piping fittings can be assumed using Darcy-Weisbach equation [37]:

$$\Delta p_{\text{pf}} = f\left(\frac{L_{\text{pi}}}{D_{\text{pi}}}\right)\left(\frac{\rho u_w{}^2}{2}\right) \tag{58}$$

where Δp_{pf} is the pressure drop due to friction, f is the Darcy friction coefficient, and L_{p} is the length of the pipe, D_{p} is the hydraulic diameter of the pipe, and v is the velocity of the flow. Darcy friction coefficient can be calculated using Colebrook correlation [37]:

$$\frac{1}{f^{0.5}} = -2\log\left(\frac{2.51}{Re_D f^{0.5}} + \frac{\alpha}{3.72 D_p}\right) \tag{59}$$

where α is the absolute roughness, which is 0.0015 mm assuming the pipe is made of copper [56]. Figure 2.22 presents the calculated pressure drops along with flow velocity and pipe length.
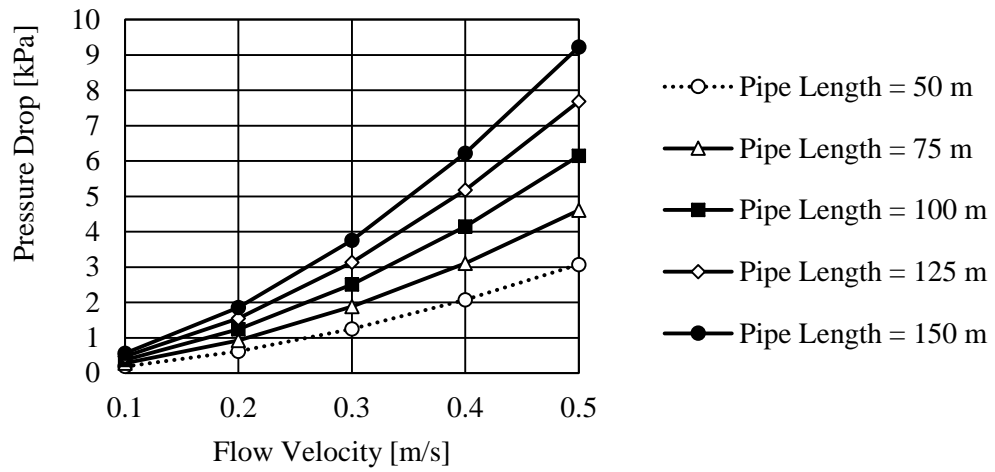
Figure 2.22. Pressure Drop in Pipe Fittings with a Pipe Diameter of 50 mm

In the presented study, the pressure drop in pipe fittings is assumed to be 30 kPa in order to account for more complex fittings and longer length of pipe arrangements that may be used.

CHAPTER 3

RESULTS AND DISCUSSIONS

3.1 Scenario A

3.1.1 Combined Model (Heat Exchanger & DX System)

The presented model in Section 2.1 calculates cold side mass flow rate needed for heat removal under different environmental conditions. The rotary regenerative heat exchanger is modeled in MATLAB, based on the equations presented in the previous chapter. Using the fact that the cold side mass flow rate is always lower or equal to the hot side mass flow rate, solution is obtained by an iterative method. The iteration starts with an initial guess of cold side mass flow rate, which increases by 0.0005 kg/s following each iteration, until the overall effectiveness calculated by Equation (17) agrees with the one calculated by Equation (13). When the two effectiveness values at a mass flow rate have a difference less than 0.000001, the mass flow rate is computed. The MATLAB codes used for this model can be seen in Appendix C. Figure 3.1 shows the mass flow rates of the cold side with varying rotational speed of the wheel and ambient temperature.
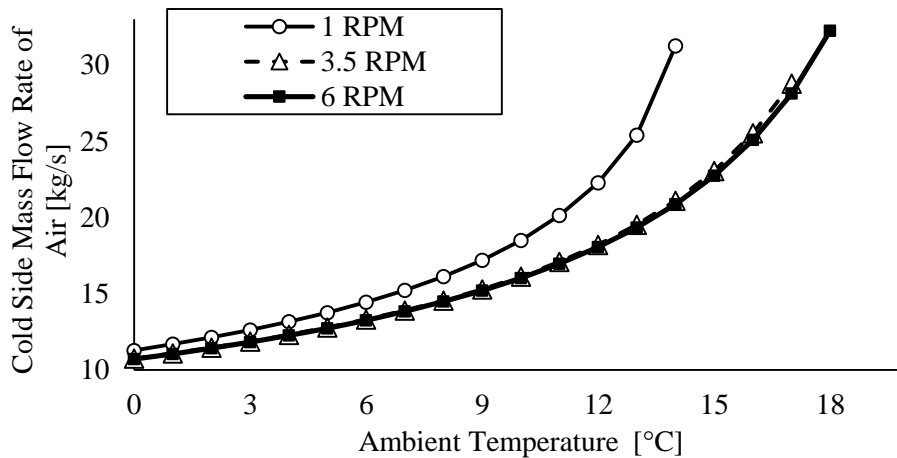
Figure 3.1 Required Mass Flow rate of the Cold Side versus Ambient Temperature with Different Rotational Speed of the Wheel.

In general, for all RPM cases, it can be observed that the required mass flow rate increases as the ambient temperature increases. Also, for higher rotational speeds, lower mass flow rates are required. As can be seen in Figure 3.1, at 1 RPM, the cold side mass flow rate exceeds 32.7 kg/s when the ambient temperature reaches 13 °C, which means the regenerative system is not capable of cooling the assigned load, 400 kW at any temperature greater than 13 °C. At 6 RPM, the regenerative system can handle the cooling load by itself when the ambient temperature is below 18 °C. Another observation is that there is not much of difference between the result for 3.5 RPM and 6 RPM. This suggests that it is better to rotate the wheel at a lower speed when the ambient temperature is relatively cold.

The temperature of the return air entering the thermal wheel of hot side is always set to 39 °C. Although the desired temperature of the cooled air that leaves the thermal wheel is 27 °C, the temperature can actually be higher than 27 °C when ambient temperature exceeds 18 °C. Figure 3.2 shows the relationship.
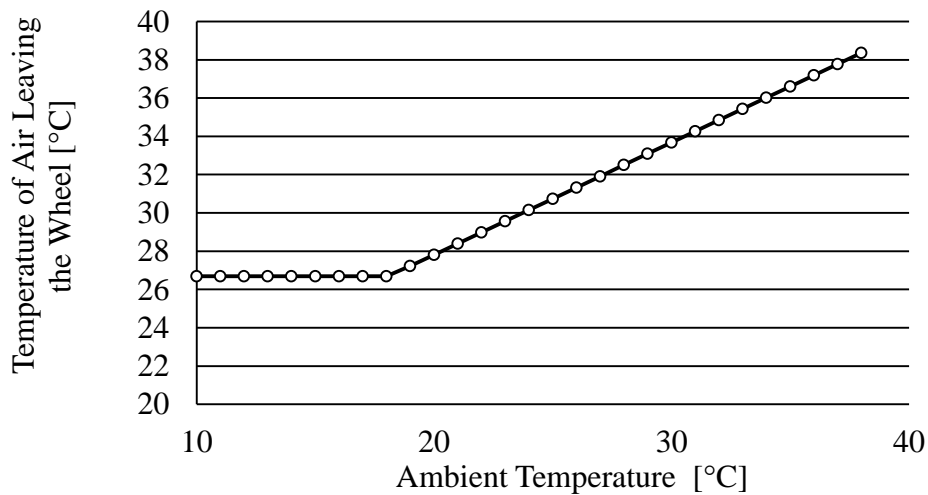
Figure 3.2 Temperature of the Cooled Air Leaving the Thermal Wheel with Respect to Ambient Temperature.

It can be seen that the temperature of the cooled air by the wheel linearly increases as the ambient temperature increases beyond 18 °C. For this ambient temperature region, the overall effectiveness

(ε) in Equation (17) remains constant. According to Equation (14), however, the maximum possible heat transfer rate (Q_{max}) linearly decreases as the ambient temperature ($T_{c,i}$) increases. This means that the cooling load (Q) must be reduced by the same amount as Q_{max}, which explains the linear relationship. A linear equation can be obtained from Figure 3.2 and used to connect the heat exchanger model and the EnergyPlus results. Figure 3.3 explains how the different models are connected to estimate power usage by the DX system.
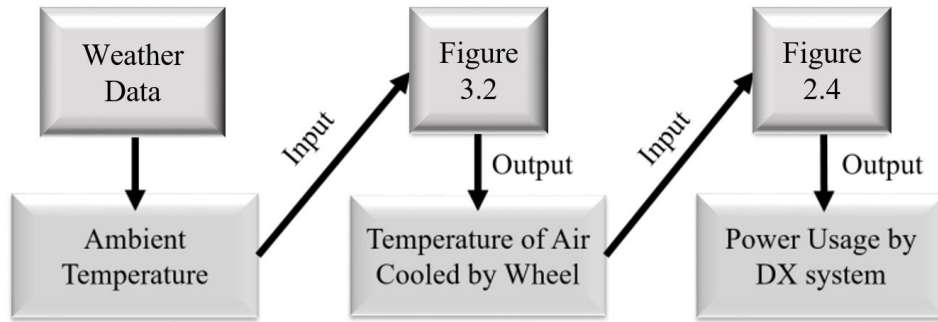
Figure 3.3 The Process of Estimating Power Usage by DX system from Weather Data

Power usage effectiveness is a measure on energy efficiency on data centers defined as

$$\text{PUE} = \frac{\text{Total Facility Power}}{\text{IT Equipment Power}} \tag{40}$$

In the present simulations, the IT equipment consumes 400 kW. Total facility power is the sum of the power consumption by the IT equipment, hot side fans, cold side fans, wheel, and DX system. The power consumed by the fans is obtained from the mass flow rate calculated by the heat exchanger model. The power consumption by DX is calculated using the EnergyPlus model. The power needed to rotate the thermal wheel is 1.1 kW at 6 RPM [30]. The power consumption by the wheel decreases with the rotational speed and is assumed to follow the affinity laws [57]:

$$\frac{WP}{WP_X} = \left(\frac{N_6}{N_X}\right)^3 \tag{57}$$

where WP is the power consumption of the wheel and N is the rotational speed. The subscripts indicate what RPM the parameter is evaluated at. The optimal speeds for the wheel are determined by performing parametric simulations and presented in Table 3.1.

Table 3.1 Optimal Rotating Speed of the Wheel

Ambient Temperature Range	Optimal Speed [RPM]
$T_{c,i} \leq 12.6\ °C$	2
$12.6 < T_{c,i} \leq 15.1\ °C$	3
$15.1 < T_{c,i} \leq 16.4\ °C$	4
$16.4 < T_{c,i} \leq 17.5\ °C$	5
$17.5\ °C < T_{c,i} \leq 37.1\ °C$	6
$37.1\ °C \leq T_{c,i}$	0

Though more sophisticated optimization may be done, it is reasonable enough to set up five operating conditions, considering the fact that the wheel consumes very small amount of power compared to other components. The wheel operates until the ambient temperature reaches 37.1°C, where the temperature of the air leaving the wheel becomes 39 °C. At this point, the wheel does not provide any benefits and stops rotating. Figure 3.4 presents power consumption by each component with respect to the ambient temperature when the wheel turns at an optimal speed.
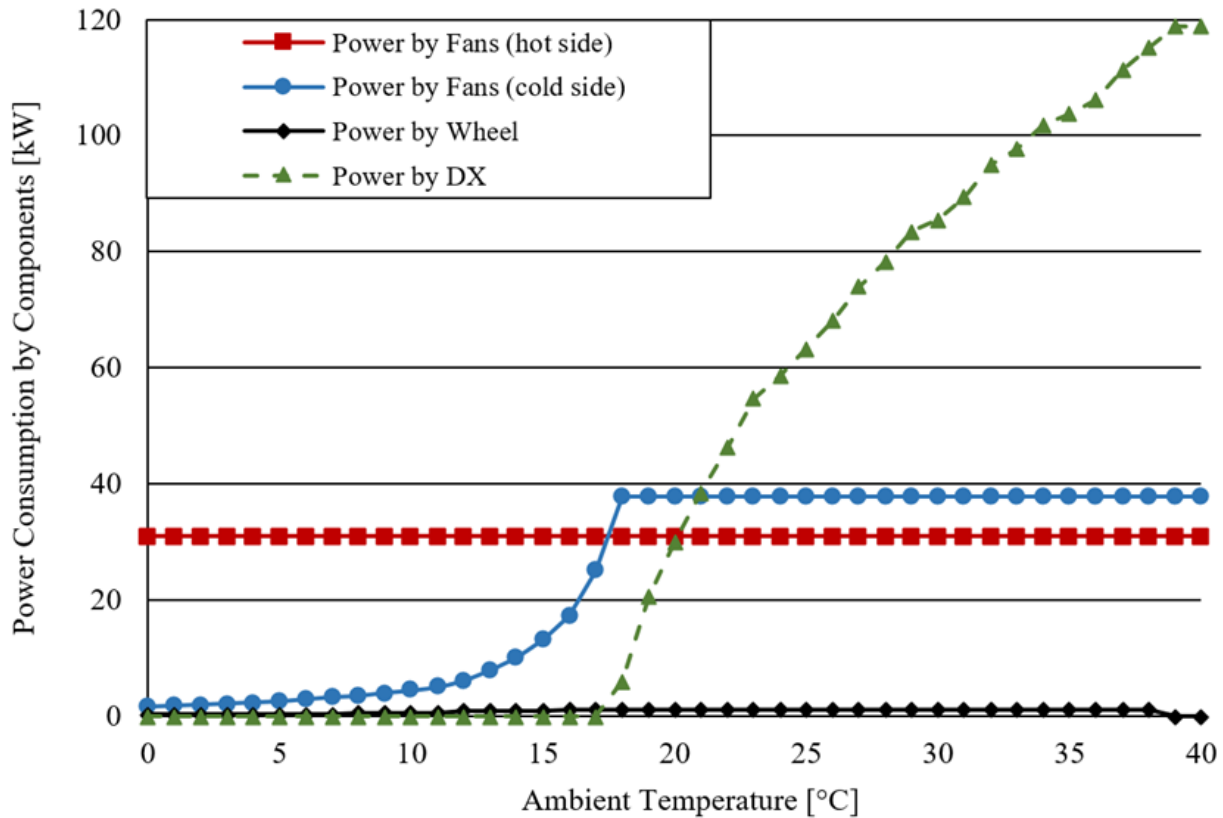
Figure 3.4 Power Usage by Components with Respect to Ambient Temperature. (Overall Fan Efficiency = 0.6)

As the system has a constant cooling load, the power consumed by the hot side fans remains constant at around 32 kW. The power usage by the cold side fans rapidly rises up to 38 kW until 18 °C and remains constant at higher ambient temperature. The 6 kW difference comes from the fact that the hot side and cold side fans face different total pressure drops, even if the volumetric flow rates of the air are the same. The DX system stays turned off until 18 °C, where it starts to consume power. Also, it can be seen that the hot/cold side fans constantly deliver the maximum amount of air, even after the DX system starts to aid. When the ambient temperature reaches around 38 °C, the wheel stops as it provides no cooling. After this temperature point, the DX system cools down the entire cooling load and its power consumption stays constant. The power consumption by the wheel ranges from 0.1 % to 2.2 % of the total power needed for cooling, which is relatively low, compared to the other components.

Year-long energy simulations have been performed for five cities around the world. The weather data files are obtained from the U.S. Department of Energy. Figure 3.5 and 3.6 presents the annual PUE results for the selected locations.
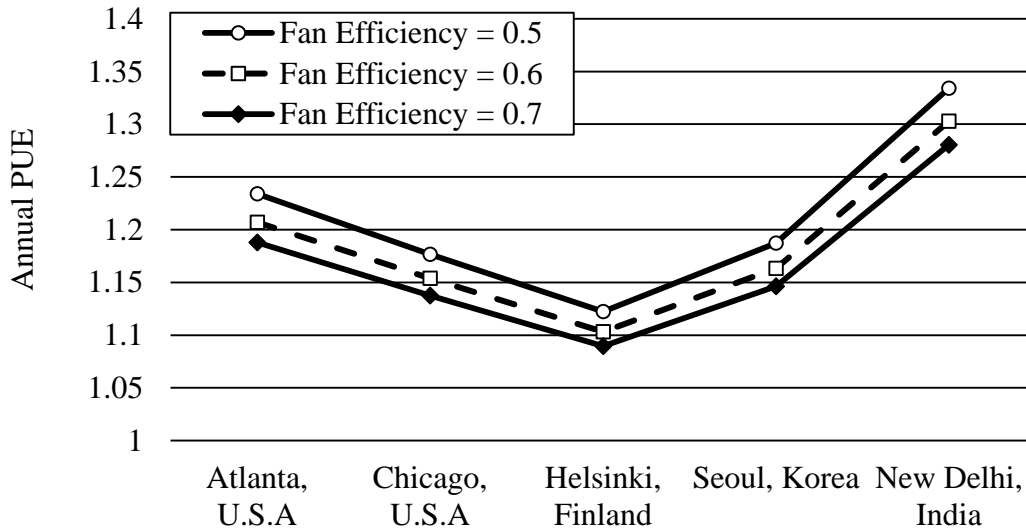
Figure 3.5 Annual PUE of Selected Cities Worldwide (Scenario A)
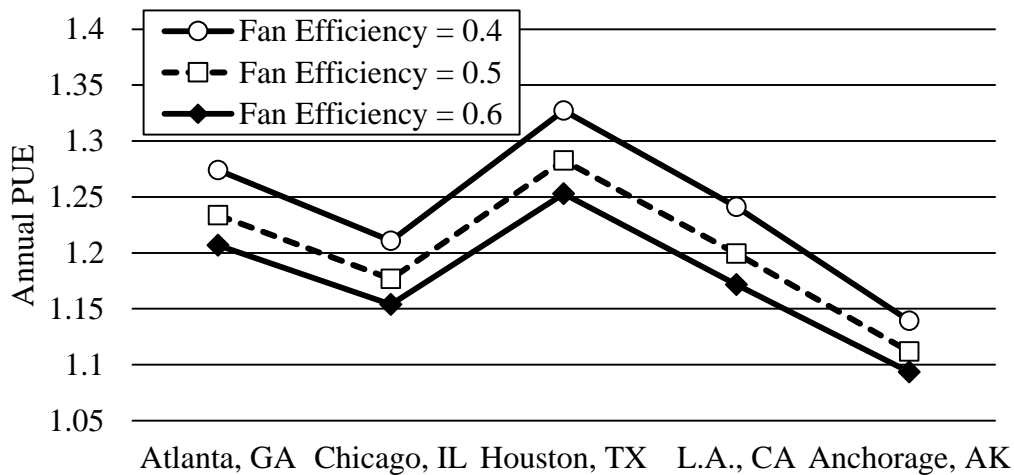
Figure 3.6 Annual PUE of Selected Cities in the U.S. (Scenario A)

A lower value of PUE indicates that the data center uses energy more efficiently for cooling. The annual PUE calculated with a fan efficiency of 0.6 can be as low as 1.10 in Helsinki, where the average annual temperature is 5.18 °C. When the efficiency is assumed to be 0.7, a 1.09 of PUE can be achieved. The PUE calculated for Anchorage is as attractive as the one for Helsinki. For Chicago, where the average temperature is 9.80 °C, the PUE values are 1.14, 1.15, and 1.17 with a fan efficiency of 0.5, 0.6, and 0.7, respectively. For a warmer climate, such as New Delhi, where the average temperature is 24.7 °C, the PUE value goes up to 1.3 when the fan efficiency is 0.6. Even the slightest difference in the PUE can result in a large difference in total power consumption. For example, if the difference in PUE is 0.1 with a cooling load of 400 kW, the data center with the higher PUE will consume 40 kWh more energy every hour. This is about 350 MWh every year.

3.1.3 Waste Heat Re-use – Domestic Heating in Winter

The model discussed in Section 2.8 calculates the air flow rate needed for heating up the house when the supply air temperature is constant at 32 °C. Figure 3.7 below presents 4 outputs calculated for 72 hours period. The outputs are following: zone mean temperature in the house, mass flow rate of supply air needed, outdoor dry-bulb temperature, and supply air temperature.

Hourly Frequency
06/01/2002 00:00 - 12/01/2002 23:00, Hourly Frequency
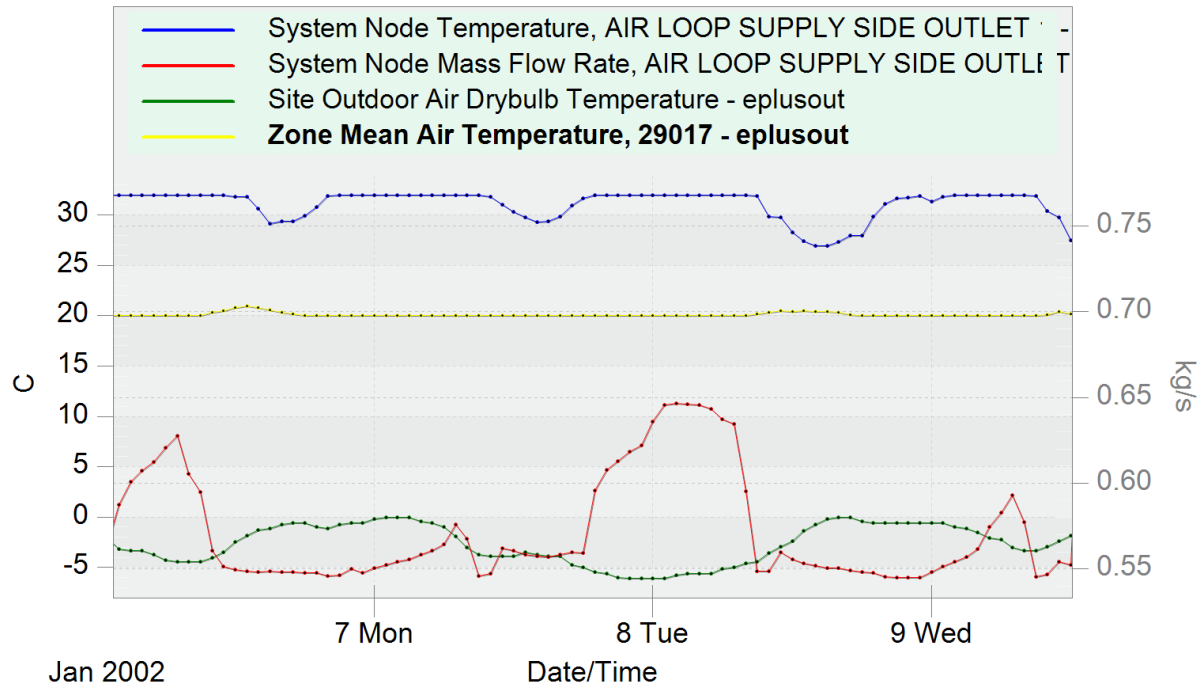
Figure 3.7 EnergyPlus Result from Waste Heat Re-use Model (Domestic Heating)

It can be seen that zone mean temperature is maintained at 20 °C while outdoor air temperature varies from -7 °C to 0 °C. A higher air flow rate is required when outside air temperature is relatively low. This implies that the house will need no more than air flow rate of 0.65 kg/s, which is from the peak point of the red curve, when ambient temperature is above -7 °C. According to Figure 2.16 showing how much waste heat is produced from the 400 kW data center, air flow rate at 9.62 kg/s will be available for building heating when ambient temperature is -7 °C. With these numbers, data center can provide heated air that is enough to heat up at least 14 houses during winter. To estimate how much energy the house needs to consume for heating, another simulation was done using the same model but without fixing the supply air temperature to 32 °C. Figure 3.8 shows natural gas usage for a particular period in Atlanta.

Hourly Frequency
01/10/2002 00:00 - 31/03/2002 23:00, Hourly Frequency
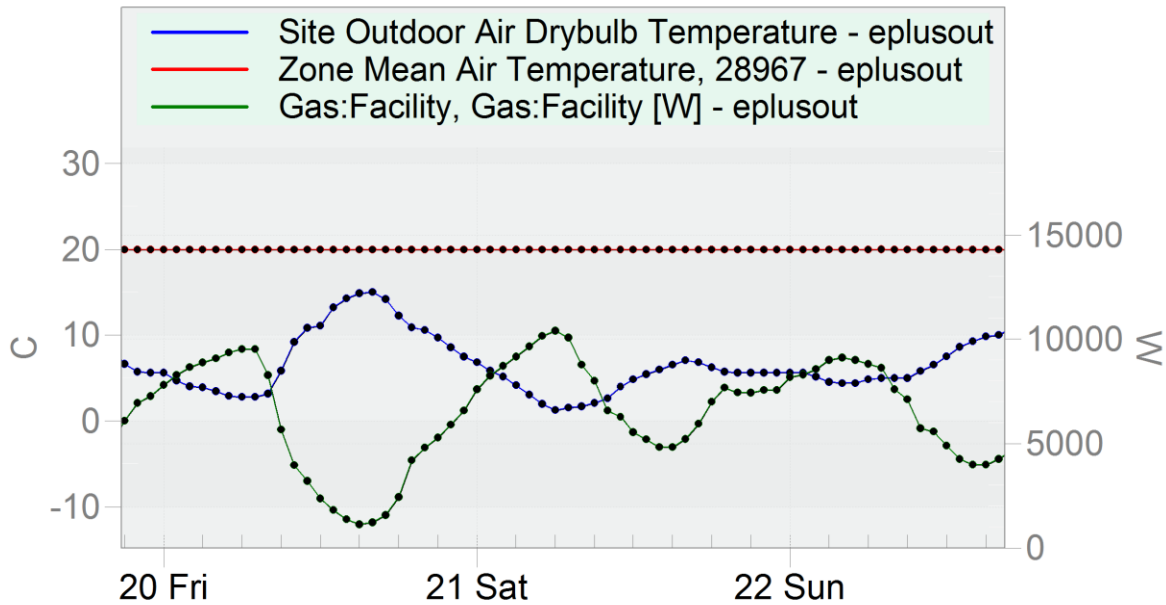
Figure 3.8 Natural Gas Usage from EnergyPlus Result

This figure only shows the result for 3 days for clarity. The straight red line indicates that the zone mean air temperature of the house is maintained at 20 °C as we have set. It can also be seen in the figure that as outdoor air temperature changes, the natural gas usage for heating changes. Whole winter simulation from October 1 to Mar 31 reports that 6445.27 kWh of natural gas was needed for heating for the model house located in Atlanta. This is equivalent to about $880/year/house according to Bureau of Labor Statistics. As the waste heat as air from 400 kW data center can be used for heating up at least 14 houses at peak time, total savings would be $12,320 per year. There is still waste heat because, the number of the houses that can enjoy free heating, is calculated based on the peak time. The number will be increased for normal hours.

3.2 Scenario B

3.2.1 DX Cooling System Results

Considering a hybrid cooled data center with a total cooling load of 408 kW, it has previously been found that 191 kW is cooled by air through DX cooling, while the remaining 217 kW is cooled by water through air-cooled chiller. Figure 3.9 and 3.10 present the EnergyPlus results for a data center with DX system in Atlanta, GA. Total pressure drop for water loop in this scenario can be expressed as

$$\Delta p_{total,1} = \Delta p_{cp} + \Delta p_{pf} \tag{58}$$

where Δp_{cp} is the pressure drop along the cold plate, which is 650 Pa, and Δp_{pf} is the pressure drop in pipe fittings, which is assumed to be 30 kPa. Pump power consumption is calculated using Equation (57) and included in the following EnergyPlus results. For reference conditions for simulations, the fan pressure rise, set point temperature, rated COP of DX coil, and fan efficiency are set to 750 Pa, 27 °C, 3.0, and 0.6, respectively. These are fixed unless varied in simulations.
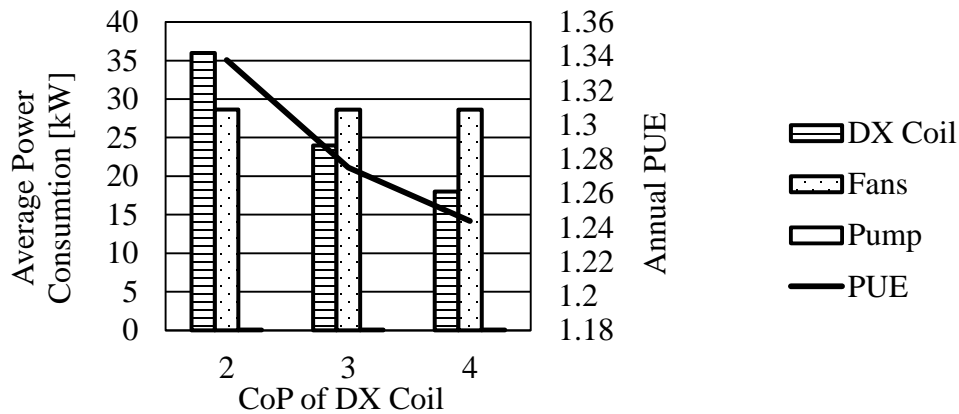
Figure 3.9. Average Power Consumption by DX System with Varying Rated COP of DX Coil

61
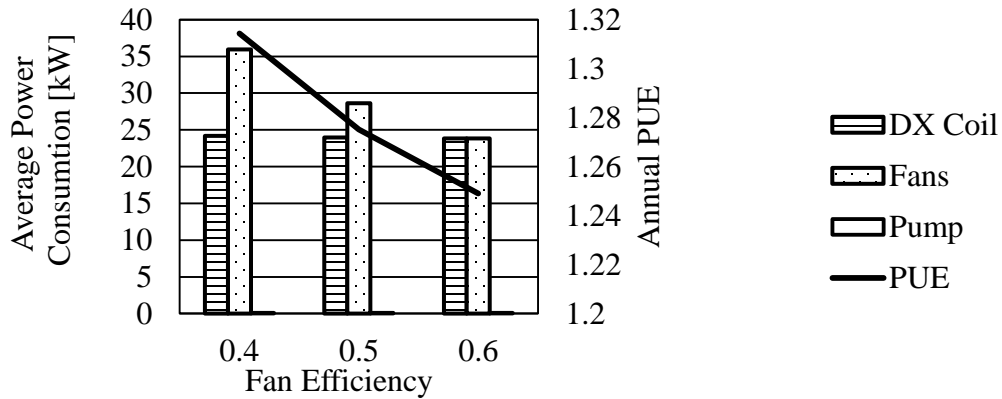
Figure 3.10 Average Power Consumption by DX System with Varying Fan Efficiency

The power consumption of the pump is hardly seen in the figures. As expected, rated COP of DX coil and fan efficiency influence the annual energy usage of the data center. For most cases, fans consume more energy than DX coil due to "free air cooling" enabled by air-side economizer. Figure 3.11 shows how the data center efficiency changes with the set point temperatures.
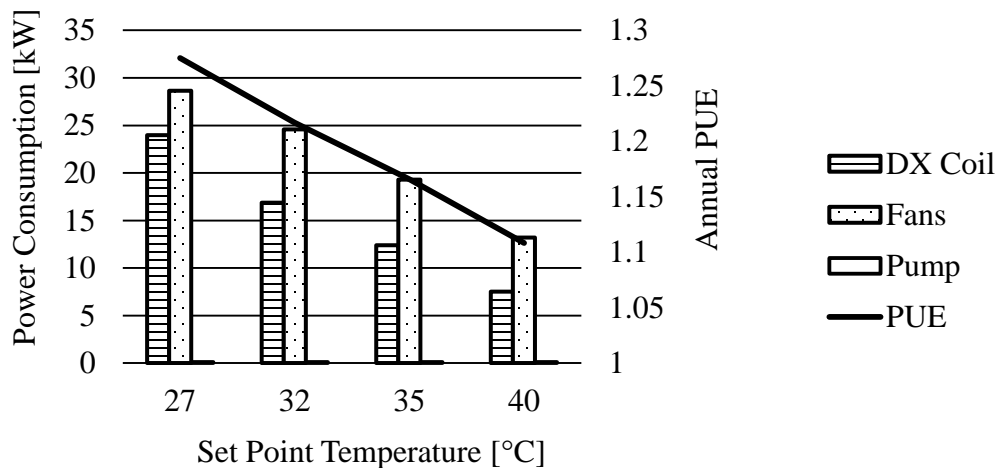
Figure 3.11. Average Power Consumption by DX System with Varying Set Point Temperature

As shown above, the annual PUE significantly drops with increasing room temperature. When the set point temperature is 40 °C, the annual PUE is 1.1 in Atlanta. This implies that having IT equipment with a wider range of operating temperature will save significant amount of energy.

3.2.2 Air-cooled Chiller Results

Since the performance of air-cooled chiller is affected by the ambient condition, EnergyPlus is used to determine the relationship between the chiller power consumption and ambient temperature, which is shown in Figure 3.12.
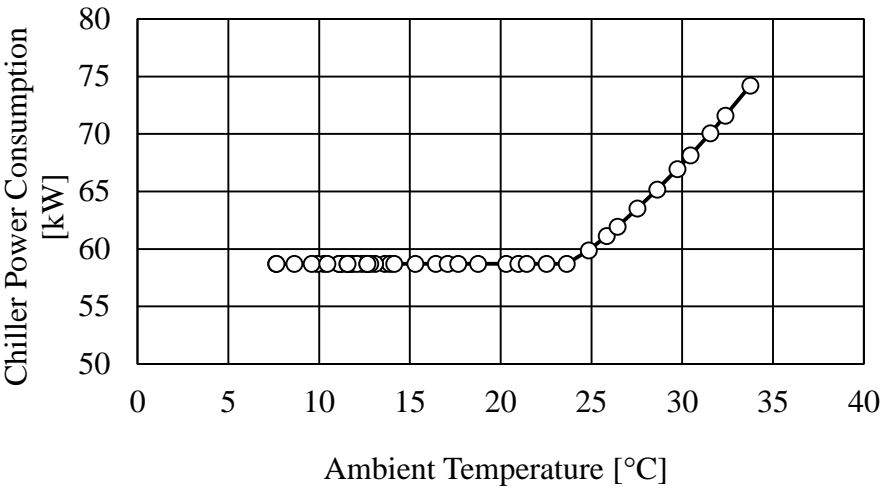
Figure 3.12 Chiller Power Consumption With Respect To Ambient Temperature

This air-cooled chiller consumes about 58 kW to cool down 217kW when the dry-bulb temperature is below 23.5 °C. Then the power consumption linearly increases with the dry-bulb temperature. It is also found that there is no strong relation between the chiller power consumption and the dew-point temperature. Pump power is also calculated using Equation (50) with the given data and assumptions previously discussed. With a pump efficiency of 0.6, the power consumption of pump is found to be about 122 W, which is less than 0.3 % of the chiller power consumption.

3.2.3 Annual PUE Results

Figure 3.13 presents annual PUE value for five selected locations in the United States.
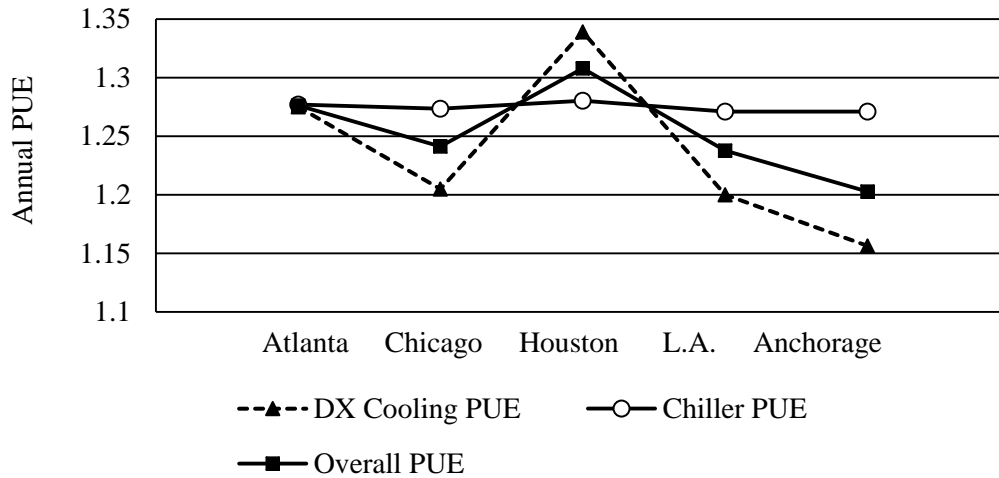
Figure 3.13 Annual PUE Results for Five Selected U.S. Cities.

DX cooling results are calculated based on the following parameters: DX COP of 3.0, fan efficiency of 0.5, and set point temperature of 27 °C. As can be seen in Figure. 3.13, chiller PUE is relatively insensitive to the ambient condition. In most of time in winter, DX coil does not consume much power due to free air cooling. Although the average annual temperature in Chicago is about 7 °C lower than the one in L.A, the PUE for L.A. is found to be slightly lower than Chicago. This means that the DX system efficiency is determined by the number of hours that free air cooling can be achieved during summer. The average summer temperature in L.A. is slightly lower than Chicago, which explains the lower PUE in L.A. Also, it is important to note that liquid cooling is not always efficient than air cooling. In Chicago and L.A, DX system PUEs lie on 1.2 while their PUEs of the chiller are about 1.27. In very cold climate DX cooling can be energy efficient with a PUE as low as 1.16.

3.2.4 Waste Heat Re-use – TEG Modules

The flow rate chosen in the CFD simulation is 1.4 L/min, which is enough to cool 28 blade servers. With inlet water temperature of 5 °C and outlet water temperature of 50 °C, optimum power generated by TEG(s) and its efficiency is plotted in Figure 3.14.

64
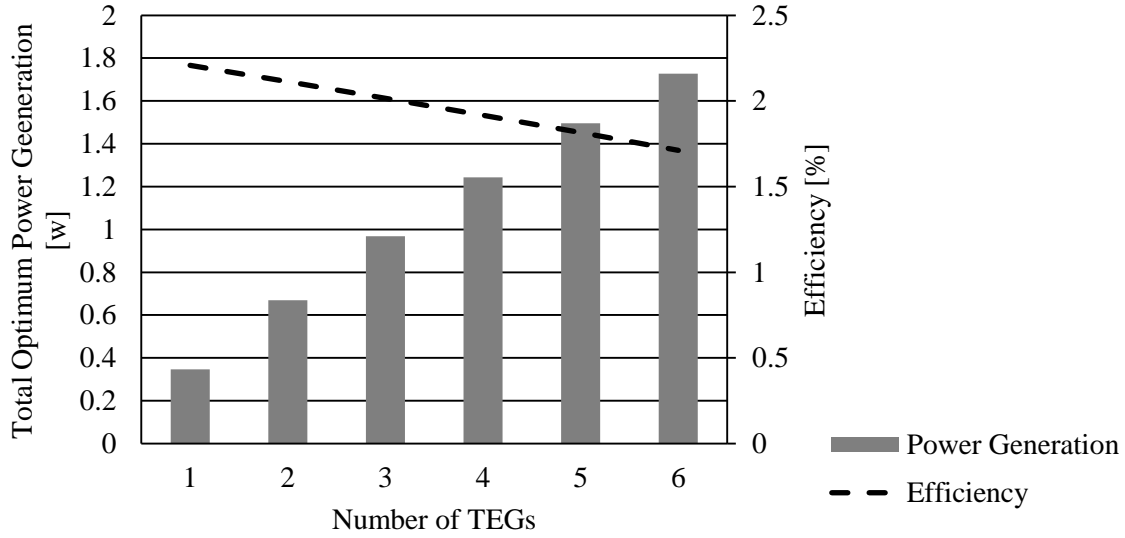
Figure 3.14: Optimum Power Output and its Efficiency with Respect to the Number of TEGs with ZT = 0.73

The efficiency is calculated using the equation below:

$$\eta_{\text{TEG}} = \frac{P_{\text{TEG}}}{Q_{\text{H}}} \tag{59}$$

where Q_H is defined as

$$Q_H = K_{\text{TEG}}(T_{\text{H}} - T_{\text{C}}) + S_{\text{TEG}}T_H I - 0.5\,I^2 R_{\text{TEG}} \tag{60}$$

$$K_{\text{TEG}} = N(k_{\text{TEG}})G \tag{61}$$

where K_{TEG} is the total thermal conductance of the N couples. As shown in Figure 3.14, the power generation by TEGs increases with increasing number of TEG placed between the flow channels. However, the efficiency decrease from 1.8 % to 1.4 % when the number of TEGs increases from 1 to 6. This concludes that power generation from a temperature difference of 45 °C is very low. More simulations have been done to see how figure of merit (ZT) value would improve the efficiency. Figure 3.15 shows optimum power generation by one TEG with different values for the figure of merit.
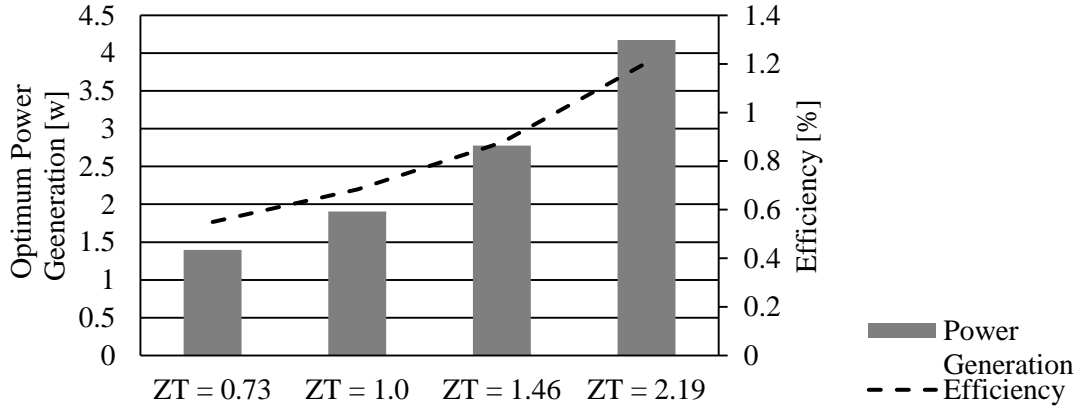
Figure 3.15: Optimum Power Output and its Efficiency with Respect to ZT Value When One TEG is Placed

As the figure of merit increases the efficiency also increases. However, it is still not attractive for TEGs to be used in data center as a waste heat re-use method due to the fact that the optimum power output is very low even with higher ZT values.

3.3 Scenario C

3.3.1 DX Cooling System Results

The DX Cooling results of the second scenario are identical to the ones of the first scenario. When cooling with groundwater, the only power consuming component is pump. Total pressure drop is defined as

$$\Delta p_{total,2} = \Delta p_{cp} + \Delta p_{ltl} + \Delta p_{pf} \tag{62}$$

where Δp_{ltl} is liquid-to-liquid heat exchanger, and other pressures drops remain the same. According to Equation. 54 and Table 2.9, the pump power consumption for one liquid-to-liquid heat exchanger is 5.8 W. As one liquid-to-liquid heat exchange can take care of one rack, 17 heat exchangers are needed. Total pump power consumption is only 98 W.

3.3.2 Results for Warm Water Cooling with Groundwater and Dry Cooler

A problem with this cooling approach is that the data center needs to constantly consume groundwater at 131 L/min, 188,640 L/day. The best way to resolve the issue is to consult with local water distributor. If it is possible to return the heated groundwater back to the distributor,

there is no problem. If the data center are neighboring on a hospital, hotels, university, and office buildings, it is a matter of finding a way to distribute the water to where it is needed. Hotels, hospitals, and university housings are one of the largest hot water consumers [58].   Average hot water usages by a university with 5000 students living on campus is 57500 L/day [58], which is about 30 % of required groundwater consumption. In case of data center facing difficulty to manage the groundwater, a secondary cooling component must be placed. Using the benefit of using warm water, this cooling scenario uses an outdoor dry cooler unit for heat rejection. IBM System & Technology has performed experimental studies regarding energy efficient warm liquid cooled servers with chiller-less cooling. They have designed a 100 % water cooled servers with an average cooling load of 13.16 kW and measured total power consumption by the dry cooler unit, consisting of an liquid-to-air heat exchanger, outdoor fans, and pump [59]. Their tested water flows ($\dot{V}_{dc}$ shown in Figure 2.14) ranged from 15.4 L/min to 30.3 L/min, and the temperate of the water entering the IT room ($T_{dc2,o}$) is as high as 40 °C [60]. Taking the flow conditions into account, Figure 2.12 shows that the maximum CPU temperature would reach 61. 2 °C at 30.3 L/min and 67.1 °C at 15.4 L/min, which are below the maximum allowable temperature of the CPU. According to their test data, in a hot summer day, the total power consumption by the dry cooler unit is 0.442 kW when the average IT load is 13.16 kW [59]. Since the outdoor fans would consume less power when the ambient temperature is cooler, it is expected that average cooling power for a full year to be significantly below 0.442 kW. We used their experiment results when estimating the power consumption by the dry cooler unit. Figure 3.16 shows the annual PUE of five selected U.S. cities with varying the availability of cooling with groundwater.
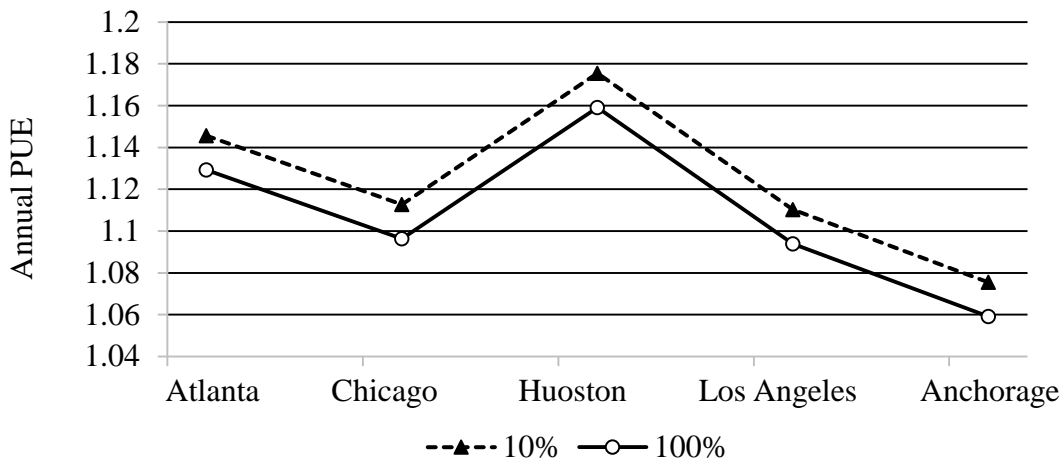
Figure 3.16 Annual PUE for Five Selected U.S. Cities with Different Availabilities of Groundwater Cooling

In Figure 3.16, the curve of 100 % availability denotes that cooling with groundwater can provide 100 % of the total water cooling. To cool 217kW completely using groundwater, 131 L of groundwater needs be used every minute. As can be seen above, utilizing groundwater is more energy efficient than using dry cooler units for all climates, but it does not mean dry coolers are inefficient. This high efficiency is due to the warmer water used for servers, which makes it possible for the data center to achieve chiller-less system.

3.3.3 Waste Heat Re-use – Preheating Water for Surrounding Buildings

Cooling with groundwater provides an additional benefit by reutilizing the waste heat. If 100% is cooled by groundwater, 5208 kWh (178 us therm) of energy can be saved every day. According to the average prices of electricity and gas in 2015 [61], the saving in terms of energy is equivalent to $60,000/year if heated using natural gas. If only 10% of the total load can be cooled using groundwater, the number simply decreases by a factor of 10.

3.4 Scenario D

3.4.1 Water-Cooled Chiller Results

      In this scenario, the entire 408 kW is entirely cooled by water through water-cooled chiller. There are two cases considered. In Case A, the condenser loop temperature in cooling tower is controlled by ambient conditions, while Case B fixes the temperature at the default value, 30 °C. The chiller supply temperature of water is 10 °C. The flow rate for the chiller is set to 382.5 L/min, which is distributed to 51 air-to-liquid heat exchangers at 7.5 L/min. This 7.5 L/min is then allocated to 28 servers at 0.27 L/min. Year-long energy simulations by EnergyPlus produce the relationship between chiller power consumption and ambient temperature for the two settings, which his plotted in the following figure.
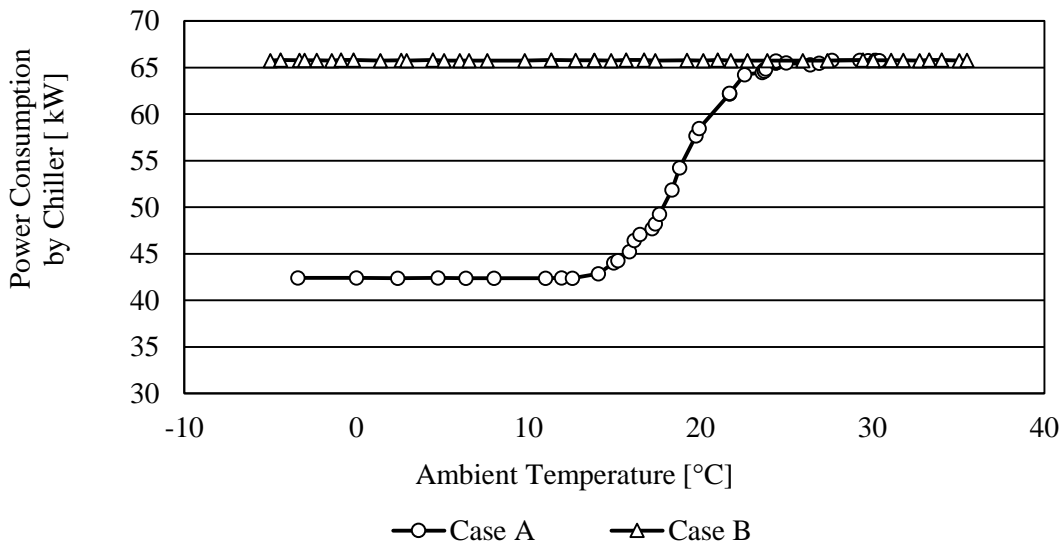
Figure 3.17. Power Consumption by Water-Cooled Chiller With Respect To Ambient Temperature

The chiller power calculated using EnergyPlus includes. The pump power is calculated using the same method presented in other scenarios. As can be seen in Figure 3.17, it turns out that there is cooling benefits from varying the condenser loop temperature until the ambient temperature reaches about 23.5°C. At this temperature, the ambient temperature is higher than the water

temperature in condenser loop. It can also be seen that the chiller power consumption stays constant with the temperatures below 10 °C. This is because the minimum value for condenser loop temperature is set to 10 °C.

3.4.2 Water Consumption of Cooling Tower

A cooling tower connected to water cooled chiller needs makeup water while operating, due to evaporation, drift/windage, and blow-down losses. Drift is entrained water in the tower discharge vapors, and we assumed that drift loss rate is 0.05 %. Blow-down discards a portion of the concentrated circulating water due to the evaporation process, and it is determined according to blow-down concentration ratio, which was set to 3 for this chiller. Figure 3.18 presents makeup water required for the cooling tower in the five selected cities.
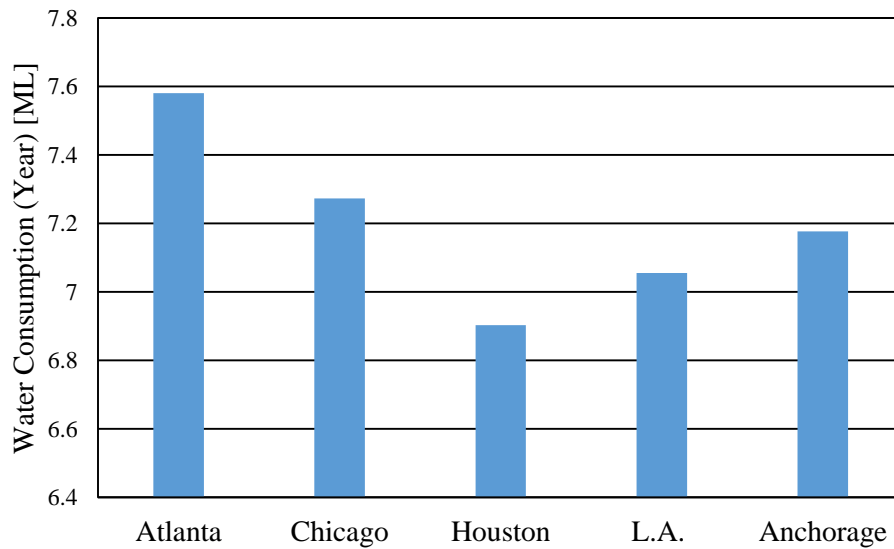
Figure 3.18 Makeup Water Needed for Cooling Tower throughout a Year

The water consumption by cooling tower highly depends on the relative humidity. As Houston is the most humid city among the five, it shows that the water consumption is the least in Houston, consuming about 6.9 ML for a year.

Figure 3.19 shows the average power consumptions of the cooling components and annual PUE with five locations.
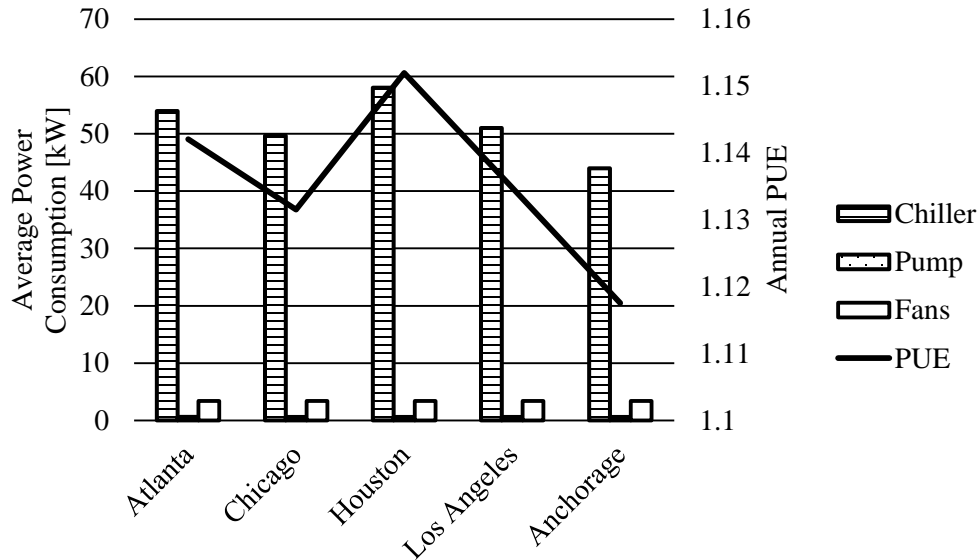
Figure 3.19 Power Consumption and Annual PUE for Five Selected U.S. Cities

Fan and pump power consumptions are severely low compare to the chiller consumption. With this cooling scenario, a data center placed in Houston can have a PUE as low as 1.15. Compared to the previously presented scenarios, this strictly water cooled data centers are generally more efficient except for extremely cold climates such as Anchorage, AK.

3.5 Overall Comparison

Annual energy simulations have been performed for all scenarios with the following conditions and assumptions: (1) Atlanta climate, (2) IT room set point temperature of 40 °C, (3) Fan efficiency of 0.5, (4) Rated DX COP of 4.0, (5) Cooling load of 408 kW. Figure 3.20 shows the annual energy usage for all scenario considered in this study.
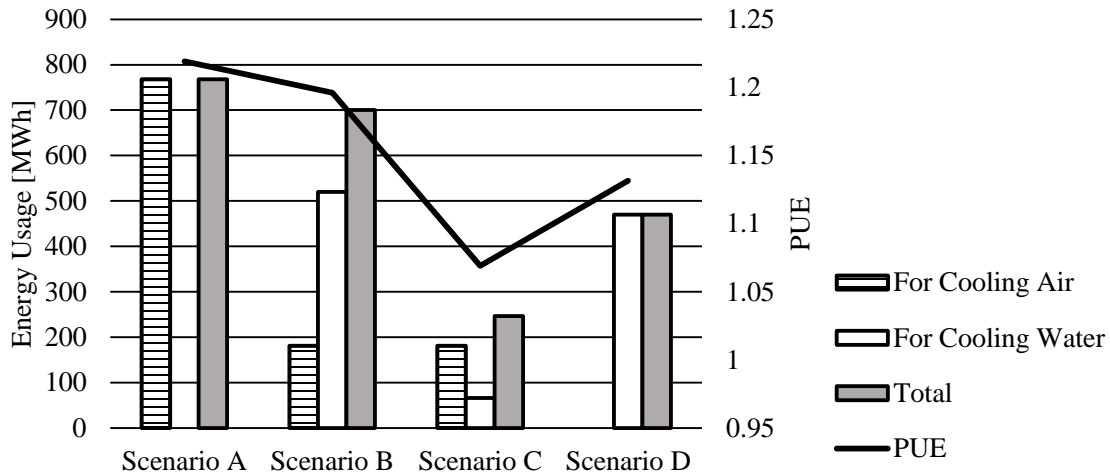
Figure 3.20 Annual Energy Usage for All Scenarios for a Notional Data Center in Atlanta

As can be seen in the figure, estimated PUEs for all scenario range from 1.07 to 1.22, suggesting that all of the systems considered are fairly efficient. The highest PUE can be observed in Scenario A, where a rotary regenerative heat exchanger and DX system are used. It should be noted that this cooling strategy has several advantages that are not represented in terms of PUE, and they are discussed in Section 1.3. Due to the fact that IT room set point temperature was set to 40 °C, it turned out to be more efficient to use DX cooling system with assisted air-side economizer than to use air-cooled chiller in Scenario B. Scenario C produced the best annual PUE, which is around 1.07. The result has been calculated for the case where 100% of water is cooled by dry coolers and shows that warm water cooing is very energy efficient. Not only Scenario C shows the best result, but also it has potential to use groundwater and distribute pre-heated water to local facility as waste heat, which is large energy savings. Scenario D with water-cooled chiller is also fairly efficient with a PUE of 1.13, but it should be concerned that this cooling approach requires about 7.6 ML/year of makeup water.

CHAPTER 4

CONCLUSION

This study aims to develop energy simulation models for four cooling scenarios that include one air-cooled data center and three hybrid liquid/air cooled data centers. As waste heat produced from data center can be reutilized for possible energy savings, three methods of re-using the waste heat are presented and linked to the data center models for evaluation.

For Scenario A, the presented method of estimating a PUE for rotary regenerative heat exchanger and DX cooling system in an air cooled data center involves developing two separate models interacting with each other. It is found that the performance of the regenerative heat exchanger highly depends on climate, as the overall effectiveness of the system is proportional to the ambient temperature. Since the power consumption by fans is significant, the overall fan efficiency plays an important role in producing a lower PUE. As expected, the PUE for a relatively cold location, such as Helsinki, Finland, can be 1.1, which signifies the facility uses only 10% of the IT load for cooling. The system still looks attractive for major cities with warmer environment such as Chicago, IL and Seoul, Korea with PUE values lower than 1.2, when the fan efficiency was higher than 0.5. The presented model can be further used to determine the performance of the system with varying location, cooling load, wheel design, temperature set points, and type of fan.

For Scenario B, C, and D, it is found that the efficiency of DX cooling systems is affected by fan efficiency, DX coil COP, ambient temperature, and temperature set point of IT room. Through using free cooling, air-cooled data centers can be more energy efficient than liquid cooled data centers with chillers at cold climates. This implies that liquid cooling is not always more energy efficient than air cooling. Water-cooled chillers are found to be considerably more efficient than air-cooled chillers, even with a cooling load of about 400 kW. It is also observed that warm water cooled servers can use a liquid-to-liquid heat exchanger to reject the heat to groundwater very efficiently. However, in order to completely cool the cooling load through using groundwater, the data center must be able to manage 136 L/min of water as waste heat. Since pumps power consumption is very low compared to fans and chillers, the results show that warm water cooling is very efficient compared to cooling with air-cooled chiller. In addition, the use of groundwater as coolant produces enormous amount of waste heat as heated water. If the heated water can be

distributed to neighboring buildings, a data center with 408 kW can save 5.2 MWh a day. The energy efficiency of hybrid cooled data centers is still relying on how efficient it is to cool the air. Among Scenario B, C, and D, estimated PUEs from Scenario D are the least affected by the ambient condition.

Overall, the results from all Scenarios show that the DX system, a conventional refrigeration-based cooling system, can be inefficient when it is not assisted with an air-side economizer. The efficiency increases with enabling the air-side economizer, which makes the system efficiency depend on climatic conditions. Hybrid cooling scenarios (B, C, and D) look more promising than air cooling scenario simply by comparing the PUE results, especially for warmer climates. This is because the system performances of water cooling systems are relatively insensitive to the ambient condition. For data center in Atlanta, GA, Scenario C had the highest efficiency, and it is expected that many other cities around the world would have similar results. It should be noted that waste heat re-use by thermoelectric generators in Scenario B was very inefficient while domestic heating in Scenario A and pre-heating water in Scenario C would provide considerable energy savings.

APPENDIX A: PERFORMANCE CURVES AND
INPUT PARAMETERS USED

A.1 Data Center Model

A.1.1 Construction data (templates available in EnergyPlus)

External wall	super insulated brick/block external wall
Below grade walls	super insulated brick/block external wall
Flat roof	flat roof – 19mm asphalt
Pitched roof (occupied)	clay tiles (25mm) on air gap (20mm) on roofing felt (5mm)
Pitched roof (unoccupied)	uninsulated Pitched roof, lightweight
Glazing	no window
Vent type	grille, small, light slates
Lighting	off

A.1.2 DX coil data

Coil type	single speed
Rated cooling capacity	variable
Rated sensible heat ratio (SHR)	Autosize
Rated COP	variable
Evaporator fan power per vol. (W/(m3/s)	1100
Availability schedule	on 24/7
Condenser type	air-cooled
Run setting	run on sensible and latent load both

Performance curve 1:
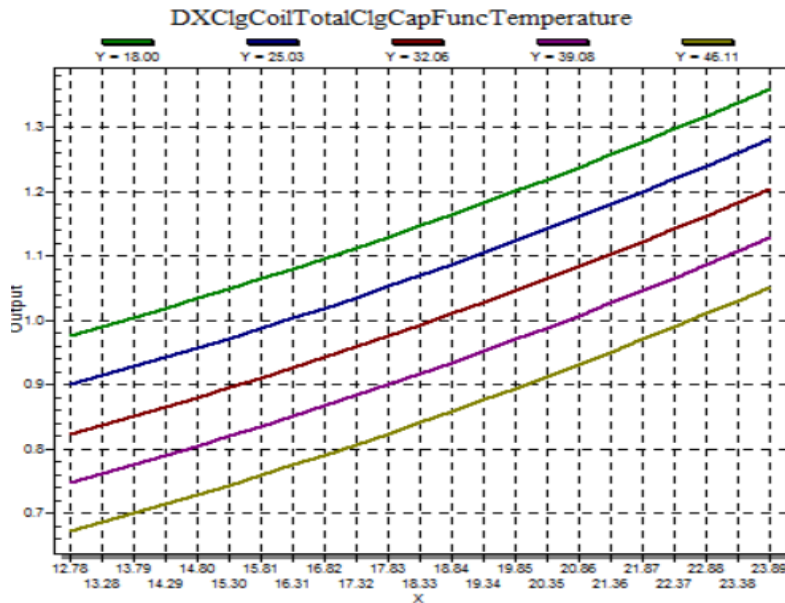
Figure A.1 Total cooling capacity function of temperature curve

Category	bi-quadratic
Source	EnergyPlus
Coefficient 1	0.942587793
Coefficient 2	0.009543347
Coefficient 3	0.00068377
Coefficient 4	-0.011042676
Coefficient 5	0.000005249
Coefficient 6	-0.00000972
Minimum value of x	12.77778
Maximum value of x	23.88889
Minimum value of y	18
Maximum value of y	46.11111
Input unit type for x	temperature
Input unit type for y	temperature
Output units	dimensionless

Performance curve 2:
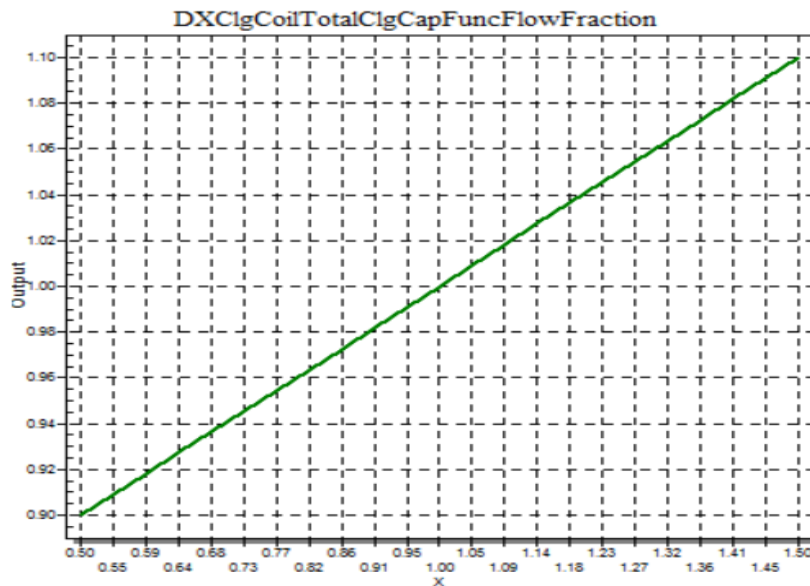
Figure A.2 Total cooling capacity function of flow fraction curve

Category	quadratic
Sourcre	EnergyPlus
Coefficient 1	0.8
Coefficient 2	0.2
Coefficient 3	0
Minimum value of x	0.5
Maximum value of x	1.5

Performance curve 3:
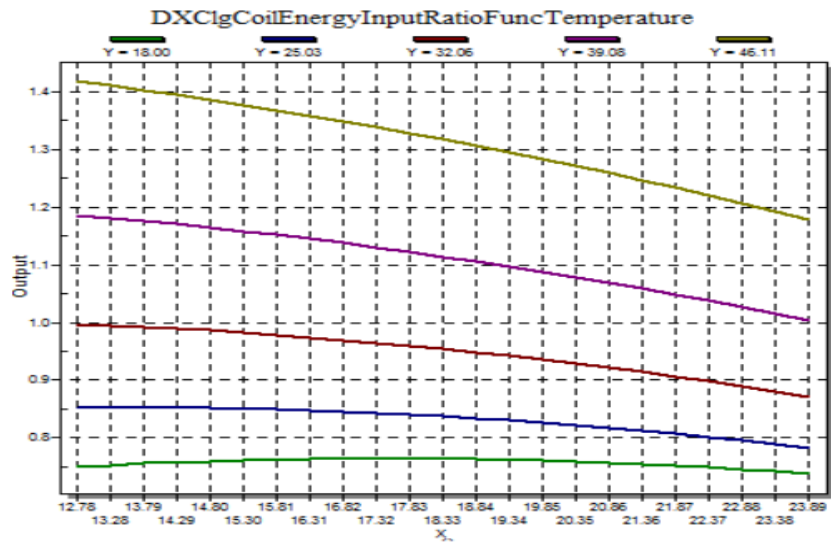
Figure A.3 Energy input ratio (EIR) function of temperature curve

Category	bi-quadratic
Source	EnergyPlus
Coefficient 1	0.342414409
Coefficient 2	0.034885008
Coefficient 3	-0.0006237
Coefficient 4	0.004977216
Coefficient 5	0.000437951
Coefficient 6	-0.000728028
Minimum value of x	12.77778
Maximum value of x	23.88889
Minimum value of y	18
Maximum value of y	46.11111
Input unit type for x	temperature
Input unit type for y	temperature
Output units	dimensionless

Performance curve 4:
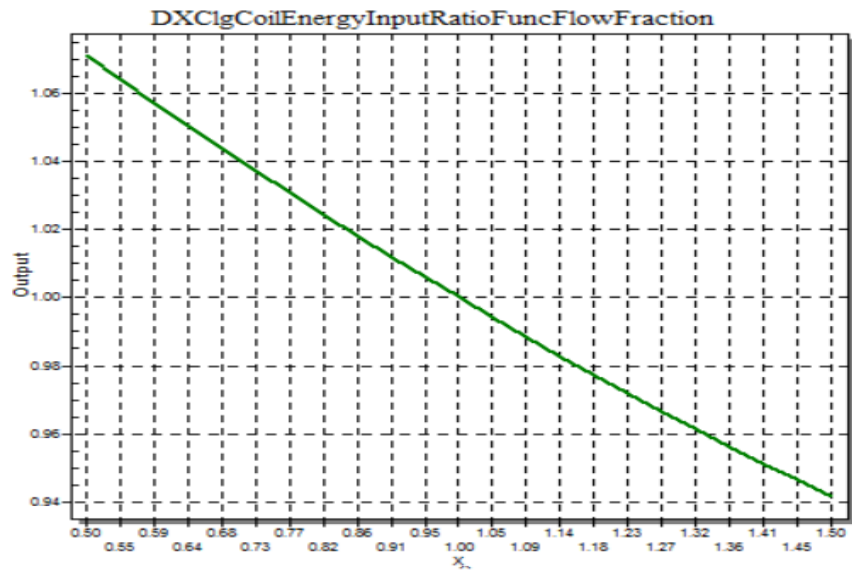
Figure A.4 Energy input ratio (EIR) function of flow fraction curve

Category	quadratic
Sourcre	EnergyPlus
Coefficient 1	1.15552
Coefficient 2	-0.1808
Coefficient 3	0.0256
Minimum value of x	0.5
Maximum value of x	1.5

Performance curve 5:
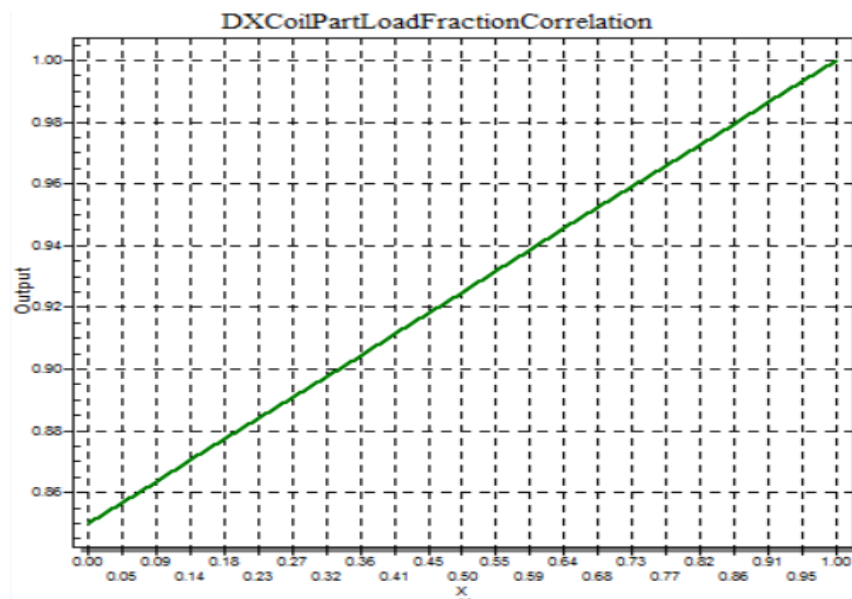
Figure A.5 Part load fraction correlation curve

Category	quadratic
Sourcre	EnergyPlus
Coefficient 1	0.85
Coefficient 2	0.15
Coefficient 3	0
Minimum value of x	0
Maximum value of x	1

A.1.3 Fan data

Fan total efficiency	variable
Pressure rise (Pa)	variable
Minimum flow fraction for fan power	0.3

Performance curve:
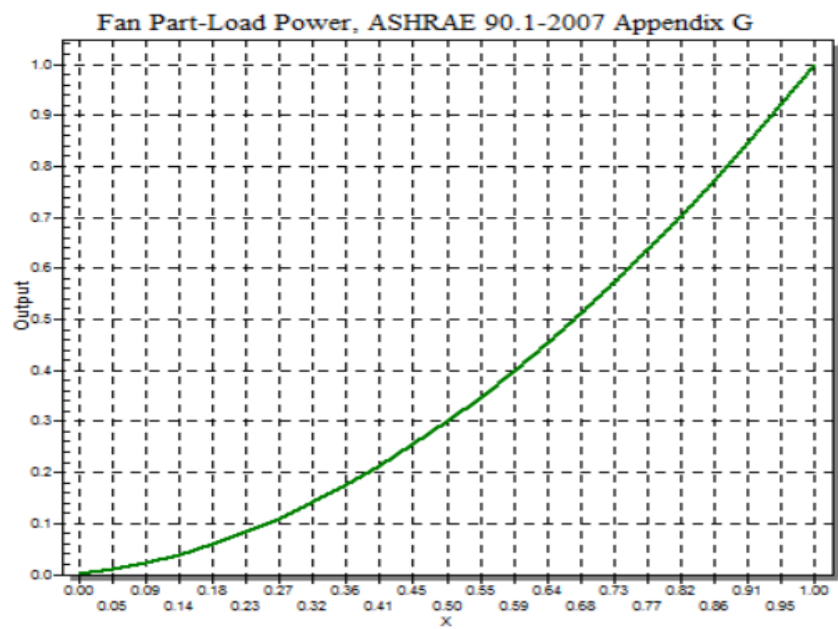
Figure A.6 Fan Part-load power, ASHREA 90.1-2007 Appendix G

Category	quadratic
Sourcre	ASHRAE
Coefficient 1	0.0013
Coefficient 2	0.147
Coefficient 3	0.9506
Coefficient 3	-0.0998
Minimum value of x	0
Maximum value of x	1

A.1.4 Air-cooled chiller data

Chiller name	Electric EIR chiller Scroll McQuay AGZ075D
Reference capacity (kW)	257
Reference COP	2.93
Compressor motor efficiency	1
Sizing factor	1
Flow rate	variable

Performance curve 1:
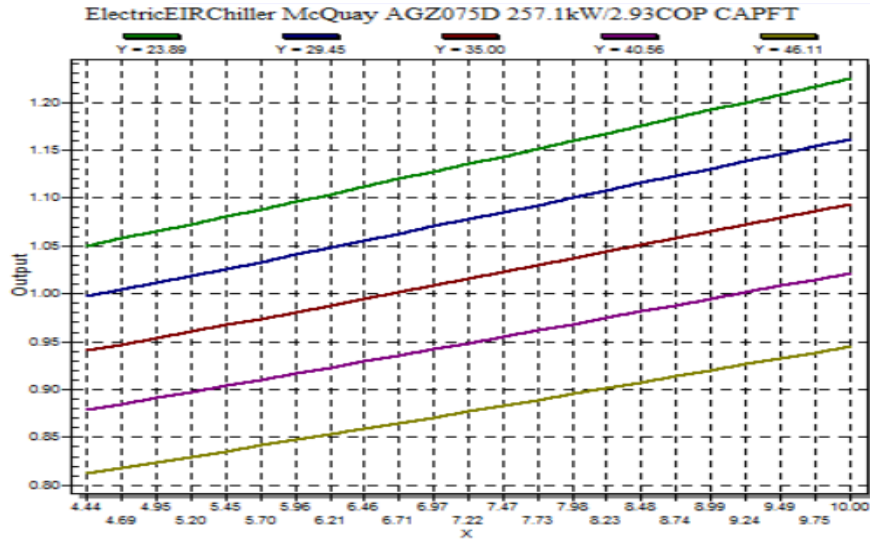
Figure A.7 Cooling capacity function of temperature curve (air-cooled chiller)

Category	bi-quadratic
Source	EnergyPlus
Coefficient 1	1.0585362843
Coefficient 2	0.0363158882
Coefficient 3	0.0002295290
Coefficient 4	-0.0040266953
Coefficient 5	-0.0000733438
Coefficient 6	-0.0003425523
Minimum value of x	4.44
Maximum value of x	10
Minimum value of y	23.89
Maximum value of y	46.11

Performance curve 2:
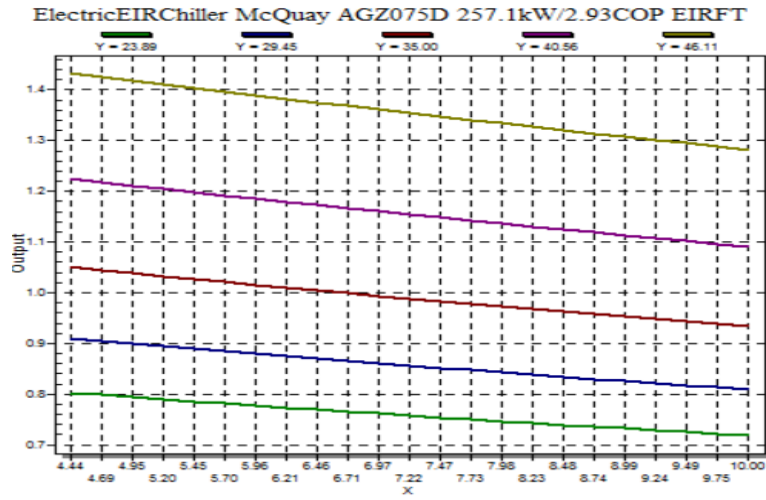
Figure A.8 Electric input to cooling output ratio function of temperature curve (air-cooled chiller)

Category	bi-quadratic
Source	EnergyPlus
Coefficient 1	0.7566566326
Coefficient 2	-0.0080094048
Coefficient 3	0.0003995600
Coefficient 4	-0.0076070096
Coefficient 5	0.0005478231
Coefficient 6	-0.0005383933
Minimum value of x	4.44
Maximum value of x	10
Minimum value of y	23.89
Maximum value of y	46.11

Performance curve 3:
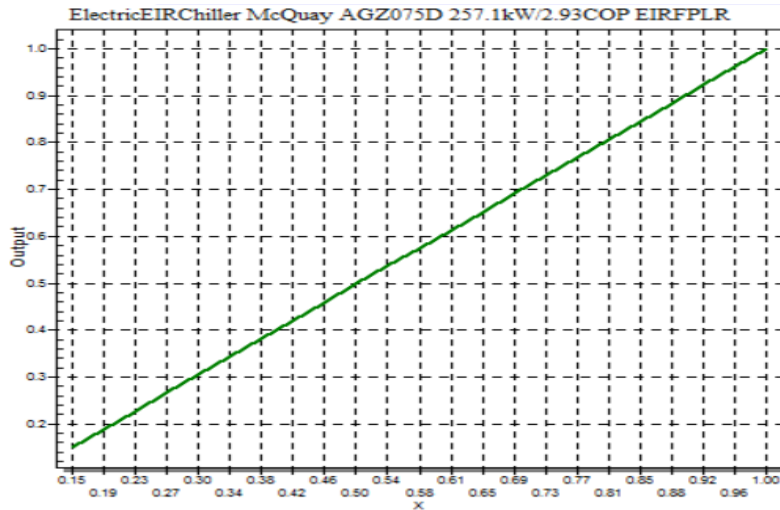
Figure A.9 Electric input to cooling output ratio function of part load curve (air-cooled chiller)

Category	quadratic
Source	EnergyPlus
Coefficient 1	0
Coefficient 2	1
Coefficient 3	0
Minimum value of x	0.15
Maximum value of x	1

A.1.5 Water-cooled chiller data

Chiller name	Reform EIR chiller Centrifugal McQuay PEH 703
Reference capacity (kW)	703
Reference COP	7.03
Compressor motor efficiency	1
Sizing factor	1
Flow rate	variable
Cooling tower type	single speed
Design air flow rate	autosize
Fan power at design air flow rate	autosize
Air flow rate in free convection regime	autosize
Evaporation loss mode	saturated exit
Drift loss percent	0.008
Heating sizing factor	1
Performance input method	UA and design water flow rate
Design water flow rate	autosize
UA at design air flow rate	autosize
UA at free convection air flow rate	autosize
Free convection air flow rate sizing factor	0.1
Capacity control	fan cycling

Performance curve 1:
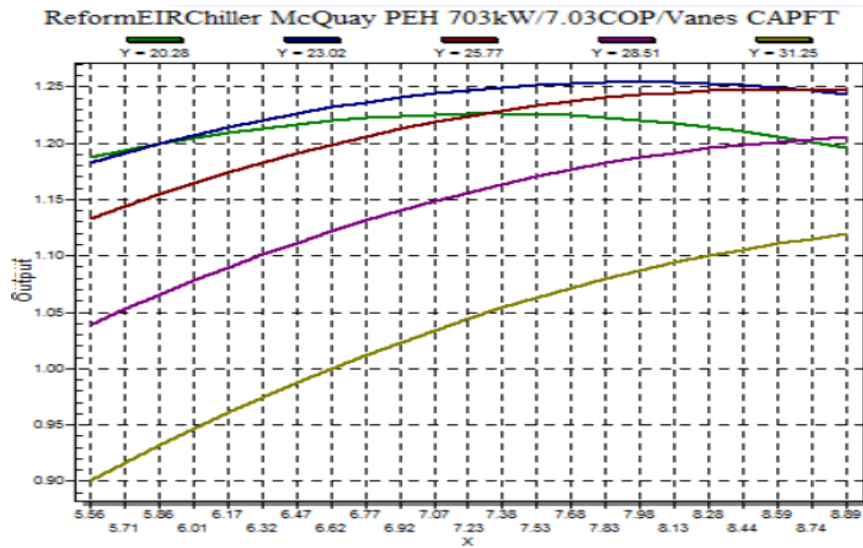
Figure A.10 Cooling capacity function of temperature curve (water-cooled chiller)

Category	bi-quadratic
Source	EnergyPlus
Coefficient 1	-0.133618
Coefficient 2	0.06473161
Coefficient 3	-0.01240446
Coefficient 4	0.09425649
Coefficient 5	-0.002958871
Coefficient 6	0.005765503
Minimum value of x	5.56
Maximum value of x	8.89
Minimum value of y	20.28
Maximum value of y	31.25

Performance curve 2:
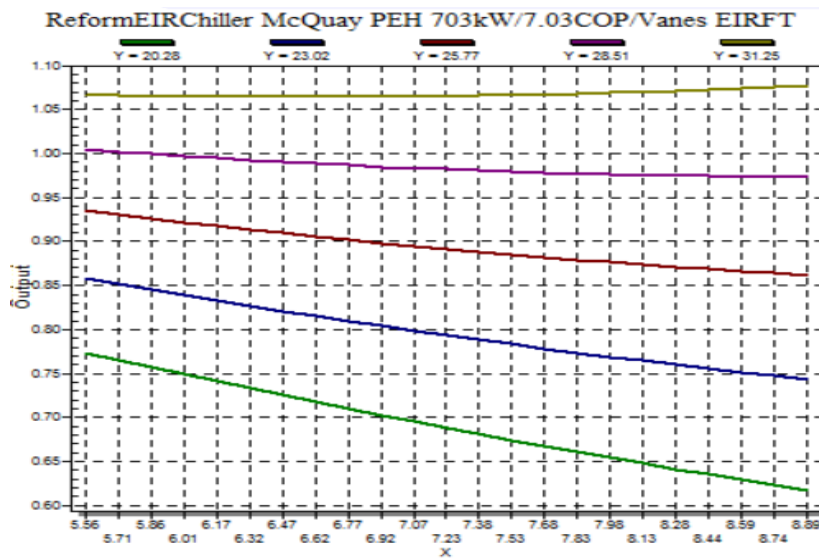
Figure A.11 Electric input to cooling output ratio function of temperature curve (water-cooled chiller)

Category	bi-quadratic
Source	EnergyPlus
Coefficient 1	0.8177961
Coefficient 2	-0.1756394
Coefficient 3	0.002510719
Coefficient 4	0.02677783
Coefficient 5	-0.0004926551
Coefficient 6	0.004559008
Minimum value of x	5.56
Maximum value of x	8.89
Minimum value of y	20.28
Maximum value of y	31.25

Performance curve 3:
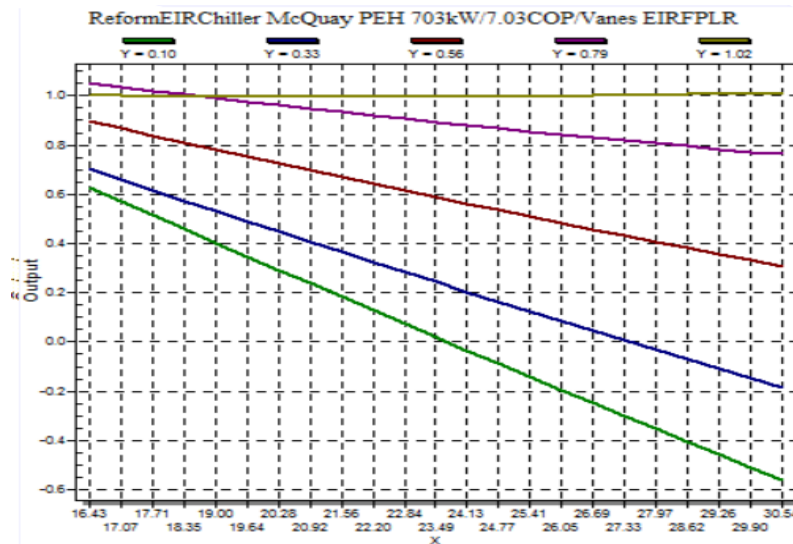
Figure A.12 Electric input to cooling output ratio function of part load ratio curve (water-cooled chiller)

Category	bi-cubic
Source	EnergyPlus
Coefficient 1	2.342644
Coefficient 2	-0.1060883
Coefficient 3	0.0002710155
Coefficient 4	-2.289108
Coefficient 5	3.338339
Coefficient 6	0.09221626
Coefficient 7	0
Coefficient 8	-2.217954
Coefficient 9	0
Coefficient 10	0
Minimum value of x	16.43
Maximum value of x	30.54
Minimum value of y	0.1
Maximum value of y	1.02

A.2 House Model

A.2.1 Construction data (templates available in EnergyPlus)

External wall	wall – typical reference – medium weight
Below grade walls	below grade wall – typical reference – medium
Flat roof	combined flat roof –typical reference – medium
Pitched roof (occupied)	pitched roof – typical reference – medium
Pitched roof (unoccupied)	pitched roof – uninsulated – lightweight
Internal partitions	lightweight 2 * 25 mm gypsum plasterboard with 100mm cavity
Model infiltration	0.7

Glazing	1.5m, 30% glazed
Window height (m)	1.5
Window spacing (m)	5
Still height (m)	0.8
Window frame	painted wooden window frame
Vent type	grille, small, light slates
Lighting	on
Normalized power density (W/m^2)	15
Schedule	Dwell_Dom_CommonAreas_Lights
Target illuminance (lux)	100
Luminaire type	0.42
Visible fraction	0.18

A.2.2 Activity data

Occupancy (people/m^2)	0.0196
Occupied volume (m^3)	256.3
Metabolism	light manual work
CO_2 generation rate (m^3/s-W)	0.0000000382
Heating setpoint temperature (°C)	20
Heating setback temperature (°C)	15
Minimum fresh air (l/s-person)	10
Heat gain from equipment (W/m^2)	2.16
Radiant fraction from equipment	0.2

A.2.3 Hot water boiler data

Boiler template	gas-fired condensing boiler
Nominal capacity (kW)	autosize
Parasitic electric load (W)	25
Nominal thermal efficiency	0.89
Efficiency curve temperature evaluation	leaving boiler

Performance curve:
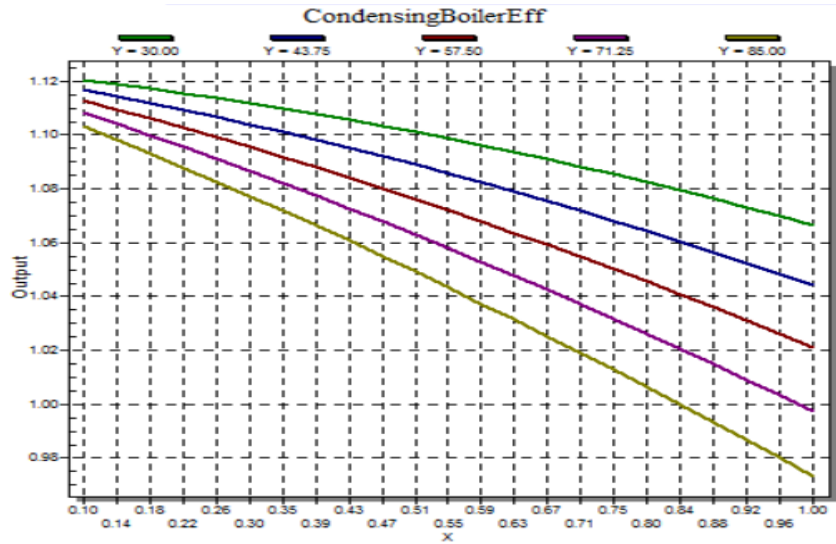
Figure A.13 Normalized boiler efficiency curve

Category	bi-quadratic
Source	EnergyPlus
Coefficient 1	1.124970374
Coefficient 2	0.014963852
Coefficient 3	-0.02599835
Coefficient 4	0.02677783
Coefficient 5	-0.0000014046
Coefficient 6	-0.00153624
Minimum value of x	0.1
Maximum value of x	1
Minimum value of y	30
Maximum value of y	85

APPENDIX B: MEASUREMENT AND ENERGYPLUS RESULTS FOR VALIDATION

* Measured data was obtained from Demetriou et al. [16]
* % difference is defined as $\frac{P_{model} - P_{measured}}{P_{measured}} * 100$

Chiller 1 (Electric EIR Chiller Centrifugal Carrier 19EX 4667kW Vanes)

Measurement No.	Measured cooling load	Measured chiller power	Average chiller power calculated by EnergyPlus	% difference (chiller)	Measured cooling tower power	Average cooling tower power calculated by EnergyPlus	% difference (cooling tower)
1	4310	470	483.6228751	2.898484074	44.7	44.31	-0.872483221
2	4350	472.5	488.554454	3.397768039	44.7	44.31	-0.872483221
3	4450	476.5	496.4937035	4.195950367	44.7	44.31	-0.872483221
4	4470	477	502.3013653	5.304269454	44.7	44.31	-0.872483221
5	4500	483.5	505.2799823	4.50464987	44.7	44.31	-0.872483221
6	4540	490	511.0874244	4.303556007	44.7	44.31	-0.872483221
7	4540	490	511.0874244	4.303556007	44.7	44.31	-0.872483221
8	4610	497.5	515.9673402	3.712028176	44.7	44.31	-0.872483221
9	4660	503.5	521.6958308	3.613869072	44.7	44.31	-0.872483221
10	5380	660	596.626589	-9.602031974	44.7	44.31	-0.872483221

Chiller 2 (Electric EIR Chiller Centrifugal York YK 4396 kW Vanes)

Measurement No.	Measured cooling load	Measured chiller power	Average chiller power calculated by EnergyPlus	% difference (chiller)
1	4310	470	470.0238589	0.005076351
2	4350	472.5	478.5808528	1.286952976
3	4450	476.5	484.0503285	1.584539041
4	4470	477	487.4443294	2.189586881
5	4500	483.5	494.7217172	2.320934264
6	4540	490	497.0955368	1.44806873
7	4540	490	497.0955368	1.44806873
8	4610	497.5	508.4683926	2.20470203
9	4660	503.5	521.7836501	3.631310842
10	5380	660	586.7552766	-11.09768536

APPENDIX C: MATLAB CODE USED

B.1 Scenario_A.m

This code takes weather data files and three functions (Find_V.m, Convert_V.m, and DX_power.m) to estimate overall data center efficiency. These functions are introduced later in this section.

```matlab
clc; clear;

weather= dlmread('weather.csv');
T_ci_vec = weather(:,10) % 6: Atlanta 4: Helsinki 3: Seoul 2: New Delhi 7:
Chicago 8: Houston 9: LA, 10: Anchorage
%T_ci_vec = [18]

Q_vec = [400]
n= 0;

CoP = 4.0; % Rated CoP of DX D
PUE = ones;

fan_eff = 0.6;

for j = 1:length(Q_vec)
    Q = Q_vec(j);

P_kwh = 0; % reset Power (a new CoP is used)
P_DX_Total = 0;
P_Fans_Supply = 0;
P_Fans_Outside = 0;

for i = 1:length(T_ci_vec)

    T_ci = T_ci_vec(i);
      if T_ci <= 12.6

        N = 2;
        P_wheel = (N^3)*1.1/(6^3);

        V_outside = Find_V(T_ci,Q,N);
        V_supply = 56474.63837; % units in CFM
        P_outside = conv_outside(V_outside)/fan_eff;
        P_supply = conv_supply(V_supply)/fan_eff;
```

```
        P_kwh = P_kwh + P_supply + P_outside + P_wheel;
        P_Fans_Supply = P_Fans_Supply + P_supply;
        P_Fans_Outside = P_Fans_Outside + P_outside;

    elseif T_ci <= 15.1

        N = 3;
        P_wheel = (N^3)*1.1/(6^3);


        V_outside = Find_V(T_ci,Q,N);
        V_supply = 56474.63837;
        P_outside = conv_outside(V_outside)/fan_eff;
        P_supply = conv_supply(V_supply)/fan_eff;

        P_kwh = P_kwh + P_supply + P_outside + P_wheel;
        P_Fans_Supply = P_Fans_Supply + P_supply;
        P_Fans_Outside = P_Fans_Outside + P_outside;

elseif T_ci <= 16.4

        N = 4;
        P_wheel = (N^3)*1.1/(6^3);


        V_outside = Find_V(T_ci,Q,N);
        V_supply = 56474.63837;
        P_outside = conv_outside(V_outside)/fan_eff;
        P_supply = conv_supply(V_supply)/fan_eff;

        P_kwh = P_kwh + P_supply + P_outside + P_wheel;
        P_Fans_Supply = P_Fans_Supply + P_supply;
        P_Fans_Outside = P_Fans_Outside + P_outside;

elseif T_ci <= 17.5

        N = 5;
        P_wheel = (N^3)*1.1/(6^3);

        V_outside = Find_V(T_ci,Q,N);
        V_supply = 56474.63837;
        P_outside = conv_outside(V_outside)/fan_eff;
        P_supply = conv_supply(V_supply)/fan_eff;

        P_kwh = P_kwh + P_supply + P_outside + P_wheel;
        P_Fans_Supply = P_Fans_Supply + P_supply;
        P_Fans_Outside = P_Fans_Outside + P_outside;

elseif T_ci <= 18.0


        N = 6;
        P_wheel = 1.1 ; % 1.1 kW at 6 RPM
```

```matlab
        V_outside = Find_V(T_ci,Q,N);
        V_supply = 56474.63837;

        P_outside = conv_outside(V_outside)/fan_eff;
        P_supply = conv_supply(V_supply)/fan_eff;
        P_kwh = P_kwh + P_supply + P_outside + P_wheel;
        P_Fans_Supply = P_Fans_Supply + P_supply;
        P_Fans_Outside = P_Fans_Outside + P_outside;


    elseif T_ci < 37.1
        N = 6;

        T_ho_warm = 0.5824*T_ci + 16.251; % This is to calculate the T_ho
when ambient temp exceeds 18 degree C
        % DX_Eplus.xls has the linear equation plotted.

        V_supply = 56474.63837;
        P_supply = conv(V_supply);

        V_outside = 32.6502*2118.88/1.157;
        P_outside = conv_outside(V_outside)/fan_eff;
        P_supply = conv_supply(V_supply)/fan_eff;
        P_DX = DX_power(T_ho_warm)/1000; % power is calculated using E+
result


        P_wheel = 1.1;
        P_kwh = P_kwh + P_supply + P_outside + P_DX + P_wheel;
        P_Fans_Supply = P_Fans_Supply + P_supply;
        P_Fans_Outside = P_Fans_Outside + P_outside;
        P_DX_Total = P_DX_Total + P_DX;
    else
        N = 6;
        V_supply = 56474.63837;
        P_supply = conv(V_supply);
        P_DX = 111789.1472 /1000; %from energy plus

        V_outside = 32.6502*2118.88/1.157;
        P_outside = conv_outside(V_outside)/fan_eff;
        P_supply = conv_supply(V_supply)/fan_eff;


        P_kwh = P_kwh + P_supply + P_outside + P_DX;
        P_Fans_Supply = P_Fans_Supply + P_supply;
        P_Fans_Outside = P_Fans_Outside + P_outside;
        P_DX_Total = P_DX_Total + P_DX;

    end

n = n+1;
processing = 100*n/length(T_ci_vec)/length(Q_vec);
A = num2str(processing) ;
```

```matlab
B = ' %';
Z = ['Running...' A B ];
disp(Z)


end



P_lighting = 105186.84;
P_IT = 400*length(T_ci_vec);
PUE(1,j) = CoP;
PUE(2,j) = N;
PUE(3,j) = Q;
PUE(4,j) = (P_IT + P_kwh) / P_IT %%% <<---- PUE
PUE(5,j) = P_IT;
PUE(6,j) = P_kwh;
PUE(7,j) = P_Fans_Supply;
PUE(8,j) = P_Fans_Outside;
PUE(10,j) = P_DX_Total;
PUE(9,j) = P_kwh - (P_Fans_Supply + P_Fans_Outside +P_DX_Total);

PUE(7,2) = P_Fans_Supply/P_kwh*100;
PUE(8,2) = P_Fans_Outside/P_kwh*100;


PUE(9,2) = PUE(9,1)/P_kwh*100;
PUE(10,2) = P_DX_Total / P_kwh *100;

end

PUE = PUE'
```

B.2 Find_V.m

This function takes the cooling load, rotational speed of the wheel, and the ambient temperature to calculate the mass flow rate of air in the cold side using the effective NTU method presented in the paper.

```matlab
function out2 = Find_V(T_ci,Q_in,RPM_in)

T_ho = 26.7; % "Supply Air Temperature in Celsius"
T_hi = 38.9 ; % "Return Air Temperature in Celsius"

RPM = RPM_in ;
p_kwh = 0;

Q = Q_in*1000; %[W]
C_h = Q/(T_hi-T_ho);

% -------------------"Properties"-----------------------------------------
Cp_c = 1005;
Cp_h = 1004;
Pr_hot = 0.7268;
Pr_cold = 0.73;
k = 0.02588;

m_dot_c = 9; % This is an initial value. We know m_dot_c won't be lower than
             9 kg/s

Ef2 = 1;
Ef1 = 10;
compare = Ef1 - Ef2;

while compare > 0.000001

C_c = m_dot_c*Cp_c;
m_dot_h = C_h/Cp_h;
C_min = C_c;
Q_h = m_dot_h*2118.88/1.157;


% -------------" C_h > C_c" ---------------------------------

C_max = C_h;
C_c = C_min ;
Q_max = (m_dot_c*Cp_c)*(T_hi-T_ci) ;
C_star = C_min / C_max;


EEE = Q/Q_max ;
```

```matlab
%"-----------------Find Nu_inf ------------------------------------"

d_star = 1; % " equilateral triangle"
delta_phi_max = (7*1d0^(-3)*d_star^8)/((1+10*d_star^(-28))*(1+64*10^(-
8)*d_star^28)^0.5);
n = 1.653; % " equilateral triangle... Eq. (16)"
delta_phi = delta_phi_max*(0.95*(n-1)^0.5)/(1+0.038*(n-1)^3);
phi_inf = 0.5155*d_star/(3-d_star);
phi = 1 + (phi_inf-1)/(1+(1/(n-1)))+delta_phi;


Nus_inf = 3.657*phi;


%"------------------Find Shape Factor (psi) ----------------------------

psi_inf = 3/8*d_star^2*(3-d_star);
psi = 1+((psi_inf-1)/(1+0.33*d_star^2.25/(n-1)));


%"---------------------Find Heat Transfer Factor (big_phi)---------------

big_phi = 1+ ((3*(d_star/2)^(7/8)/(1+d_star))-1)/(1+0.25/(n-1));



%"--------------------Find dimensionless coordinate (Z)------------------

A_1 = 9.59479706644007/2; %" Area for Airflow, [m^2]"

%%----------------------------------------------------------------------%%%

a = 3.711E-3 ; % [m] "side length of triangle"
%a = 0.0019 ; % [m] "side length of triangle"


%%----------------------------------------------------------------------%%%

F = sqrt(3)/4*a^2;
P = a*3;
D_eq = 4*F/P ; %  "Equivalent Diameter "

u_hot = m_dot_h / 1.1649 / A_1;
Re_hot = u_hot*D_eq/ 1.6036e-5;
Z_hot = 0.2/D_eq/Re_hot/Pr_hot;

u_cold = m_dot_c / 1.1649 / A_1;
Re_cold = u_cold*D_eq/ 1.6036e-5;
Z_cold = 0.2/D_eq/Re_cold/Pr_cold;



X_hot = Z_hot*Nus_inf^3 / ( big_phi^3 * psi);
Y_hot = 1+ 1.615*X_hot^(-1/3)/(1+1.88*X_hot^(1/3)+3.93*X_hot^(4/3))^0.;
Nus_hot = Y_hot*Nus_inf;
h_hot = Nus_hot*k/D_eq;

X_cold = Z_cold*Nus_inf^3 / ( big_phi^3 * psi);
Y_cold = 1+ 1.615*X_cold^(-1/3)/(1+1.88*X_cold^(1/3)+3.93*X_cold^(4/3))^0.;
```

```matlab
Nus_cold = Y_cold*Nus_inf;
h_cold = Nus_cold*k/D_eq;


%%------------------------------------------------------------------------%%%
%%------------------------------------------------------------------------%%%


area = 2302/2; % [m^2] %%% This is from Table 2.1


%%------------------------------------------------------------------------%%%
%%------------------------------------------------------------------------%%%


UA = (1/(h_hot*area)+1/(h_cold*area))^(-1);
NTU = UA/C_min;


E_0 = (1-exp(-NTU*(1-C_star)))/(1-C_star*exp(-NTU*(1-C_star)));


N = RPM; % [rpm]
m_al = 1555.82;
C_p_al = 910; % [J/kg-k]
C_r = m_al* C_p_al*N/60;
C_r_star = C_r /(m_dot_c*Cp_c);


% E_r = 1 - (1/(9*(C_r /(m_dot_c*Cp_c))^1.93))
E_r = 1- (0.114*(1-exp(-NTU)))/(C_star^0.44*C_r_star^1.93); % [Eq. 28]


Ef2 = E_r*E_0 ;
Ef1 = EEE;


compare = Ef1 - Ef2;
m_dot_c = m_dot_c + 0.0005; % Iteration

if m_dot_c > m_dot_h
    compare = 0;
    m_dot_c = 999;
end


V_c = m_dot_c*2118.88/1.157;
V_h = m_dot_h*2118.88/1.157;


end  %end of the second "for" loop end  %


out2 = V_c;


out3 = Q_max;
out4 = Q;


m_dot_h;
m_dot_c;


EEE;
T_co = T_ci+Q/(m_dot_c*Cp_c);
```

B.3 Convert_V.m

This function takes the calculated mass flow rate from Find_V.m and convert the value to power consumption by the fans using the fan data. Fan data can be seen in Figure 2.3.

```matlab
function out = Convert_Supply(V)

fan=dlmread('fandata.csv');
CFM = fan(:,1);
Watt = fan(:,3);




if V >= CFM(2)
    power_out = Watt(2) + (Watt(1)-Watt(2))*(V - CFM(2))/(CFM(1)-CFM(2));
n=1;
elseif V >= CFM(3)
    power_out = Watt(3) + (Watt(2)-Watt(3))*(V - CFM(3))/(CFM(2)-CFM(3));
   n=2 ;

elseif V>= CFM(4)
    power_out = Watt(4) + (Watt(3)-Watt(4))*(V - CFM(4))/(CFM(3)-CFM(4));
n=3;
elseif V>= CFM(5)
    power_out = Watt(5) + (Watt(4)-Watt(5))*(V - CFM(5))/(CFM(4)-CFM(5));
n=4;
elseif V>= CFM(6)
    power_out = Watt(6) + (Watt(5)-Watt(6))*(V - CFM(6))/(CFM(5)-CFM(6));
   n=5 ;
elseif V>= CFM(7)
    power_out = Watt(7) + (Watt(6)-Watt(7))*(V - CFM(7))/(CFM(6)-CFM(7));
    n=6;
elseif V>= CFM(8)
    power_out = Watt(8) + (Watt(7)-Watt(8))*(V - CFM(8))/(CFM(7)-CFM(8));
n=7;
else
    power_out = Watt(9) + (Watt(8)-Watt(9))*(V - CFM(9))/(CFM(8)-CFM(9));


end

out = power_out;
end
```

B.4 DX_power.m

This function takes the temperature of the air leaving the thermal wheel when the ambient temperature is above 18 °C. (Figure 3.2) Then it converts the temperature value to the power usage by DX system using Figure 2.4, which is implemented here as "DX_Eplus_1.csv".

```matlab
function out =  DX_power(T_ho_warm)

A = dlmread('DX_Eplus_1.csv') ;
T_ho_vec = A(:,1);
DX_power_vec = A(:,2);
kk = 999 ;


for i = 1:length(T_ho_vec) - 1
    T_ho_compare1 = T_ho_vec(i);
    T_ho_compare2 = T_ho_vec(i+1);
    DX_power1 = DX_power_vec(i);
    DX_power2 = DX_power_vec(i+1);

    if T_ho_warm < 26.8
        out1 = 6000;
        kk = 0;
    elseif T_ho_compare2 >= T_ho_warm && T_ho_warm >= T_ho_compare1
        out2 = (T_ho_warm - T_ho_compare1)*(DX_power2 -
DX_power1)/(T_ho_compare2-T_ho_compare1) + DX_power1 ;
        kk=0;
    else
        out3 = DX_power_vec(end);

        kk =0;
    end
end


if T_ho_warm < 26.8
    out = out1;
elseif T_ho_warm < 38.9
    out = out2;
else
    out = out3;
end
end
```

REFERENCES

[1]   Koomey, J., 2011, "Growth in Data center Electricity Use 2005 to 2011," Analytics Press, Oakland, CA, http:// www.an alytic spress.com/datacenters.html

[2]   Jackson, J. M., Koomey, J. G., Blazek, M., and Nordman, B., 2002, "National and Regional Implications of Internet Data Center Growth in the U.S.," Resoures, Conservation and Recycling, 36(3), pp. 175-185.

[3]   Delforge, P., "America's Data Centers Consuming and Wasting Growing Amounts of Energy ", Nrdc.org, 2014. [Online]. Available: http://www.nrdc.org/energy/data-center-efficiency-assessment.asp. [Accessed: 10- Mar- 2016].

[4]   Schmidt, R., Chu, R. C., Ellsworth, M. Iyengar, M., and Porter, D., 2005, "Maintaining Datacom Rack Inlet Air Temperatures with Water-cooled Heat Exchanger," Proc. ASME InterPACK05, San Francisco, CA, Paper No. IPACK2005-73468.

[5]   Sasser, J., "A Look at Data Center Cooling Technologies" Uptown Institute Journal. [Online]. Available: https://journal.uptimeinstitute.com/a-look-at-data-center-cooling-technologies [Accessed: 10- Apr- 2016].

[6]   Rubenstein, L., Brandon, A., Zeighami, R., and Peterson, E., 2010, "Hybrid Cooled Data Center Using above Ambient Liquid Cooling," Thermal and Thermomechanical Phenomena in Electronic Systems (ITherm), 12th IEEE Intersociety Conference on. IEEE, Las Vegas, NV.

[7]   Harris, C., "3M and allied control debut first-of-its-kind immersion cooling data center at SC13" (2013, Nov 18). Business Wire Retrieved, [Online]. Available: http://prx.library.gatech.edu/login?url=http://search.proquest.com.prx.library.gatech.edu/docview/1459183418?accountid=11107

[8]   Rambo, Jeffrey, and Yogendra Joshi. "Modeling of data center airflow and heat transfer: State of the art and future trends." Distributed and Parallel Databases 21.2-3 (2007): 193-225.

[9]   Kang, S. R.R. Schmidt, K.M. Kelkar, A. Radmehr, and S.V. Patankar, "A methodology for the design of perforated tiles in a raised floor data center using computational flow analysis," presented at ITHERM 2000 – Intersociety Conference on Thermal and Thermomechanical Phenomena in Electronic Systems, Las Vegas, NV, 2000.

[10]   Patel, C.D., C.E. Bash, C. Belady, L. Stahl, and D. Sullivan, "Computational fluid dynamics modeling of high compute density data centers to assure system inlet air specifications," Presented at Proc. IPACK'01 – The Pacific Rim/ASME International Electronics Packaging Technical Conference and Exhibition Kauai, HI, 2001.

[11]   Shrivastava, S., Iyengar, M., Sammakia, B., Schmidt, R., and VanGilder, J. 2006. Experimental-Numerical Comparison for a High Density Data Center: Hot Spot Heat Fluxes in Excess of 500 W/ft2. Proceedings of ITHERM '06. San Diego, California.

[12]   Schmidt R., "Effect of Data Center Characteristics on Data Processing Equipment Inlet Temperatures", Advances in Electronic Packaging, Proceedings of the Pacific Rim/ASME International Electronic Packaging Technical Conference and Exhibition (Interpack), Vol. 2, Paper IPACK2001-15870, Kauai, Hawaii, July 8-13, pp. 1097-1106 (2001).

[13]   Bhopte S., Iyengar M., Sammakia B., Schmidt R and Agonafer D., "Numerical modeling of data center clusters – immpact of model complexity", Proceedings of the International Mechanical Engineering Congress and Exposition, Chicago, Illinois, November (2006).

[14]   Bhopte S., Agonafer D., Schmidt R. and Sammakia B., "Optimization of Data Center Room Layout to Minimize Rack Inlet Air Temperature", Journal of Electronic Packaging, December 2006, Vol. 128, Issue 4, pp. 380 – 387.

[15]   Gondipalli, Srujan, et al. "Numerical modeling of data center with transient boundary conditions." Thermal and Thermomechanical Phenomena in Electronic Systems (ITherm), 2010 12th IEEE Intersociety Conference on. IEEE, 2010.

[16]   Demetriou, Dustin W., et al. "Development of a Dynamic Energy Use Modeling Tool for Data Center Cooling Infrastructure." ASHRAE Transactions117.2 (2011).

[17]   Mani, K., and Jee, B., 2007, On the Edge: A Comprehensive Guide to Blade Server Technology, John Wiley & Sons, pp. 108.

[18]   Romie F. E., Transient Response of Rotary Regenerators, Transactions of ASME, Journal of Heat Transfer, vol. 110, pp. 836–840, 1988.

[19]   Yilmaz T. and Büyükalaca, O., "Design of Regenerative Heat Exchangers", Heat Transfer Engineering, vol. 24, no. 4, pp. 32-38, 2003.

[20]   Worsøe-Schmidt, P., "Effect of fresh air purging on the efficiency of energy recovery from exhaust air in rotary regenerators", International Journal of Refrigeration, vol. 14, no. 4, pp. 233-239, 1991.

[21]   "KyotoCooling| Smarter Cooling for Data Centers", Kyotocooling.com. [Online]. Available: http://www.kyotocooling.com/. [Accessed: 10- Mar- 2016].

[22]   Sullivan, R. R., "Analysis of the KyotoCooling Process: Introduction to the New KPN CyberCenters", in Green Enterprise IT Symposium, New York City, 2009.

[23]   Iyengar, M., David, M., Parida, P., Kamath, V., Kochuparambil, B., Graybill, D., …, and Chainer, T., 2012, "Server Liquid Cooling with Chiller-less Data Center Design to Enable Significant Energy Savings," In Semiconductor Thermal Measurement and Management Symposium (SEMI-THERM), 28th Annual IEEE, pp. 212-223.

[24]   DesignBuilder Official Website, [Online]. Available: http://www.designbuilder.co.uk/

[25]   Henderson, H., Rengarajan, K., and Shirey, D., "The impact of comfort control on air conditioner energy use in humid climates", ASHRAE Transactions, vol. 98, no. 2, pp. 104-113, Atlanta, GA, 1992.

[26]   ASHRAE, HVAC2 Toolkit: A Toolkit for Secondary HVAC System Energy Calculation. Atlanta: American Society of Heating, Refrigerating and Air-Conditioning Engineers, In, 1993.

[27]   B. LLC, "Coils: Engineering Reference — EnergyPlus 8.2", Bigladdersoftware.com, 2015. [Online].   Available: http://bigladdersoftware.com/epx/docs/8-2/engineering-reference/coils.html#single-speed-electric-dx-air-cooling-coil. [Accessed: 12- Dec- 2015].

[28]   Shah, R. K., and London, A. L., Laminar Flow Forced Convection in Ducts, Academic Press, New York, NY, 1978.

[29]   Yilmazand T., and Cihan, E., General Equation for Heat Transfer for Laminar Flow in Ducts of Arbitrary Cross-sections, Int. J. Heat Mass Transfer, vol. 36, no. 13, pp. 3265-3270, 1993.

[30]   Air Enterprises, LLC, "Data Hall Submittal", 2015.

[31]   Turner, M., and Comair, R., "All You Need to Know about Fans", Electronics Cooling, vol. 2, no. 2, pp. 10-13, 1996.

[32]   NREL, Improving Fan System Performance, the Department of Energy, Energy Efficiency and Renewable Energy, 2003.

[33]   Jone, G., "Using fans in series and parallel: performance guidelines", Ebmpapst.

[34]   Haines, R., Control Systems for Heating, Ventilating, and Air Conditioning. New York: Van Nostrand Reinhold Co., 1987, pp. 88.

[35]   ASHRAE TC 9.9., 2011, Thermal Guidelines for Data Processing Environments – Expanded Data Center Classes and Usage Guidance.

[36]   Clark, J., 2012, "Humidity in the Data Center: Do We Still Need to Sweat IT," Data Center Journal.

[37]   Ghiaasiaan, S. M., 2011, Convective Heat and Mass Transfer, Cambridge University Press.

[38]   Lytron, CP20G03 Flat Tube Cold Plate Performance Data, [Online] Available at: http://www.lytrondirect.com/cp20g03 -flat-tube-cold-plate/cp20g03/

[39]   IBM, 2006, AMD LS20 for IBM BladeCenter, [Online] Available at: http://www-07.ibm.com/kr/partnerworld/ down loads /bcls_20_sales_guide1.pdf.

[40]   Dow Corning, Silicone Grease Solutions for Your Thermal Interface Needs, [Online] Available at: https://www. dowcorning.com/content/publishedlit/11-1712-01.pdf.

[41]   Lytron, M14-250 Copper OEM Coil Tube-Fin Heat Exchanger Performance Data, [Online] Available at: http://www.lytrondirect.com/m14-240-copper-oem-coil-tube-fin-heat-exchanger/m14-240/

[42]   Lytron, Ostro Fan Performance Data, [Online] Available at: http://www.lytron.com/Tools-and-Technical-Reference/Fans-Pumps/Heat-Exchanger-Fans/Ostro-Fan

[43]   Chang, C. K., Fui, S. K., and Bin, N. W., 2013, "Of Air-Cooled Chiller, Water-Cooled Chiller and Hybrid Evaporative Air-Cooled Chiller in Malaysia – A Review" Conference of the International Journal of Art and Science.

[44]   Kellner, E., Hubbart, J., 2015, "Agricultural and Forested Land Use Impacts on Floodplain Shallow Groundwater Temperature Regime," Hydrological Processes, 30, pp. 625-636.

[45]   United State Environmental Protection Agency (EPA), 2016, Average Temperature of Shallow Groundwater, Ecosystems Research, Athens, GA.

[46]   Lytron, LCS20 Liquid-to-Liquid Cooling System Performance Data, [Online] Available at: http://www. lytron.com/Cooling-Systems/Standard/Liquid-to-Liquid-Cooling-Systems/LCS20?tab=specs

[47]   Xing Niu, Jianlin Yu, Shuzhong Wang, Experimental study on low-temperature waste heat thermoelectric generator, Journal of Power Sources, Volume 188, Issue 2, 15 March 2009, Pages 621-626, ISSN 0378-7753

[48]   Eakburanatwat J, Boonyaroonate I. Development of a thermoelectric batterycharger with microcontroller-based maximum power point tracking technique. Appl Energy 2006; 83:687–704.

[49]   Lange RG, Carroll WP. Review of recent advances of radioisotope power systems. Energy Convers Manage 2008;49:393–401.

[50]   O'Brien RC, Ambrossi RM, Bannister NP, Howe SD, Atkinson HV. Safe radioisotope thermoelectric generators and heat sources for space applications. J Nucl Mater 2008;377:506–21.

[51]   Korzhuev, M. "Conflict Between Internal Combustion Engine And Thermoelectric Generator During Waste Heat Recovery In Cars." Technical Physics Letters 37.2 (2011): 151-153. Academic Search Complete. Web. 21 May 2016.

[52]   Crane DT, Jackson GS. Optimization of cross flow heat exchangers for thermoelectric waste heat recovery. Energy Convers Manage 2004;45:1565–82

[53]   Bitschi, A., "Modelling of thermoelectric devices for electric power generation", Dissertation submitted to the Swiss Federal Institute Of Technology Zurich, Available: http://e-collection.library.ethz.ch/eserv/eth:470/eth-470-02.pdf

[54]   Marlow, TG12-6 Data Sheets, [Online]. Available at: http://www.marlow.com /downloads/dl/file/id/155/product/113/tg12_6_data_sheet_revk.pdf

[55]   ASHRAE Standing Standard Project Committee 90.1, 2012, Energy Standard for Buildings Except Low-Rise Residential Buildings, ASHRAE, pp. 34

[56]   Neutrium, 2012, Absolute Roughness of Pipe Material, [Online] Available at: https://neutrium.net /fluid_flow/ab solute-roughness/

[57]   Vaillencourt, R. R., The correct formula for using the affinity laws when there is a minimum pressure requirement. Energy engineering, vol. 102, no. 4, pp. 32-46, 2005.

[58]   CIBSE, 2014, CIBSE Guide G: Public Health and Plumbing Engineering 2014, Chartered Institution of Building Services Engineers.

[59]   Iyengar, M., David, M., Parida, P., Kamath, V., Kochuparambil, B., Graybill, D., ..., and Chainer, T., 2012, "Extreme Energy Efficiency Using Water Cooled Servers Inside a Chiller-less Data Center," In Thermal and Thermomechanical Phenomena in Electronic Systems (ITherm), 2012 13th IEEE Intersociety Conference, pp. 137-149.

[60]   David, M., Iyengar, M., Parida, P., Simons, R., Schultz, M., Gaynes, M., Schmidt, R., and Chainer, T., 2012, "Experimental Characterization of an Energy Efficient Chiller-less Data Center Test Facility with Warm Water Cooled Servers," Proc. of SEMI-THERM Conf., San Jose, CA.

[61]   Bureau of Labor Statistics, 2016, Average Energy Prices, Washington-Baltimore – February 2016, U.S. Dept. of Labor